NOAA Technical Memorandum OAR ETL-300

SPARK DISCHARGES IN WATER
(A Hydrodynamical Description)

K.A. Naugolnykh
N.A. Roi

Environmental Technology Laboratory
Boulder, Colorado
December 2000

noaa NATIONAL OCEANIC AND ATMOSPHERIC ADMINISTRATION / Oceanic and Atmospheric Research Laboratories

NOAA Technical Memorandum OAR ETL-300

SPARK DISCHARGES IN WATER
(A Hydrodynamical Description)

Konstantin A. Naugolnykh
Nikolai A. Roi

Environmental Technology Laboratory
Boulder, Colorado
December 2000

UNITED STATES DEPARTMENT OF COMMERCE

Norman Y. Mineta
Secretary

NATIONAL OCEANIC AND ATMOSPHERIC ADMINISTRATION

D. JAMES BAKER
Under Secretary for Oceans
and Atmosphere/Administrator

Oceanic and Atmospheric
Research Laboratories

David L. Evans
Director

NOTICE

Mention of a commercial company or product does not constitute an endorsement by the NOAA Oceanic and Atmospheric Research Laboratories. Use of information from this publication concerning proprietary products or the test of such products for publicity or advertising purposes is not authorized.

For sale by the National Technical Information Service, 5285 Port Royal Road
Springfield, VA 22061

CONTENTS

ABSTRACT

The development of technology presents physics with the problem of investigating processes involving large concentration of energy, high pressure and high temperatures. The impulsive spark discharge in a liquid is one such process. As a result of the fast release of the capacitor energy into the discharge channel high temperatures and pressures are generated,accompanied by the intense sound wave radiation. The purpose of the present book is to give theoretical description and present results of experimental investigations of hydrodynamic and thermodynamic phenomena stimulated by the underwater pulse discharge. A qualitative picture of the phenomena occurring in a spark discharge in water and of the actual sequence in which they take place is given. The methods used in experiment for the initiation of spark discharges in a liquid are described. The processes occurring in the discharge channel and the properties of the matter in it are examined. The experimental information on the electric characteristics of the discharge, the rate of the channel expansion and also estimates of pressure and temperature in the discharge channel is given. The properties of the dense low-temperature plasma generated in the discharge channel are examined and the equation of energy balance is derived. The concrete form of this equation depends on the form of the equation which determines the pressure in the channel as a function of the channel radius and its derivatives. In order to find this dependence for various cases, the hydrodynamic problem of the expansion of a bubble in a liquid is considered. Then the theoretical models for the pulse park discharge in water are developed and the results of theoretical considerations are compared with the experiments. In this book we examine mainly spark discharges in water with moderate energy densities in the discharge channel, because this case is of utmost interest for many applications of spark discharges as sources of pressure pulses. The fundamental equations governed the process of underwater spark are derived and some solutions for the most important cases are obtained. The theoretical approach developed can be used in further investigations of underwater spark and sonoluminescence.. The simple engineering equations obtained are useful for many practical applications allowing to perform estimates of the hydrodynamic and thermodynamical effects of the spark at given electrical parameters of the circuit. The present report based on the translation of the monograph "ELEKTRICHESKIE RAZRJADY V VODE" by K. Naugolnykh and N. Roy, published by Nauka, Moskva, 1971.

Chapter I

INSTEAD OF AN INTRODUCTION

1.1 Spark discharges in fluids as a process with a high concentration of energy

The development of science presents physics with the problem of investigating processes involving a large concentration of energy, high pressure and high temperature.A impulsive spark discharge in a liquid is one such process. As a result of the fast release of the capacitor energy into the discharge channel high temperatures and pressures are generated. These properties of the impulsive spark discharges in liquids are widely used in the development of new technological processes for the treatment of various materials and for the creation of new means for of transformation of energy.

In 1944 B .R .Lazarenko and N. I. Lazarenko [1] reported the possibility of using the impulsive spark discharges in liquids for the treatment of metals. Today this method is widely used in many types of industry. In the electro-spark treatment of metals , one uses mainly the capability of the impulsive discharges in liquids to generate a dense high-temperature plasma. The role of liquids in this case reduces to slowing down the expansion of the channel, which leads to an increase of the density of the energy liberated in the channel with the consequent increase of the temperature and pressure of the plasma in the channel. The basic physics of the electro-spark treatment of metals is the subject of intensive investigations [2].

Due to the high temperature and pressure of the channel plasma, the impulsive spark discharges in water can serve as a source of bright light [3].

Many researchers have, at different times, focused their attention on the possibility of creating high pressures in water using impulsive spark discharges. The fact that a discharge in a liquid can have destructive power had already been mentioned in 1767 by Lane [4] and in 1769 by Priestly [5]. Pokrovskij and Stanjukovich [6] in 1944 cited the possibility of creating cumulative jets by using the pressure created in a spark discharge in liquids.

Frungel [7] carried out the first attempt to measure the electromechanical efficiency of a discharge in water. The possibility of using a spark discharge for seismic studies was mentioned in 1952 by Vogel [8], and by Mazov and Meyer in 1955 [9]. The active publicity on the applications of this effect by Jutkin [10] promoted wide use of impulsive spark discharges in water for the improvement of such classic technological processes as stamping, casting, casting decontamination and others. The impulsive spark discharges in water are used also as powerful sources of sound in hydroacoustic and hydrogeological researches [11,12] .

In practical applications, discharges with very different parameters are used .The main parameters, discharge energy and durations, may have a wide range of variations. Thus, in the electro-spark treatment of metals, the discharge energy amounts to a few joules, while in technological processes and devices, in which the discharge serves as a source of pressure pulses, the discharge energy reaches 10^3–10^4 joules. The discharge durations may vary also in a similarly extreme manner. Usually, one uses discharges in a near-critical regime, because such a regime provides the fastest energy transfer from the storage device into the channel discharge, and, as we shall show later, also the highest electro-acoustic efficiency. The discharge duration in this case is approximately given by the quantity $2\pi\sqrt{LC}$, where L and C are,respecticely, the inductance and capacity of the discharge loop. The discharge duration varies in a range from a few tenths to hundreds of microseconds. The impulsive power developed in a discharge can reach values on the order of 10^2–$10^5 kW$. Depending on the energy and duration of the discharge, the energy density in the channel may also vary considerably,reaching in certain cases values on the order of 10^2–$10^3 J/cm^3$. Note that these values are only one order of magnitude lower than the energy density occurring in explosions of solid explosive materials. The pressure in the channel rises to several thousand of atmospheres, and the temperature to several tens of thousands of degrees. In certain cases, when the density of the magnetic energy is comparable with the density of the gaskinetic energy of the particles in the channel, the effect of the magnetic pressure on the channel may be considerable (pinch-effect). In practice, one uses mainly discharges with moderate energy densities in the channel . In these, the channel expansion causes a perturbation in the density of the surrounding water, which is small compared to the equilibrium density, and the magnetic pressure is small compared to the gaskinetic pressure.

The physical phenomenona taking place in a spark discharge have not been fully investigated. In particular, the studies of the hydrodynamic characteristics of the discharges, which are important for practical applications, are inadequate . The present monograph is dedicated to the study of spark discharges from a hydrodynamical prospective.

In this book we examine mainly spark discharges in water with moderate energy densities in the discharge channel, because this case is of utmost interest for many applications of spark discharges as sources of pressure pulses.

A qualitative picture of the phenomena occurring in a spark discharge in water and of the actual sequence in which they take place is given in the next section of the present chapter.

In Chapter II we describe the methods used in experiments for the initiation of spark discharges in a liquid. In Chapter III we examine the processes occurring in the discharge channel and the properties of the matter in it. We give experimental information on the electric characteristics of the discharge, the rate of the channel expansion , and also estimates of pressure and temperature in the discharge channel. We examine the properties of the dense low-temperature plasma generated in the discharge channel and derive an equation of energy

balance. The concrete form of this equation depends on the form of the equation that determines the pressure in the channel as a function of the channel radius and its derivatives. In order to find this dependence for various cases, in Chapter IV, we examine the hydrodynamic problem of the expansion of a bubble in a liquid.

On the basis of the results of Chapters III and IV, in Chapter V we build theoretical models for the spark discharge in water. In Chapter VI the results of the calculations are compared with experiments.

The present monograph is based mainly on the work of the authors and their co-workers: D. P. Frolov, N. I. Charushina, A. I. Ioffe, B. E .Gordeev, K .P. Krivosheev, V. I . Nemchenko, B. N. Drapezo, N. G. Kozhelupova and R .A. Volchenkova, who at various stages of the work have collaborated with us. The authors express their

sincere gratitude to them . They also thank L.M. Kvasova for her help in the preparation of the manuscript.

1.2. Physics of spark discharges in water

In the present section we give a brief description of the main physical phenomena that characterize a spark discharge in a liquid. First, we examine the so-called pre-discharge stage, in which there occurs the formation of the discharge channel which shunts the interelectrode gap; then, we consider the phenomena taking place during the release of the capacitor energy into the discharge channel; and, finally, we examine the pulsation of the gas bubble after the discharge.

A typical process for the initiation of a discharge is the breakdown of the interelectrode gap cauged by the electric voltage generated on the electrodes when the charged capacitor is connected to them. Within the voltage range of 1–100 kV used in practice, two breakdown mechanisms are known: the streamer or leader mechanism, which works at high voltages, and the thermal mechanism, which works at low voltages. The more favorable conditions for a leader breakdown are created by high-voltage nonhomogeneous fields between a positive point and a negative plate. As a result of the formation of electron avalanches "running" towards the point, leaders are generated, which then grow in the direction of the ionization centers from which the electron avalanches originated. This process reminds one of the breakdown of a gas. The collection of leaders on the positive point has the shape of a corona. The shunting of the interelectrode gap by one of the leaders completes the process of the discharge channel formation. This mechanism provides the breakdown of gaps with a width of several cm at voltages of several tens of kV. The breakdown delay, i.e., the time between the application of the voltage and the formation of the channel, in the case of a leader breakdown is practically independent of the value of the hydrostatic pressure,up to at least 1000 atm.

At low voltages, the leader mechanism is replaced by the thermal mechanism. Due to the effect of the conduction current, the water around the electrodes heats up and evaporates. As a result, a gas "bridge" forms between the electrodes, which then becomes the route for the breakdown of the discharge channel. The distinctive features of this mechanism of discharge initiation are

long breakdown delays, which may reach several milliseconds, small gap widths, and a strong increase of the breakdown delay with the hydrostatic pressure. If the circumstances require it, the discharge initiation can be realized also with the help of auxiliary means.

After the formation of the channel, a strong discharge current, which may reach tens and hundreds of kA, heats the plasma already in the initial stage up to a temperature on the order of $10^4\,^\circ K$. During the discharge, at the time when the current flows, the temperature of the plasma changes insignificantly, dropping after the end of the discharge.

The heating of the plasma causes an increase of the pressure in the channel, which leads to an expansion of the channel itself. The pressure in the channel during a discharge goes through a maximum. In the initial stage the pressure rises in spite of the volume increase, and drops only towards the end of the discharge. For moderate energy density in the channel, the pressure in the channel reaches, at its peak value, values of the order of $10^3\,atm$.

The density of the plasma during a discharge varies insignificantly and stays around 10^{20} particles per cm^3. This is because the decrease of the plasma density due to the channel expansion is compensated by the arrival of new particles as a result of the evaporation of the water from the walls of the channel.

During the first stage of the discharge, the channel resistance drops due to the increase of the channel crosssection and to some increase of the specific conductivity of the plasma. Towards the end of the discharge, the resistance rises, in spite of the continuing expansion of the channel. This is connected to the cooling of the plasma and the ensuing deionization process.

The expansion of the channel continues also after the energy release has ended, at first under the effect of the pressure, which is higher than the hydrostatic value, and then due to the inertia of the moving liquid. In the after-discharge stage, the channel transforms into a gas bubble. The expansion of the bubble continues until the kinetic energy of the moving liquid is completely transformed into potential energy of the bubble, whose internal pressure is significantly lower than the hydrostatic pressure. Then, under the effect of the hydrostatic pressure, the liquid reverses its motion. The potential energy is transformed back into the kinetic energy of the liquid stream. With the collapse of the bubble, the pressure in it sharply increases. This pressure forces the liquid back, and the process repeats, thus generating a few damping pulsations. The pulsation period and the value of the maximum bubble radius are determined by the quantity of energy liberated in the channel.

The expansion of the channel in the discharge stage and the following bubble pulsation are accompanied by the emission of compression and rarefaction waves. The compression waves are emitted in the discharge stage and during the successive collapses of the bubble, when the high pressure in the channel and then the high pressure in the compressed bubble causes a compression of the adjacent liquid layers. The compression waves alternate with relatively long rarefaction waves, which are emitted in the stages when the pressure in the bubble is lower than the hydrostatic pressure. A typical profile of the compression

waves generated in a liquid during a spark discharge is shown in Figs. 1.1 and 1.2.

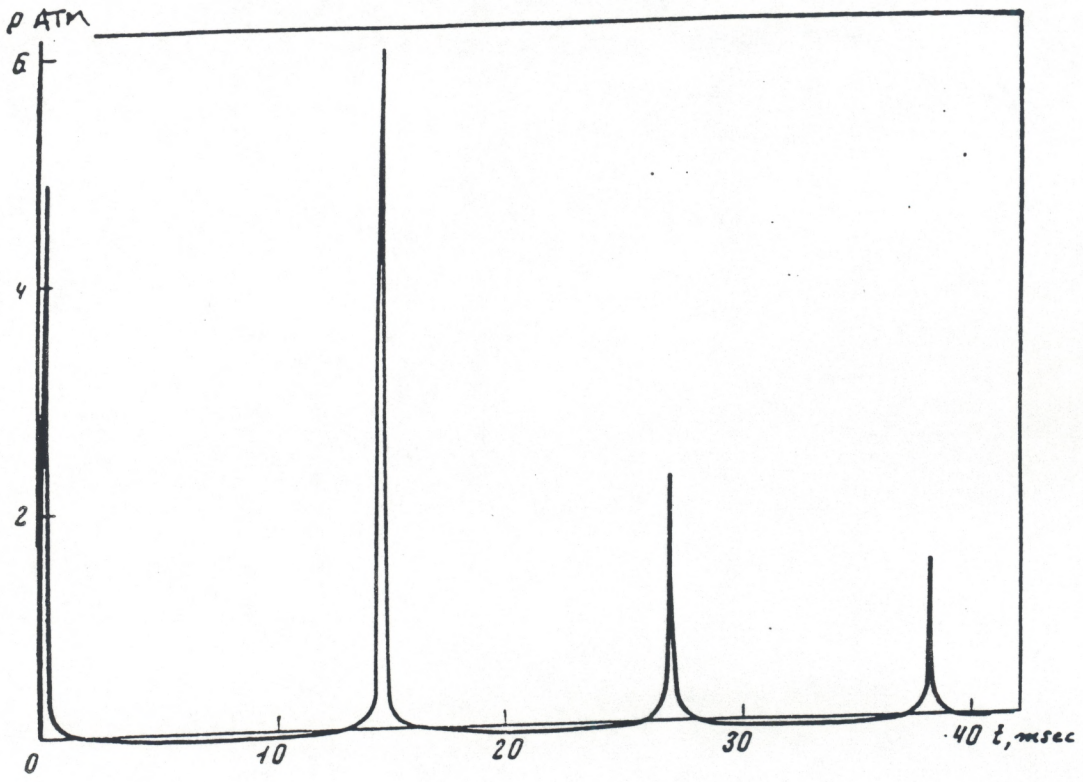

Fig. 1.1. Profile of a compression wave radiated in an electric discharge in a liquid.

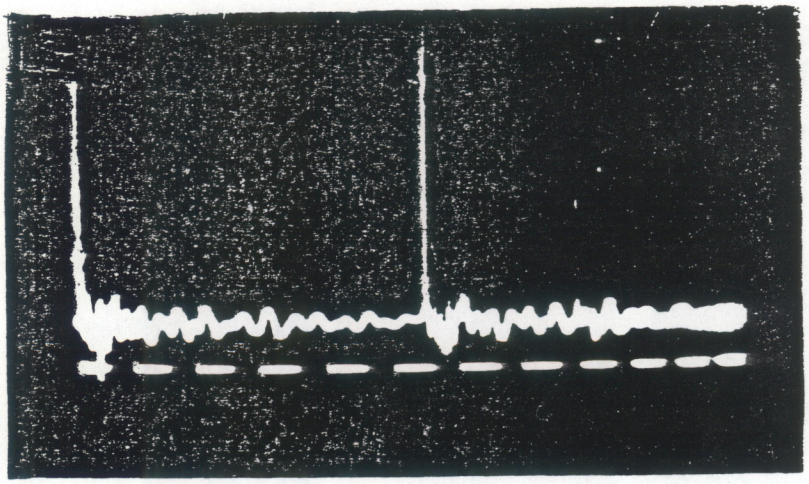

Fig. 1.2. Oscillogram of a compression wave at a distance of $1\,m$ from the discharge.

If the energy release is intense, the speed of the channel expansion can become comparable with and even exceed the speed of sound in the liquid. In such cases the compression wave propagating in the liquid becomes a shock wave in the immediate proximity of the channel; sometimes it has already been emitted as a shock wave.

The energy liberated in the discharge channel is used up mainly for the work done by the channel during the expansion (about 50%) and for the heating of the matter in the discharge channel.The work done by the channel divides into the energy of the compression waves, emitted in the stage of the discharge (up to 20%), and the energy of the bubble pulsations, which is equal to the potential energy of the bubble at the time of maximum volume (up to 30%). The pulsation energy is gradually released in the form of compression and rarefaction waves and other losses.

Fig. 1.1 shows the schematic profile of a pressure wave, and Fig. 1.2 shows the experimental profile taken at a distance of $1\,m$ from the discharge channel. The parameters are as follows: capacitance $0.9\,\mu F$, voltage $30\,kV$, length of the channel $6\,cm$, inductance of the discharge loop $3\,\mu H$, time interval $1\,msec$, amplitude of the compression pulse emitted by the discharge in the direction perpendicular to the channel $9\,atm$. In the channel of this particular discharge, which occurred in a near-critical regime, there was released about $350\,J$ of energy in a $10\,\mu sec$ time interval. The oscillogram shows the compression pulses and the pulses reflected from the container walls and from the free surface of the water.

REFERENCES to Chapter I

[1] Lazarenko B.R., Lazarenko N.I., *Electric Erosion of Metals*, Moscow, Gosenergoizdat (1944).

[2] *Physical Fundamentals of electro-spark treatment of materials*, (Collection of articles), Moscow, Nauka (1966).

[3] Early H.C., Martin E.A., "The underwater spark; a photographic light source of high intrinsic brilliance,", Trans. Amer. Inst. Elect. Engrs. I **74,** 788-790 (1956).

[4] Lane T., "Description of an Electrometer invented by Mr. lane; with an account of some experiments made by him with it: In a Letter to Bejamin Franklin," Philos. Trans., 451 460 (1867).

[5] Priestly J., " Experiments on the lateral Force of Electrical Explosions,' Philos. Trans., 57 -62 (1769).

[6] Pokrovskij G.I., Stanjukovich K.P., Izvestija Akademii Nauk, Serija Fizicheskaja, **8**, 214 (1944).

[7] Frungee F., "Zum mechanishen wirkungsgrad von flussigkeitsfunken," Optik, **3**, 124-127 (1948).

[8] Vogel C.B., "A seismic velocity logging method," Geophysics **17,** 586-597 (1952).

[9] Mazov M.V., Meyer G. Ja., *Trudy laboratorii aerometodov* (*Reports of the laboratory of aeromethods*)**4**, 119 (1955).

[10] Jutkin L.A., *Electro-hydraulic Effect*, Moscow, Mashgiz (1955).

[11] Bur. Ships J. **3**, 4 (1962).

[12] Reenan E.Y., Marine Sciences Instrument, **3** Proc 3 Nat. Marine Sci. Sympos. N.Y. Plenum Press (1956).

Chapter II

DISCHARGE INITIATION

2.1. Introduction

By initiation of a discharge is meant the process of creating a conducting channel in a fluid, which short-circuits an interelectrode gap. Various physical phenomena may be responsible for such process. The most important among them is fluid breakdown caused by voltage applied to the electrodes. At high enough intensity of an electric field, the fluid breakdown is similar to the breakdown of a gas and is characterized by the formation of leaders which develop from one electrode to the other. At small intensities of the electric field , in fluids with large enough conductivity,the formation of a gas cavity between the electrodes takes place first, along which then occurs the electric breakdown.

Besides the effects mentioned above, there are other methods one can use to initiate a discharge , for instance, the evaporation of metallic wires short-circuiting the electrodes. To initiate a discharge one can use the preliminary breakdown of the interelectrode gap caused by high voltage from an auxiliary source, as well as the breakdown of a gas bubble artificially created between the electrodes.

The variety of existing techniques for the initiation of discharges is a result of the need to generate discharges under different conditions, more specifically, under different initial working voltages in fluids with different conductivity and under different hydrostatic pressures, as well as the necessity of forming discharge channels with different parameters. The latter aspect is important for matching the channel resistance to the resistance of the supply circuit so as to minimize the losses in the transmission of energy from the capacitor into the channel.

Furthermore, in order for electric discharges to be used as sources of compression pulses, it is necessary that the time average of the channel resistance be close to the critical resistance of the discharge circuit. The fulfillment of this condition guarantees, as we will show later, the maximum efficiency of the discharge. Sometimes, for purposes of research, it is necessary to obtain a channel of a known shape, for instance, cylindrical; this can be easily achieved through initiation by evaporation of wires.

The usual requirements that an initiation method has to satisfy are: small duration of the initiation process with respect to the duration of the discharge itself, stability of the discharge, and small energy consumption.

In the following sections of this chapter we will examine a few methods for initiating discharges in water.

2.2. Discharge initiation by high voltage breakdown in low conductivity water

The conductivity of water has an essential effect on the processes of initiation of a discharge. In cases of practical importance, the conductivity can vary within a rather large range: from values of the order of $10^{-4}(ohm \cdot cm)^{-1}$ for tap water in the water-supply system, to values of the order of $10^{-2}(ohm \cdot cm)^{-1}$ for salt water. More widely used are discharges in water with low conductivity. In this case initiation of the discharge is usually achieved through breakdown of the interelectrode gap caused by high voltages applied to the electrodes. The voltages used can reach a value of 100 kV. The mechanism of the breakdown that takes place as a result of high voltages consists of the formation and evolution of leaders up to the point in time when one of them short-circuits the interelectrode gap.

The condition needed for the formation of leaders is that the intensity of the field near the surface of the electrode is higher than the discharge threshold by a few tens of kilovolts per cm. In order to obtain the highest possible intensities of the field, one uses electrodes of the point-plate or point-point type, which generate strongly nonhomogeneous fields. The intensity of the electric field near a point with a radius of curvature r much smaller than the length of the interelectrode gap l, can be determined with the approximate formula

$$E \approx \frac{2u}{rln\frac{4l}{r}} \tag{2.1}$$

for electrodes of the point-plate type, and with the formula

$$E \approx \frac{u}{rln\frac{2l}{r}} \tag{2.2}$$

or electrodes of the point-point type.

These formulae show that the intensity of the field near a point is determined mainly by the radius of curvature r and voltage u, and furthermore that such intensity is higher for the case of electrodes of the point-plate type.

Using the formula (2.1) we can find that the minimum field intensity at which leaders are still generated is approximately $36\,kV/cm$, which corresponds to the case in which the point is positive and the plate is negative [1]. This result was obtained in experiments using an edge in the shape of a rod insulated by a tube of vacuum-grade rubber $8\,mm$ in diameter, with an end shaped into a 30° cone. The radius of curvature of the point was 0.5–5 mm, and the area of contact with the water 0.8–4 cm^2. The voltages used lie in the range of 16–100 kV, the capacitance of the accumulator varied within the limits 0.01–10 μF. The reliability of the minimum value of the intensity corresponding to the leader formation threshold is unknown for other conditions. This is due not so much to the approximate nature of the formula used for the calculation, but rather to the distortions of the field near the electrode-point, which may be caused by various factors. An important role in the formation of a leader is played by the roughness of the electrode surface. A strong delay was observed in the formation of leaders after polishing the point [2]. It is possible that during the delay time the current warms up the water and as a result a gas film is formed

on the electrode, the breaking of which is the factor that initiates the formation of leaders.

The presence of roughness facilitates the formation of gas bubbles in various spots. A significant role in the formation of leaders is played by the insulation of the lateral surface of the point. The insulation is necessary to prevent contact of the high- voltage electrode with other parts of the device. Its presence causes deformations in the field induced by the charges that accumulate on the surface of the insulating dielectric. Thus, the formation of leaders takes place, as a rule, not on the point where the calculated intensity of the field is greatest, but rather on the boundary between the electrode and the insulating material. This effect can be easily seen in a photograph of the discharge between two electrodes shaped in the form of rods $10\,mm$ in diameter and with an interelectrode gap of $2.5\,cm$. The voltage on the electrodes before the breakdown was $50\,kV$ (Figs. 2.1 and 2.2). This effect leads to the destruction of the insulation and limits the operating life of the electrodes.

A visible effect on the formation of leaders is caused by the polarity of the electrodes. The pre-leader time, i.e., the the time needed for the formation of leaders, is somewhat less for the case of a negative point and a positive plate than for the case of a positive point, provided that the intensity of the field does not exceed $85\,kV/cm$. For strong fields, say $\sim 350\,kV/cm$, the situation is reversed. In this case the pre-leader time does not exceed $0.5\,\mu s$ for the positive point, and equals 1–$2\,\mu s$ for the negative one [1].

The evolution of the leaders in the gaps between a point and a plate occurs in drastically different ways depending on the polarity of the point [3]. In the case of a positive point, the electron avalanches, rushing toward a point from different ionization centers, "trace" the way for the growth of the leaders. In Figs. 2.3 and 2.4 are shown photographs of streamer patterns generated in interelectrode gaps, with separations of 17.5 and $16.5cm$ respectively, by a positive point and a grounded plate in tap water. The working voltage of the accumulator was $108\,kV$ and the capacitance $0.1\,\mu F$. The positive electrode was the end of an RK-3 cable, with the external insulation and braid removed. The diameter of the high voltage insulation was $9\,mm$ and the diameter of the inner wire $1.37\,mm$.

In the case of a negative point the electric field "pushes" electrons away from the point, evidently in a more uniform way. Around the point the formation of a space charge takes place. This decreases the intensity of the field in the negative electrode zone. This effect makes the formation of leaders more difficult. In such a situation, an important role is played by the positive surface charge on the insulation of the electrode.

The picture of the field is drastically changed by these charges. Strong field gradients are generated in a direction from the point to the insulation surface; and it is in this direction that the formation of the leaders takes place. In the photograph shown in Fig. 2.5, one can see a leader that spreads along the surface of the insulation of the negative point-electrode. This photograph was taken under conditions that differ from those of the photographs shown in Figs. 2.3

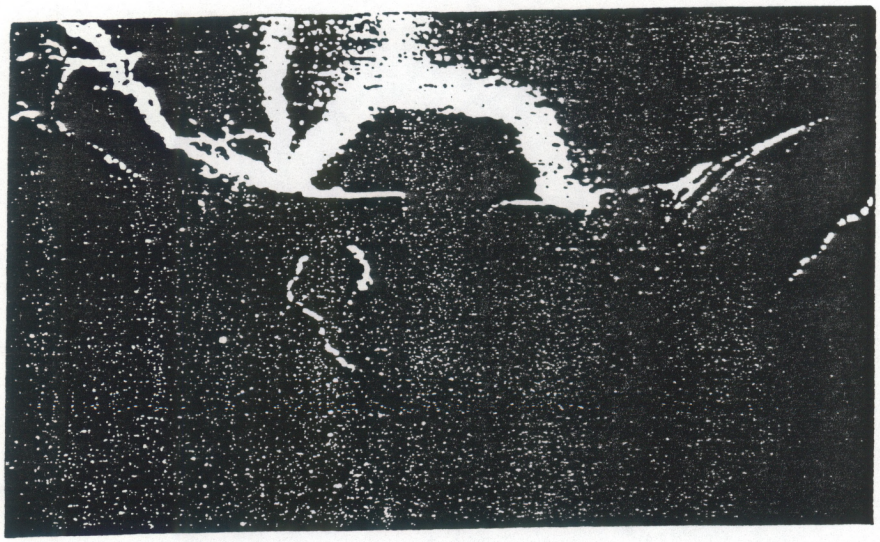

Fig. 2.1. Discharge channel.

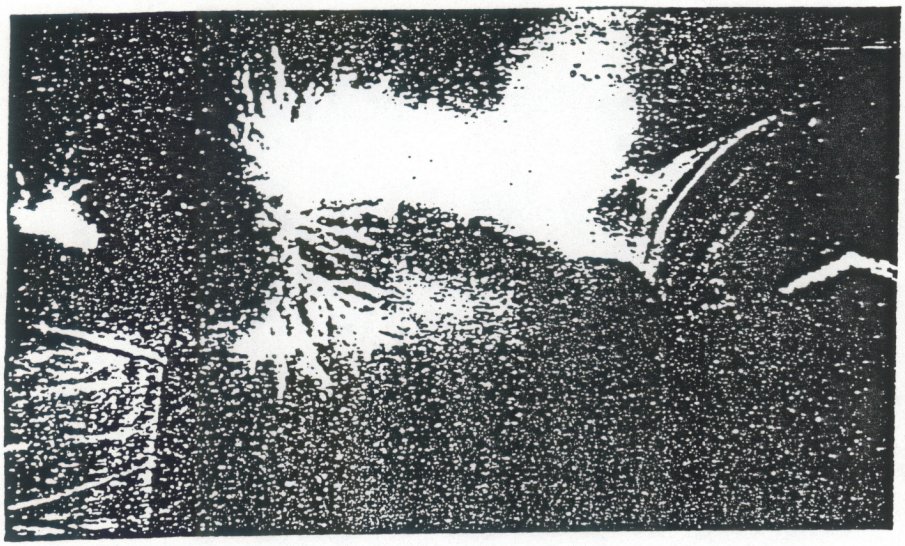

Fig. 2.2. Discharge channel.

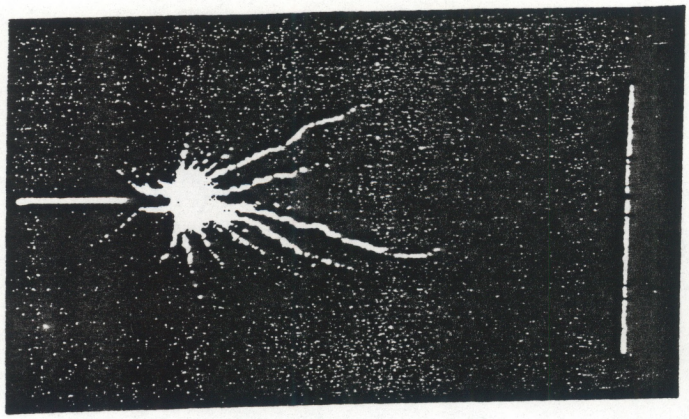

Fig. 2.3. Development of streamers in tap water. The positive electrode is a point, the negative a plate; $u_0 = 108\,kV$, interelectrode gap 17.5 *cm*.

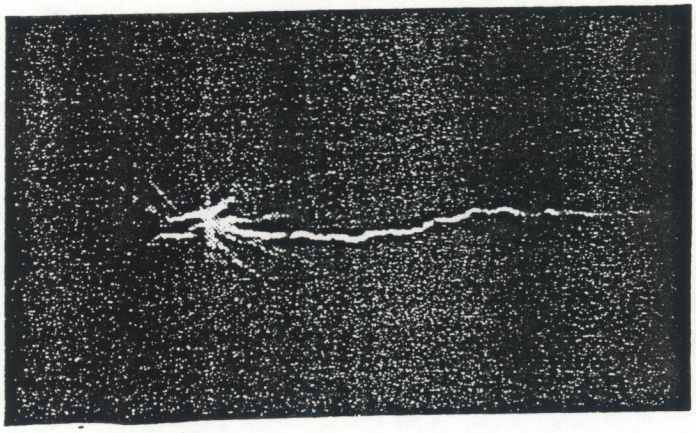

Fig. 2.4. Development of streamers in tap water. The positive electrod is a point, the negative a plate; $u_0 = 108\,kV$, interelectrode gap 16.5 *cm*.

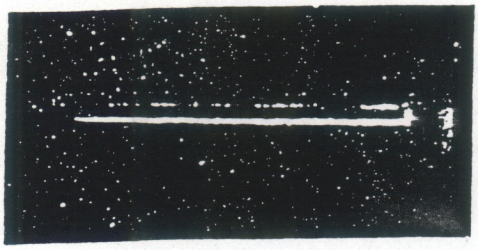

Fig. 2.5. Development of streamers in tap water. The negative electrod is a point, the positive a plate; u_0 = 108 kV, interelectrode gap 1.5cm.

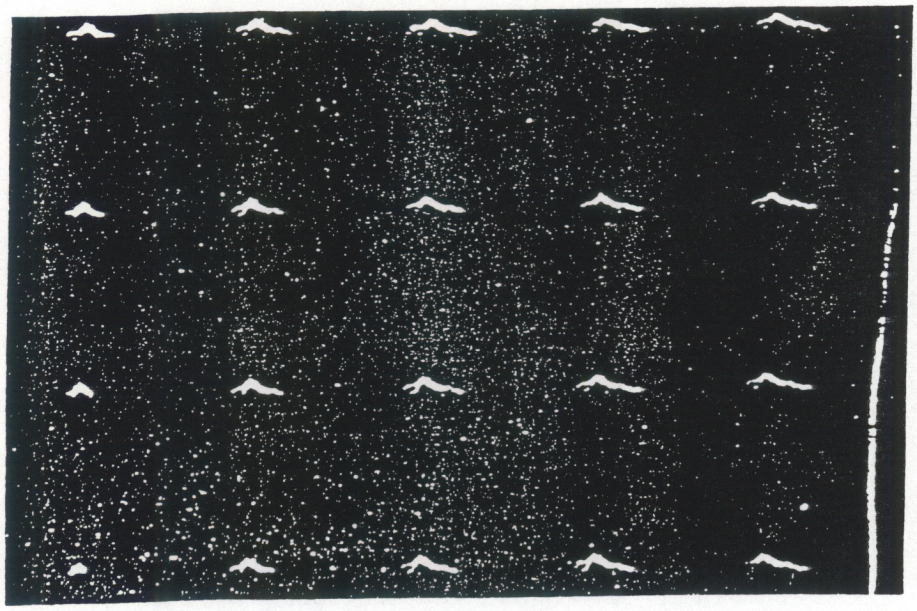

Fig. 2.6. Photograph of developing streamers.

and 2.4 only by the fact that the polarity of the electrodes was inverted and the interelectrode separation was decreased to $1.5\,cm$.

Thus, the most favorable conditions for the formation of leaders, which are indispensable for bridging the interelectrode gap, exist on a positive high- voltage point. The dynamics of the leader growth in the interelectrode gap formed by a positive point and a negative plate depend on the voltage, the capacitance of the accumulator, and on the area of the point electrode that comes into contact with water. Information about the leader formation is usually obtained by taking photographs of the leaders: (i) by the self-exposure method, examples of which are shown in Figs. 2.3 and 2.4; (ii) by high-speed film, an example of which is shown in Fig. 2.6; (iii) using an image-converter tube [4]; (iv) filming passing-through lighting with[5]. Still another way of gathering information about leaders is by recording the oscillographs of the discharge current and voltage in the interelectrode gap.

By analyzing the experimental data on the leader formation, we can observe the following fundamental regularities. The strength of the field near the point, which depends on the voltage and radius of curvature of the point surface in contact with the water, determines the number of leaders being formed. The higher the field strength, the larger is the number of .leaders. A qualitative interpretation of this dependence can be obtained from the photographs of impulsive coronas in Fig. 2.3, taken at $108\,kV$, and in Figs. 2.7 and 2.8, which were taken with the same electrodes but at $36\,kV$, capacitance of the condensar $0.33\,\mu F$ and gap separation respectively equal to 10 and $9\,cm$. From these pictures one sees that at $36\,kV$ the number of leaders is significantly less than at $108\,kV$. The explanation for this is that with the increase of the strength, the electron avalanches are formed on the nucleus having a higher ionization potential.

Once the leaders are formed, their growth is controlled by the field strength at the leader head. When the strength falls below some critical value, the formation of electron avalanches becomes impossible and the growth of the leaders stops. The field strength at the head of the leader decreases : because of the drop in voltage over the length of the leader, and because of the voltage drop on the electrodes caused by the discharge of the capacitor. Thus, the higher the voltage in the capacitor and the higher its capacitance, the greater the limiting length of the leaders. For example, for a $0.1\,\mu F$ capacitance and voltages 10, 30 and $100\,kV$, the limiting length of leaders that form on a positive electrode made of PK-3 cable is equal to 1, 4 and $15\,cm$ respectively. If we keep the voltage at $30\,kV$ and set the capacitance at $0.1, 0.2, 0.4, 0.9$ and $1.6\,\mu F$, the limiting length of the leaders equals, respectively, $4.0, 4.5, 5.0, 5.5$ and $6.0\,cm$. If the energy of the accumulator is held constant, the limiting length of the leaders goes through a maximum as the voltage is increased. In this case, the effect of the increasing voltage is at first compensated for, and then eliminated by the shortening of the duration of the discharge of the capacitor brought about by the decreased capacitance, and also by a drop in the resistance of the interelectrode gap, the latter due to the increased branching of the corona.

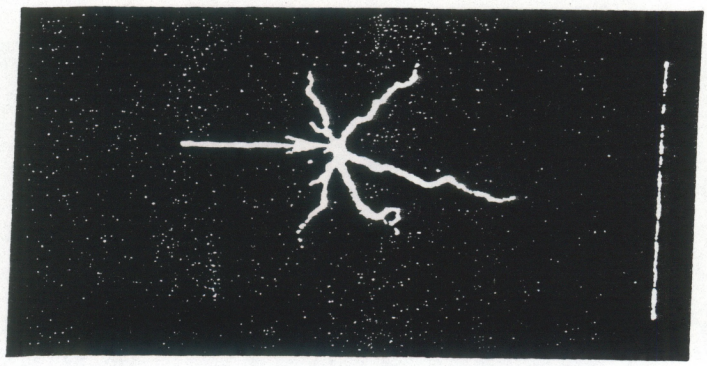

Fig. 2.7. Branching corona. Positive electrode is a point.

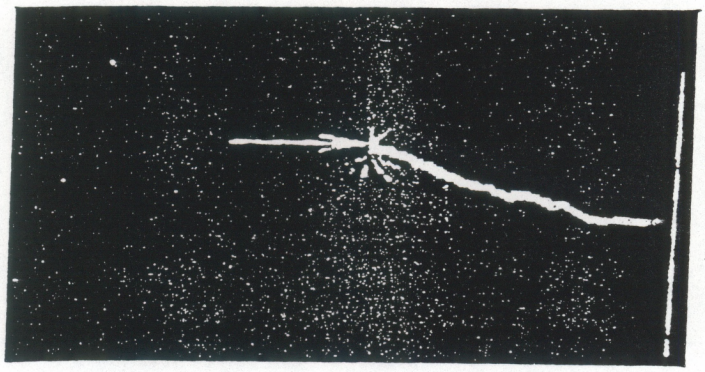

Fig. 2.8. Branching corona. Positive electrode is a point.

In ref. [1] empirical formulae were derived to describe the growth of positive leaders. These formulae are valid for the following regimes: voltage range $u = 15\text{–}100\,kV$, capacitance range $C = 0.1\text{–}10.0\,\mu F$, point area $S = 0.8\text{–}4.0\,cm^2$. The point electrode is a rod with diameter $8\,mm$, with an end machined into a 30° cone, and a radius of curvature of the cone top $r = 0.5\text{–}4.0\,mm$. The conductivity of the water is $\sigma \sim 10^{-4}(ohm \cdot cm)^{-1}$, with a plate as the negative electrode.

Under the above conditions, the limiting length of the leaders, and consequently, the maximum breakdown length of the interelectrode gap, is given by the expression

$$l_{max} = \sqrt{\frac{2.5Cu_0^2\left(\frac{u^2}{u_0^2} - 4\frac{u}{u_0} + \ln 12\frac{u^2}{u_0^2}\right)}{4\sqrt{\pi S}\sigma a} + 1.25^2} - 1.25[cm]\,. \qquad (2.3)$$

Here $u_0 = 18 \cdot 10^3 ln\frac{4l}{r}$ is the voltage corresponding to the minimum field strength at which the formation of leaders still takes place ($36\,kV/cm$); a is a constant equal to $3600\,sec \cdot V^2/cm$; and l is the interelectrode separation.

The interelectrode separation requiring no more than 10% of the accumulator energy for the breakdown is given by

$$l_{\Delta W=10\%} = \sqrt{\frac{0.035C(u-u_0)^2}{\sqrt{S}a\sigma} + 1.25^2} - 1.25[cm]\,. \qquad (2.4)$$

These formulae will give incorrect results, in particular, if the point area is smaller that the lower boundary for the range of S given above. This is the case, for example, for the electrode made of RK-3 cable, for which the area is only a few square millimeters.

Let us consider the time evolution of the leaders. As the high-speed film shows [2], the "growth" of a leader is an intermittent process. The pauses are evidently caused by two factors: the encounters of the leader head with gas bubbles (cavitation nucleus) which lead to an increase of the radius of curvature of the leader head, thus decreasing the field strength near it; and delays in the formation of avalanches due to the temporary absence in the water surrounding the leader head of ionization centers with a sufficiently low ionization potential. The number of pauses and their durations depend on the voltage; these quantities decrease as the voltage increases. As a result, the mean growth rate of a leader, defined as the ratio of the gap separation to the delay in the breakdown, depends on the voltage. The mean growth rate so defined depends also on the delay in the formation of the leader on the electrode; the latter, in turn, depends not only on the voltage, but also on the shape and construction of the electrode

We will now give experimental data relative to the dependency of the mean growth rate of the leaders on the voltage for two different types of positive point-electrodes. The first was made of a rod $8\,mm$ in diameter, insulated by a

vacuum tube. One end of the rod was machined into a 30° cone with a radius of curvature of 0.5–4.0 mm. The mean rate was found to be $2 \cdot 10^4 cm/sec$ at $20kV$ and $5 \cdot 10^6 cm/sec$ at $100\,kV$ [1].

The second electrode was the end of an RK-3 cable. In Table 2.1 we give the values for the separation gap l, the breakdown delay τ, and the mean rate of growth of the leaders l/τ at different working voltages. The value of the energy of the capacitor during the experiment was held constant at $45\,J$ [6].

Table 2.1

u [kV]	l[cm]	τ	l/τ
52	5	2.5	$2 \cdot 10^6$
30	5	4	$1.3 \cdot 10^6$
21.2	2.5	15	$1.7 \cdot 10^5$
15	1.2	22	$5.5 \cdot 10^4$

The data of Table 2.1 show that in the case of the point-electrode made out of an RK-3 cable, which has a significantly smaller area of contact with the water than the electrode in the first case (which was made of a rod), the mean rate of growth of the leaders at equal voltages is somewhat higher. This effect is evidently related to the significantly shorter delay in the formation of the leaders on an electrode with a smaller radius of curvature.

If the interelectrode gap is greater than the limiting length of the leaders, the lifetime of the leaders is not confined to the time period of growth. The leaders continue to exist even after attaining the limiting length; furthermore, the total lifetime sometimes exceeds by two orders of magnitude the time period of growth. To illustrate this, in Figs. 2.9 and 2.10 are shown the oscillograms of the discharge current and voltage on the electrodes, taken for discharges of capacitors with capacitance 0.4 and $0.9\,\mu F$ at $30\,kV$ for the case when the growth of the leaders does not end with the breakdown of the interelectrode gap (Fig. 2.9, electrode separation $6\,cm$), and for the breakdown case (Fig. 2.10, separation $5\,cm$) [3].

In Figs. 2.9 and 2.11 is also plotted the time dependence of the resistance of the interelectrode gap calculated on the basis of the above oscillograms.

The evolution of the leaders at strengths of the electric field at a point-electrode greater than a few hundreds kilovolts per centimeter does not depend, in practice, on the hydrostatic pressure up to the maximum pressure realized in the experiments, which was $1000\,atm$. This points, apparently, to the fact that the matter density in the channels of the leaders during of their growth period is very high. The expansion of the leader channels , which can be seen in pictures taken with a certain delay with respect to the discharge, show that the matter in the leader channels is heated and is under increased pressure. However, the electroacoustic efficiency of the discharges in which the formation of the channel does not take place is small: the ratio of the energy of the compression wave to the energy stored in the capacitor does not exceed a few tenths of a percent [3].

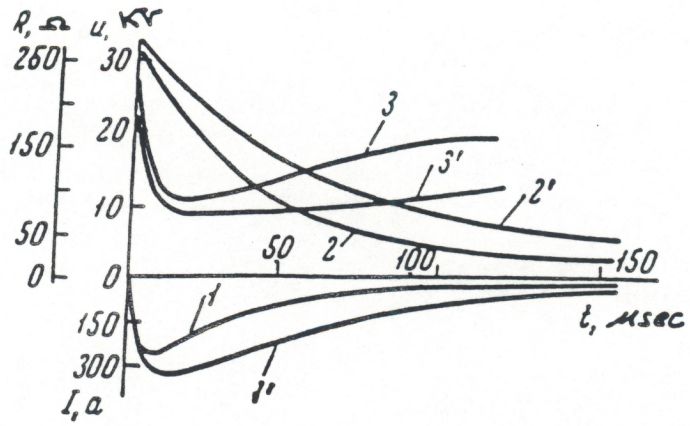

Fig. 2.9. Electric characteristics of a discharge in the absense of breakdown. Gap separation is 6 cm, voltage 30 kV. Lines 1.2 and 3 correspond to current, voltage and resistance for the discharge of a 0.4 μF capacitor; Lines 1', 2' and 3' same quantities, but pertaining to the discharge of a 0.6 μF capacitor.

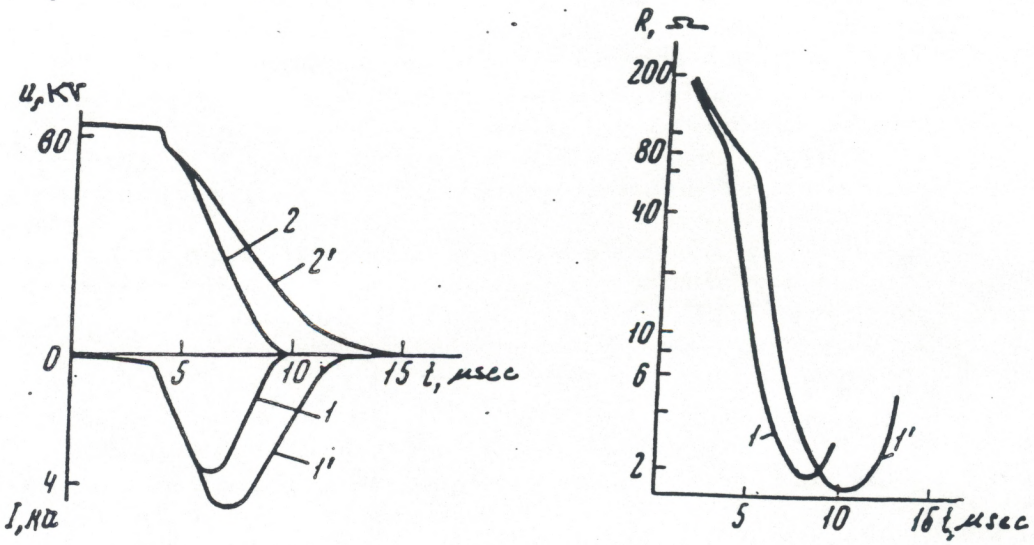

Fig. 2.10. Electric characteristics of a discharge at breakdown. Gap separation 5 cm, voltage 30 kV. Lines 1, 2 and 1', 2' correspond to current and voltage a for the discharge of a 0.4 μF and 0.9 μF capacitor, respectively.

Fig. 2.11. Time dependence of the resistance in a breakdown; interelectrode gap 5 cm, voltage 30 kV. Lines 1 and 1' correspond to discharges of a 0.4 and 0.9 μF capacitor respectively.

This is related to the fact that, as a consequence of a large ballast resistance of the water, the energy released in the leader channels is not large.

In conclusion, let us note that the initiation of discharges in water with low conductivity through the breakdown induced by high voltages (i) takes place in very short intervals of time, usually of the order of a few microseconds; (ii) requires modest energy consumptions, approximately a few Joules; and (iii) is a highly stable process provided that (a) the positive electrode has a sufficiently small open area (of the order of $10\,mm^2$), (b) the applied voltage is of the order of a few tens of kilovolts, and, finally (c) the interelectrode gap does not exceed two- thirds of the limiting length of the leaders for a given voltage.

2.3. Discharge initiation by high-voltage breakdown in high conductivity water

As the conductivity of the water increases from values of the order of $10^{-4}(ohm \cdot cm)^{-1}$, which correspond to tap water, up to values of the order of $10^{-2}(ohm \cdot cm)^{-1}$, which is in the conductivity range of sea (salt) water, the structure of the branching corona changes drastically. The changes mainly reduce to the following [3]. The leaders, which form on the positive point, begin to branch out very strongly, and their limiting length for a given capacitance decreases significantly. The corona at the negative point becomes a dense "brush" of short rectilinear leaders. In Figs. 2.12 and 2.13 are shown the photographs of a corona near the positive and negative electrodes. (The electrodes were constructed out of the end of an RK-2 cable with the insulation and braid removed.) The diameter of the high voltage insulation was $7\,mm$, and the diameter of the inner wire was $0.6\,mm$. The capacitance of the capacitor (energy storage) was $0.9\,\mu F$, the initial voltage was $30\,kV$. The water contained approximately 5% in weight of $NaCl$ and the conductivity was $0.069\,(ohm \cdot cm)^{-1}$. From these photographs we can determine that the limiting length of the leaders at the positive point is about $1\,cm$, while for tap water with conductivity of about $2.8 \cdot 10^{-4}(ohm \cdot cm)^{-1}$, all the other parameters being unchanged, the limiting length of the leaders could be $6\,cm$.

The increased branching of the corona together with the higher conductivity of the water reduces the duration of discharge not terminating in a complete breakdown. Figures 2.14 and 2.15 show the oscillograms of discharge current and voltage on positive and negative point electrodes, respectively, relative to a grounded electrode shaped as a spherical brass grid with $5 \times 5\,mm^2$ cells encompassing the point-electrode. The radius of the sphere is several centimeters. In practice, the value of the radius has no effect on the characteristics of the discharge. Lines 1 and $1'$ correspond to the discharge of a $0.9\,\mu F$ capacitor at 30 and $10\,kV$; lines 2 and $2'$ to the discharge of a $0.1\,\mu F$ capacitor at 30 and $10\,kV$, and the inductance of the discharge loop amounts to a few μH. Figure 2.16 shows the dependence of the interelectrode resistance at the instant when the current reaches its maximum for various values of the capacitance and initial voltage.

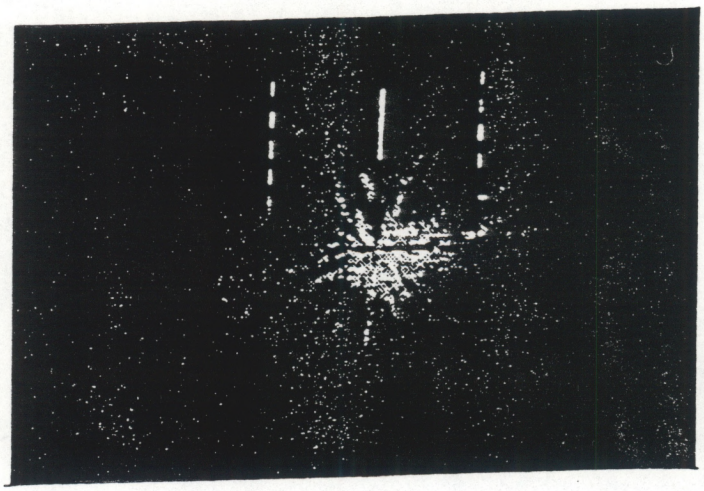

Fig. 2.12. Corona on a positive point in salt water.

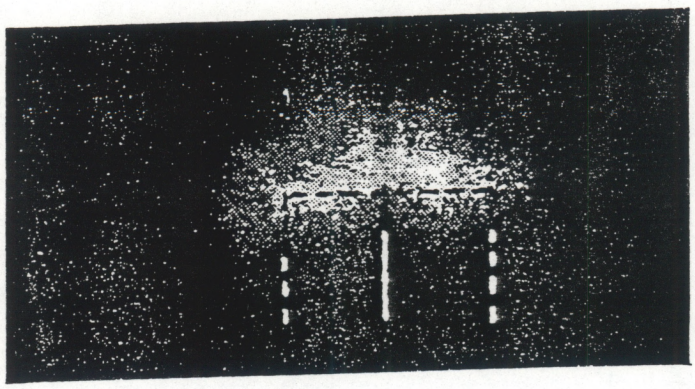

Fig. 2.13. Corona on a negative point in salt water.

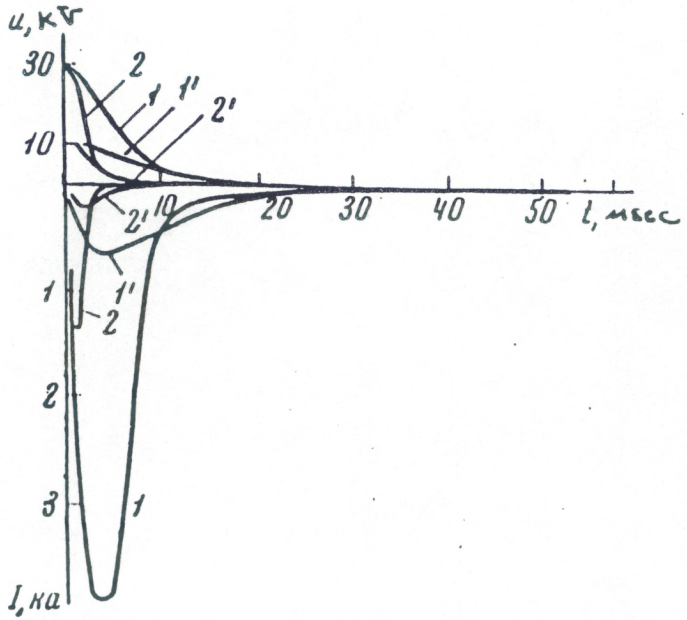

2.14

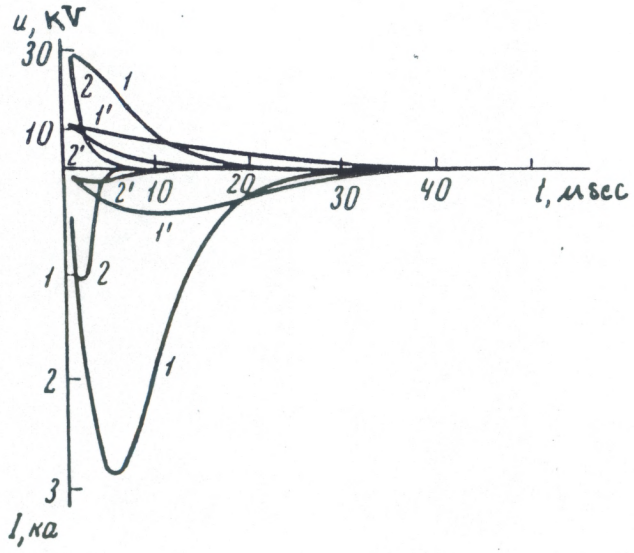

2.15

Fig. 2.14. Oscillograms of discharge current (1 ,2) and voltage(1', 2') for a corona discharge on a positive point. Lines 1 and 1' correspond to 0.9 μF, 30 kV and 10 kV ; Lines 2 and 2' correspond to 0.1 μF, 30 kV and 10 kV;

Fig. 2.15. Oscillograms of discharge current (1.2) and voltage(1', 2') for a corona discharge on a negative point.

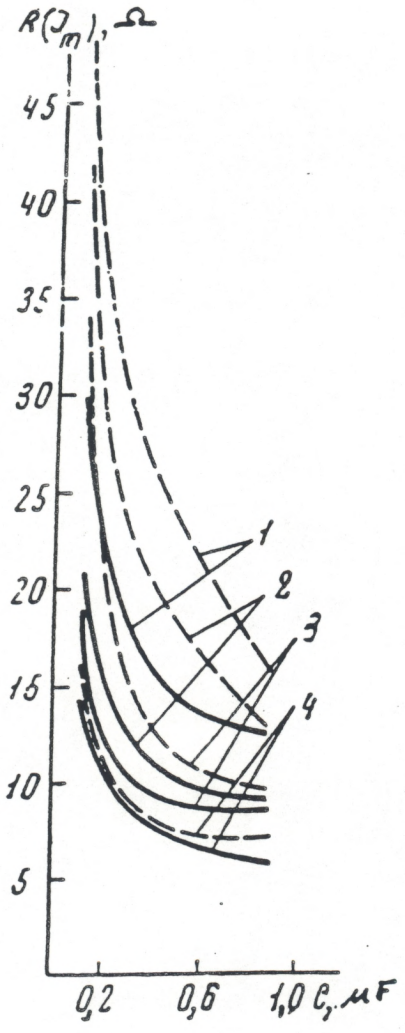

Fig. 2.16. Plot of the interelectrode resistance at peak current as a function of the capacitor capacitance for various voltages. Lines 1.2.3 and 4 correspond to 10, 15, 21 and 23 *kV*. The solid lines correspond to a corona on the positive, the dashed lines to a corona on the negative point.

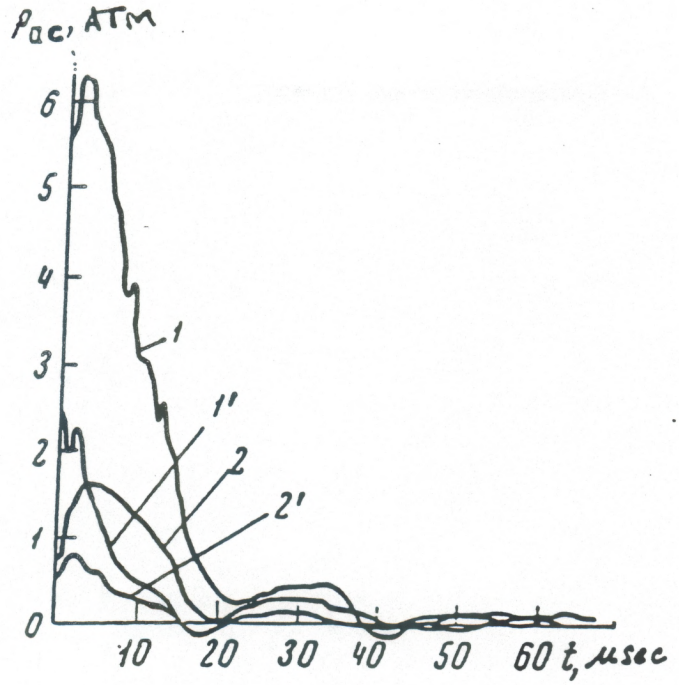

Fig. 2.17. Oscillograms of the pressure pulses radiated by a corona on a positive point.

Fig. 2.18. Oscillograms of the pressure pulses radiated by a corona on a negative point.

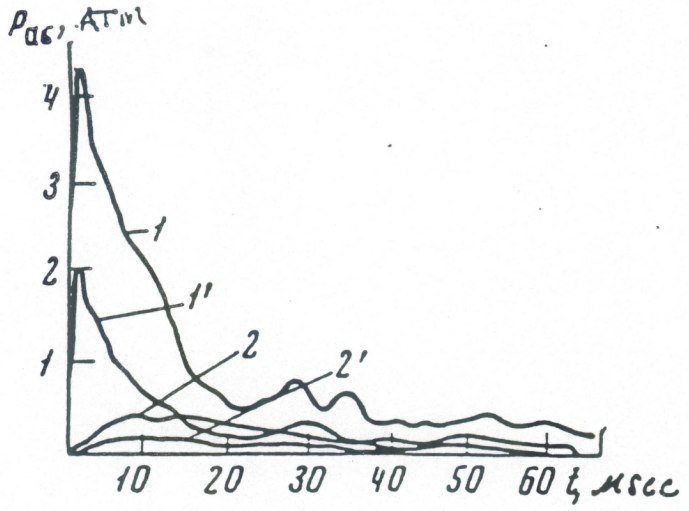

The observed changes in the structure of the corona are, apparently, related to the fact that as the concentration of the electrolyte in the water increases, so does the number of nucleusof electron avalanches with small ionization potential. This causes an increased branching of the corona on the positive point and a rise in the numbers of leaders on the negative electrode. On the other hand, the discharge of the capacitor takes place at a faster pace when the corona surface and water conductivity are increased. This causes a more rapid decrease of the field strength at the leader heads down to the threshold value, and the evolution of the leaders stops sooner than in the case of low conductivity tap water. Therefore, the breakdown interelectrode gap becomes smaller with the increase of the conductivity , and the energy used up in the pre-breakdown stage increases. While in the case of a high- voltage breakdown in low conductivity water the amount of the capacitor energy released into the leader channels is negligible, as the conductivity rises such an amount increases significantly. This can be seen from the energy characteristics of the hydroacoustic effects that accompany the discharges not ending in breakdowns in water with high conductivity. In Figs. 2.17 and 2.18 are shown the oscillograms of pressure pulses taken by a wide-band hydrophone at a distance of $50\,cm$ from the impulsive corona on the positive and negative points, respectively. The construction of the electrodes is the same as in the case of Figs. 2.14 and 2.15. Lines 1 and $1'$ correspond to discharges of a $0.9\,\mu F$ capacitor at 30 and $10\,kV$; lines 2 and $2'$ refer to discharges of a $0.1\,\mu F$ capacitor at 30 and $10\,kV$. The acoustic field generated by the discharges is spherically symmetric. The duration of the compression pulses is close to the duration of the discharge current. The compression pulses radiated by the corona are very reproducible from discharge to discharge. In Table 2.2 we give the experimental values for η_{exp}, defined as the ratio of the energy of the compression pulses to the energy of the capacitor, for various values of the capacitor energy E and initial voltages u on the positive $(+)$ and negative $(-)$ points. There are also shown the durations τ of the discharges, determined from the oscillograms. The energy of the compression pulses is calculated using the formula

$$W_{ac} = \frac{4\pi r^2}{\rho c} \int_0^{\tau} p^2 dt \,, \tag{2.5}$$

where r is the distance from the corona to the hydrophone, ρc is the wave resistance of the water, p is the pressure in the compression wave at the distance r at the time t.

Another hydroacoustic characteristic of the discharge is the energy of the pulsating bubble. In Table 2.2 are reported the pulsation periods τ_p and the percent ratio η_p of the energy of the pulsating bubble to the energy of the capacitor. The energy of the bubble is calculated by the formula [7]

$$W_b = \frac{\tau_p^3 p_0^{5/3}}{1.135\rho^{3/2}} \,, \tag{2.6}$$

where p_0 is the hydrostatic pressure and ρ is the water density.

Table 2.2

u [kV]	Polarity	E [J]	τ [μsec]	η_p [%]	τ_p [μsec]	η_{exp} [%]
Case of $0.1\,\mu F$						
10	+	5	5	3.2	1.28	0.8
	−		12.5	4.4	1.43	0.4
15	+	11.3	4.5	2.4	1.53	1
	−		8.6	4.3	1.85	0.6
21.2	+	22.5	4.1	2.4	1.91	1
	−		6.5	5.4	2.53	0.8
30	+	45	3.7	2.3	2.41	1
	−		4.7	6.2	3.33	1.3
Case of $0.2\,\mu F$						
10	+	10	7	3.8	1.71	0.8
	−		15	5.2	1.9	0.4
15	+	22.5	6.2	3.2	2.11	1
	−		11	5	2.45	0.7
21.2	+	45	5.2	2.5	2.46	0.9
	−		8.8	6	3.3	0.7
30	+	90	4.5	2.6	3.15	0.9
	−		6	7.2	4.4	1
Case of $0.4\,\mu F$						
10	+	20	11	4.5	2.28	1.1
	−		20	5.8	2.48	0.3
15	+	45	9	3.4	2.73	1.2
	−		16.5	5.9	3.27	0.4
21.2	+	90	7	3.1	3.33	1.4
	−		13	6.7	4.3	0.7
30	+	180	6	3.1	4.21	1.3
	−		92	6.3	5.33	1
Case of $0.9\,\mu F$						
10	+	45	20	5	3.1	0.9
	−		32	7.2	3.5	0.3
15	+	101	15	3.8	3.7	1
	−		27	6.8	4.5	0.5
21.2	+	202	12.5	3.5	4.55	1.1
	−		24	7	5.7	0.7
30	+	405	10.5	3.1	5.5	1
	−		18	6.4	7.2	1

From the data in the table we may conclude that the work done by a discharge not ending in a breakdown in the case of a high conductivity water can reach 7–8% of the energy of the capacitor. These kinds of discharges are used to generate pressure pulses for hydrogeological research [8].

The results reported above pertain to cases of relatively small concentrations of electrolytes. In the work of refs. [5, 9, 10–12]. there were performed investigations of breakdowns of electrolytes with conductivity and solution concentration varying in a wide range of values. The authors of the work [5, 9–11] came to to conclusion that the "high- voltage behavior" of the electrolytes is independent of the solution and is determined only by the low-voltage conductivity. In Figs 2.19 and 2.20 the breakdown distance is plotted against the conductivity of the electrolyte for positive and negative points (points made using RK-3 cable, capacitance 0.2 and $0.4\,\mu F$ and voltage $10, 14$ and $6\,kV$). While in the small concentration region there is a clear correlation between breakdown voltage and interelectrode separation, in the regions of average and high concentrations the capacitor discharges before the breakdown occurs even at strongly decreased electrode separation.

In the work [12] the investigation of the breakdown of electrolytes was extended to the region of very high concentrations of electrolytes at which the drop of conductivity occurs. For such regions it was found that the same values of conductivity as in the case of small concentrations correspond to a longer breakdown delay.

In conclusion let us note that as far as the discharge initiation is concerned the more important effects, entailed by the increase in the fluid conductivity, are the decrease of the length of the leaders and the increase of pre-breakdown currents. As a result, even at small interelectrode distances it is necessary to take into account the energy losses in the pre-breakdown stage, particularly in the case of small energies of the capacitor. The use of small interelectrode gaps requires a lowering of the active resistance and inductance of the feeding loop in order to achieve a sufficiently complete release of energy in the discharge channel with small resistance in a near-critical regime.

2.4. Discharge initiation by low- voltage breakdown of fluids

In the previous sections we considered the initiation of discharges induced by high- voltage breakdown of fluids, in which the main role is played by the formation and growth of the leaders. As the voltage is decreased the field strength on the electrodes can become insufficient for the formation of leaders. For tap water with conductivity of the order of $10^{-4}(ohm \cdot cm^{-1})$ the critical field strength is about $36\,kV/cm$, according to the data of ref. [1]. At lower field strengths the breakdown of the interelectrode gap occurs via a gas bridge formed as the result of the heating and evaporation of the water by the conduction current. Electrolysis also gives some contribution to the formation of gas bubbles on the electrodes.

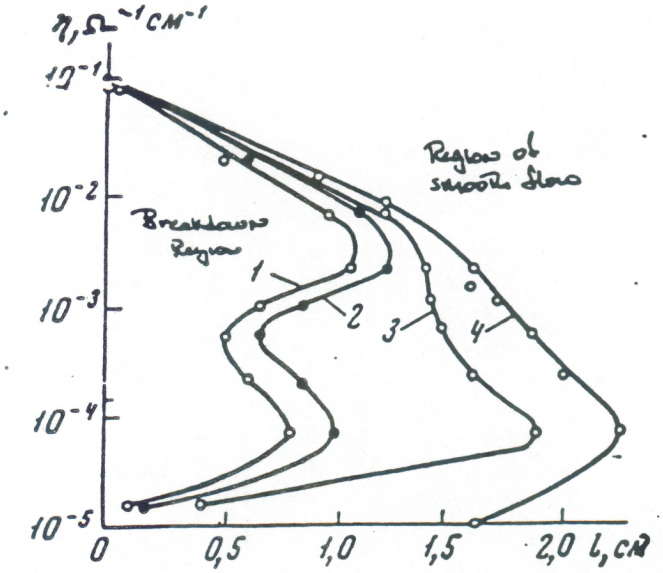

Fig. 2.19. Plot of the breakdown separation as a function of the specific electric conductivity of the solution (positive point). (1) 10 kV, 0.2 μF; (2) 10 kV, 0.4 μF; (3) 14 kV, 0.2 μF; (4) 14 kV, 0.1 μF.

Fig. 2.20. Plot of the breakdown separation as a function of the specific electric conductivity of the solution (negative point). Same notation as in Fig. 2.19.

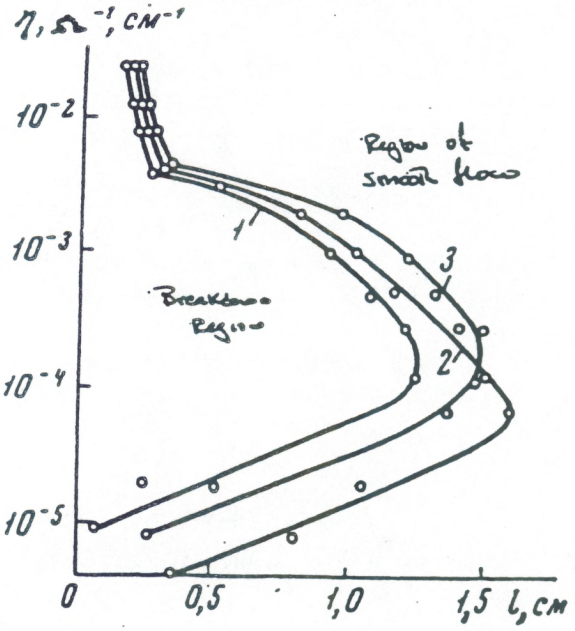

The formation of the gas bridge is an energy consuming process that takes a rather long time compared to the time of growth of the leaders in a high-voltage breakdown. In the case of tap water these time periods are measured in hundreds and thousands of microseconds depending on the construction of the electrodes, voltage and interelectrode gap. The time needed for the formation of the gas bridge decreases as the water conductivity increases.

Since the breakdown of the interelectrode gap requires that the gas bridge reaches a certain volume, the result is that the energy consumption and the duration of the breakdown stage depend on the hydrostatic pressure. These circumstances make the use of low-voltage breakdown for the initiation of the discharge very inefficient. There is, however, a solution to this problem. The solution lies in the use of electrodes with a special geometry, such that the channel that is formed after the breakdown of a relatively small interelectrode gap can become longer during the discharge. In particular, this requirement is satisfied by the discharger shown schematically drawn in Fig. 2.21. Such a device consists of coaxial electrodes, mounted one inside the other and electrically separated by the insulating sleeve. The breakdown can occur only between the edges of the ends of the two electrodes. The interelectrode gap, equal to the thickness of the two insulations, can be of the order of $1\,mm$, provided that the working voltage on the capacitor is of the order of $1\,kV$. The breakdown delay in this case amounts to a few tens of microseconds. The delay decreases with the rise of the water conductivity and depends weakly on the hydrostatic pressure, provided that the latter does not exceed 10–20 atm.

After the breakdown of the interelectrode gap has occurred, the formation of a hemispherical little bubble, filled with plasma, takes place. The electric current in it is pushed toward the surface of the bubble by its own magnetic field. As a result, the channel takes the form of an arc and the effective length of the channels increases during the discharge as the bubble in the fluid expands.

As a result of the lengthening of the channel during the discharge, its electric resistance becomes sufficiently large so as to make it technically simple to transfer the energy of the capacitor into the channel without substantial losses and, at the same time, sufficiently quickly.

As an example, in Fig. 2.22 are shown the oscillograms of the discharge current and voltage on the electrodes pertaining to the method of discharge initiation described above. The parameters are: capacitance $320\,\mu F$, initial voltage $1.6\,kV$, inductance of the discharge loop $0.1\,\mu H$, interelectrode gap $0.1\,cm$. The discharge was produced in water with 1.5% (in weight) of common (table) salt added. The breakdown delay is, as one can see from the voltage oscillogram, about $30\,\mu sec$. The energy released into the channel constitutes about 85% of the energy stored in the capacitor.

2.5. Discharge initiation by auxillary means

An effective initiation of the discharge in low-conductivity water offers no difficulties only if high voltages are used. But

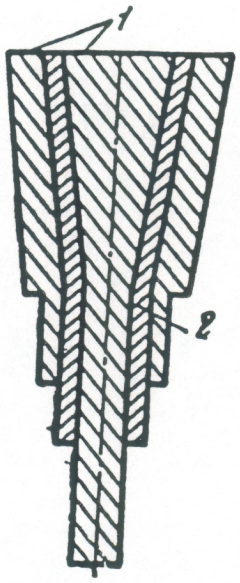

Fig. 2.21. Sketch of a discharger: (1) electrodes; (2) insulating sleeve.

Fig. 2.22. Oscillograms of the current and voltage for the discharge of a capacitor.

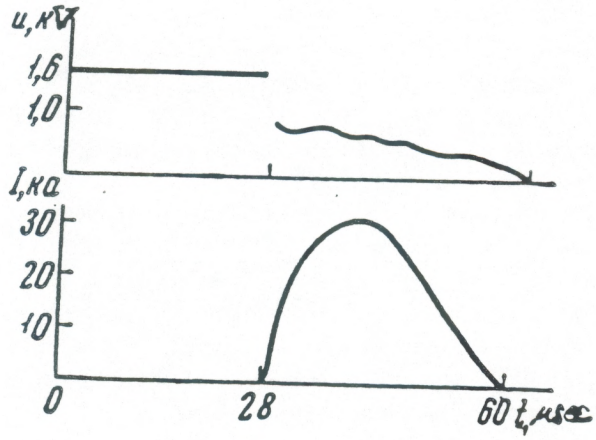

the use of high voltages does present some difficulties. The most crucial one is the necessity of providing a reliable insulation for the high-voltage circuits, which, in turn, leads inevitably to an increase in the size of the devices. The use of low-voltage discharges with the same energies allows one to build devices significantly more compact, and this is, in many cases, a decisive factor. For this reason the search for an effective method of initiation of low-voltage discharges is an important problem now.

In this section we will examine three methods of initiation of low-voltage discharges by auxiliary means: (i) initiation with wire bridges; this method is practically independent of the conductivity of the fluid; (ii) initiation of the discharge via a preliminary high-voltage breakdown; this method is suitable only for low-conductivity fluids; and (iii) initiation via breakdown by the working voltage in the gas bubble, generated beforehand in the interelectrode gap by an auxiliary corona discharge. The latter method is suitable for the initiation of discharges in fluids with sufficiently high conductivity.

The initiation of the discharge by means of wire bridges is based on the electric explosion of the wires. This physical effect has for many years attracted the attention of many researchers [13,14]. Intensive investigations were carried out mainly on the electric explosion of wires in a gas medium. The main features of such an explosion can be characterized as follows. The process taking place after the circuit is closed can be divided into three stages. During the first stage, as a result of the discharge current flow four different situations can occur.

1. Melting: the energy is insufficient for the evaporation of the wire.

2. Slow explosion: the time of evaporation of the wire is much larger than the time needed for the development of instabilities in the melted wire.

3. Fast explosion: the time of evaporation is small compared to the time for the development of instabilities.

4. Explosive ablation: the time of evaporation is small compared to the time needed for the temperature, corresponding to the boiling point, to reach a depth equal to $1/e$ of the radius of the wire. The evolution of the explosion in this situation is determined by evaporation from the surface of the wire.

The first stage ends with the transition of the wire into a non-conducting state. After this, the second stage begins: the "pause" of the current. The suspension of the current flow lasts until the density of the gas in the expanding channel does not fall to the point at which the breakdown of the gas under the effect of the voltage still remaining on the capacitor becomes possible. Then the last, third stage begins: the discharge in the gas channel.

There can be conditions under which either the second or the third stage, or both of them either are totally absent or are weakly developed. For example, if the energy of the capacitor is sufficient only for the evaporation of the wire, then the current disappears at the end of the first stage and never starts again. In the case of tungsten wires the second state, the "pause" of the current, is only weakly developed. In fact, the current decreases only so slightly after the explosion of the wire and then increases leading into the third stage of the process.

The explosion of wires in water is qualitatively similar to the explosion of wires in the air. The only differences that can be observed are in the quantitative characteristics of the various stages. At the explosion of wires in water all the stages, in particular the stage of the "pause" of current, are substantially protracted in time. This effect is due to the large inertia of the water, which makes it difficult for a wire to expand during the first stage, and makes even more difficult the expansion of the gas channel in the second and third stages.

Figure 2.23 shows the oscillograms of the current and the voltage on the electrodes during a discharge initiated by a copper wire with diameter $0.05\,mm$ and length $4\,cm$ in water (a) and air (b) (capacitance $2\,\mu F$, voltage $6.7\,kV$). From the plot one sees that the "pause" between the current pulse that vaporizes the wire (1) and the pulse generated by the vapor breakdown (2) is substantially greater for discharge in water than for discharge in the air. The duration of the "pause" increases with the diameter and length of the wire, and depends also on the material of the wire. For tungsten wires the "pause" is either absent or weakly developed. Therefore, thin tungsten wires are more suitable for the initiation of discharges in water. With tungsten wires it is possible, using working voltages of a few kV, to initiate discharges with large channel lengths and small delays, i.e. small time intervals between the instant when the voltage is applied and the discharge itself.

One interesting possibility is the initiation of discharges using wires made of materials, whose reaction with the oxygen released as a result of the water dissociation has a large thermal effect. Examples of such materials are aluminum, zirconium and beryllium. The thermal effect of exothermic reactions is capable of increasing the mechanical work done by the channel.

To illustrate this we report the experimental data obtained during the initiation of a discharge in water using an aluminum wire with diameter $0.45\,mm$ and length $10\,cm$. Other parameters: condensor capacitance $12\,\mu F$, voltage $10\,kV$, inductance of the discharge loop about $3\,\mu H$. The size of the wire was chosen so that almost the entire energy of the capacitor is used up for the evaporation of the wire. From the oscillograms of the current and voltage shown in Fig. 2.24, we can find that the evaporation of the wire occurs in about $18\,\mu sec$ and that this process uses about $420\,J$, which is about 70% of the capacitor energy.

From the amplitudes of the compression pulse radiated in a direction perpendicular to the channel axis (the oscillogram for this pulse taken at a distance of $100\,cm$ from the channel is shown in Fig. 2.25), we can estimate the acoustic energy radiated by the discharge. For this purpose we use formula (5.46), assuming that the pulse in Fig. 2.25 can be approximated by a Gaussian curve with $\tau_0 = 0.7\tau$, where τ is the duration of the compression pulse, approximately equal to $18\,\mu sec$. Then, for $p_\perp = 16\,mm$, $l = 10\,cm$, and $r = 100\,cm$ we find $W_{ac} \approx 100\,J$, which constitutes about 25% of the electric energy released into the channel. The measurements of the period of pulsation of the bubble formed this way gave a value of about $16\,msec$. If, in spite of the fact that the channel length in this case is large compared with radius, we use formula (2.6)

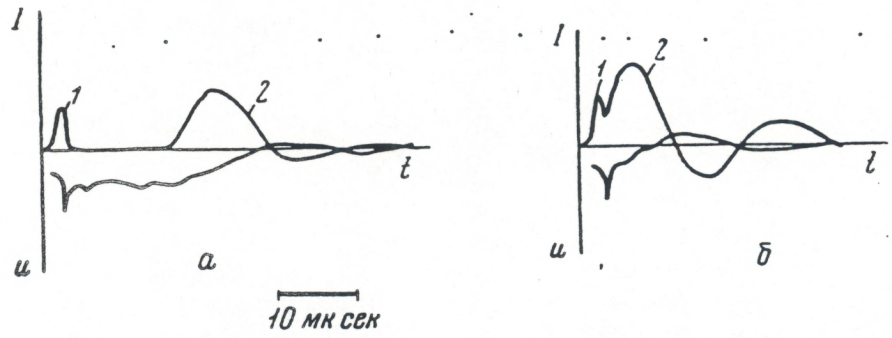

Fig. 2.23. Oscillograms of the current and voltage for a discharge initiated using a copper wire.

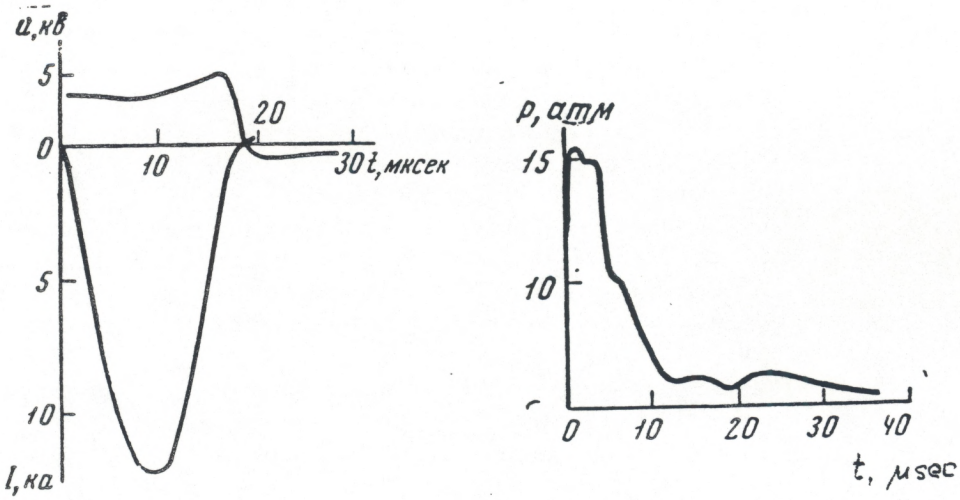

Fig. 2.24. Oscillograms of the current and voltage for a discharge in water initiated using an aluminum wire.

Fig. 2.25. Oscillogram of a compression pulse radiated by a discharge with electric characteristics given in Fig. 2.24. Direction perpendicular, distance 100 *cm*.

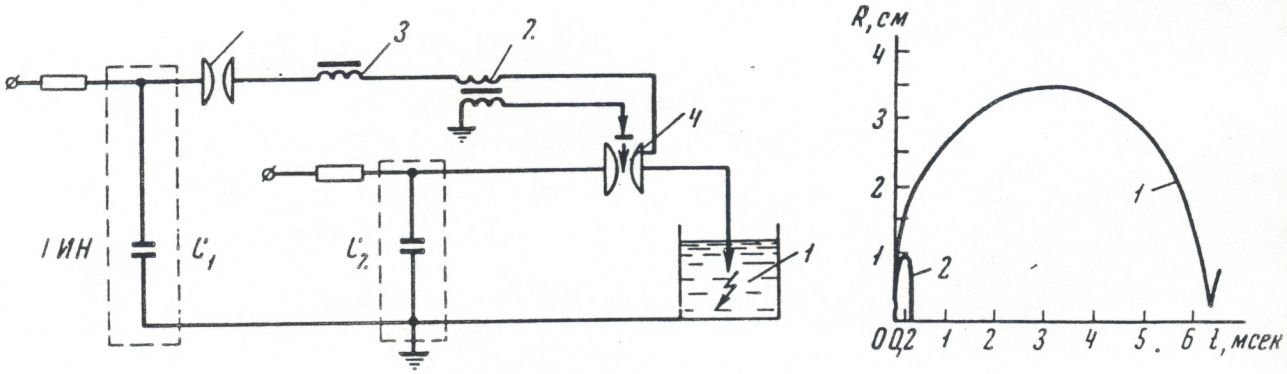

Fig. 2.26. Discharge circuit adopted for a preliminary high-voltage breakdown of the interelectrode gap.

Fig. 2.27. Plot of a bubble radius as a function of time.

to calculate the pulsation energy, and we find that this energy equals approximately $300\,J$, or 70% of the electric energy released into the channel. At the same time, for discharges initiated through high-voltage breakdown, the acoustic energy constitutes 15–20%, and the pulsation energy 25–30% of the energy released into the channel.

Let us examine the features of the initiation of low-voltage discharges in low-conductivity water based on the use of a preliminary high-voltage breakdown of the interelectrode gap. This method is known in the field of high-voltage engineering as a combination of two generators: the generator of voltage pulse (GVP) and the generator of current pulse (GCP). The difficulty in the use of this method for the initiation of discharges in water stems from the fact that the start of the GVP has to induce the breakdown of two parallel interelectrode gaps, one in the water and the other in the air. The breakdown of the air gap has to cause the connection of the GCP to the interelectrode gap in the water. However, the delay in the breakdown of the interelectrode gap in the water is substantially longer than the delay of the gap breakdown in the air. It is therefore necessary to resort to special circuits that would not be sensitive to the difference in the breakdown delays.

Figure 2.26 shows a circuit that achieves the high-voltage breakdown of the gap in the water and subsequent connection of the low-voltage capacitor. This scheme works as follows. At the breakdown of the interelectrode gap 1 caused by the voltage from GCP (C_1) there occurs a steep increase of discharge current, which in turn causes a voltage jump on the exit of transformer 2, whose primary coil is connected to the GVP loop. The voltage jump is used to ignite the discharger 4, which in turn connects the low-voltage capacitor C_2 to the discharge loop. Choke 3 with a saturating core prevents the voltage jump from taking place when the GCP is connected, which is when the current of the corona discharge appears in the discharge loop.

Let us now examine the principle of the initiation of low-voltage discharges in high-conductivity fluids. As we have already mentioned, this principle is based on the use of the breakdown of the interelectrode gap along the gas bubble which is formed in between the electrodes by a preliminary corona discharge on a third electrode introduced into the interelectrode gap [5].

Let us find the energy of the capacitor that feeds (ignites) the corona discharge. If the gap separation is l, then at time t_1, when the "power" capacitor is connected, the radius R of the bubble formed by the corona discharge will reach the value $l/2$. Since it is convenient to assemble the dischargers in a massive holder, we will examine the motion of the "starting" bubble near the solid wall. In this case, the bubble has a hemispherical shape, and its potential energy at the moment when it reaches the maximum radius R_b is connected with the energy E of the capacitor that feeds the corona by the relation

$$\frac{2}{3}\pi R_b^2 p_0 = \eta_b E\,, \tag{2.7}$$

where p_0 is the hydrostatic pressure,and η_b it the ratio of the bubble energy to

the energy of the capacitor. As we indicated in Section 2.3, this quantity can reach 6% if the water has a salinity of a few percent.

The pulsation period τ_p of the gas bubble in the case of a discharge in free space is determined by the relation (see Ch. IV)

$$\tau_p = 1.135\rho^{1/2}p_0^{-5/6}(m\eta_b E)^{1/3}\,, \quad m = 1\,, \tag{2.8}$$

where ρ is the fluid density. If the discharge occurs near solid wall, then in (2.8) we have to set $m = 2$.

For a rough estimate of the expansion of a bubble in water we can use the approximate formula

$$R = R_b\sqrt[3]{2t/\tau_p}\,, \tag{2.9}$$

where t varies in the range from 0 to $\tau_p/2$.

Using this formula, let us find the capacitor energy E needed for the ignition of a corona discharge capable of forming bubbles of radius R at the time t_1 :

$$E = \sqrt[2/3]{\frac{1.5\rho^{1/2}p_0^{1/6}}{\eta_b^{2/3}t_1}}R^2\,. \tag{2.10}$$

The initiation method examined above is not very sensitive to the hydrostatic pressure, because the radius of the bubble in the initial stage of growth depends very weakly on the values of the hydrostatic pressure, provided that the pressure in the discharge channel generating the bubble is large compared to the hydrostatic pressure. (See Ch. IV.)

To compensate for the decrease of the bubble radius with the increase in the hydrostatic pressure, one has to increase slightly the energy of the capacitor that feeds the corona discharge.

As an example, Fig. 2.27 shows how the behavior of $R(t)$ changes in going from $p_0 = 1$ to $p_0 = 40\,atm$ (lines 1 and 2) for the case of a bubble generated with a wire explosion. From the figure one sees that if $t_1 < \tau_p/2$, where τ_p is the pulsation period at $p_0 = 40\,atm$, then $R(t_1)$ experiences a very small decrease in going from $p_0 = 1$ to $p_0 = 40\,atm$.

REFERENCES to Chapter II

[1] Kuzhekin I.P., *Impulsive breakdown and discharge channel in liquids* (Dissertation), Moscow Energy Institute (1967).

[2] Trofimova I.B., *Experimental study of the breakdown of conducting non decontaminated liquids* (Dissertation), ZNILelectrom (1965).

[3] Naugolnykh K.A., Roy N.A., "Electrical and hydrodynamical characteristics of a pulse underwater crown,"Akust. Zhurnal **13**,.3, 417-425 (1967).

[4] Stekol'nikov I.S.,Ushakiv V., "An investigation of discharge phenomena in liquids," Zh. Tekh. Fiz. **35** (9), 1692 -1970 (1965), (Soviet Phys. Tech. Phys., **10** (9) 1966)

[5] Mel'nikov N.P., Ostroumov G.A., Sojak M. Ju., "The formation of electrical breakdown in aqueous of sodium chloride,"Zh. Tekh. Fiz. **34** (5), 949-951 (1964) (Soviet Phys. Tech. Phys., **9** (5) 1964).

[6] Roy N.A.,Frolov D.P.,"Generation of sound by spark discharge in water", *Proc.3 Internat. Congr.Acoustics, Elsevier Publ. Co.* (1961).

[7] Cole R. H., *Underwater explosions*, (Princeton UP, Princeton, 1948).

[8] Earl Van Reenan, "Low-voltage deep penetration marine seismic profiling system,". *Marine Sciences Instrument.3 Proc. 3 Nat. Marine Sci. Sympos. Plenum Press, N.Y.* (1965).

[9] Mel'nikov N.P., Ostroumov G.A. Schteinberg A.A., "Method of stabilization of electric discharge in water,"Vestnik LGU, **10** ,157-158 (1962). [Reports of the Leningrad State University]

[10] Mel'nikov N.P., Ostroumov G.A. Schteinberg A.A., "Some features of electric breakdown in electrolites," Doklady Akad. Nauk SSSR, **147** (4), 822-825 (1962) (Reports of the Academy of Sciences USSR)

[11] Mel'nikov N.P., Ostroumov G.A. Schteinberg A.A., Doklady Akad. Nauk SSSR, **148** (5) (1963) (Reports of the Academy of Sciences USSR)

[12] Kutzenko L.G., Kortnev A. V., "On formation of pulse discharge in aqueous solutions of lithium chloride," Ukrain. Fiz. Zh. **12** (9), 1539-1544 (1967).

[13] *Exploding wires* (Collection of articles), Moscow, IL, (1963).

[14] *Electric explosion of conductors*, Moscow, Nauka,. (1965).

[15] Roy N.A., Patent *No.* 32982, Priority date November 28, 1964.

Chapter III

THE PROPERTIES OF MATTER IN THE DISCHARGE CHANNEL

3.1. Introduction

In the present chapter we examine the processes taking place in the discharge channel and the properties of matter in it. We present experimental data on the electric characteristics of the discharge, such as the current and voltage in the interelectrode gap and the gap resistance, for typical cases that allow us to study the regimes of energy release into the channel, i.e. the typical time and energy scales of the phenomenon. In the present monograph we consider mainly discharges in which, during time intervals of tens of microseconds, there occurs an energy release of several kilojoules (which corresponds to a power of hundreds of megawatts). As for discharges corresponding to other energy regimes, we shall give only fragmentary experimental data. However, the theoretical approaches presented here are applicable, within certain limits, to a larger class of cases.

We describe experimental data on the expansion of the discharge channel obtained using high-speed photography. These data allow us to determine the speed of the channel expansion, which is typically about $10^4 - 10^5 cm/sec$, as well as to find the pressure in the discharge channel by using the hydrodynamic relations presented in Ch. V. The pressure in the channel lies in a range from a few hundreds to a thousand atm.

Knowing the resistance of the discharge gap and the channel radius, it is possible, assuming that the channel is homogeneous and neglecting the effect of the near-electrode regions, to estimate the resistance of the gas in the gap.

Let us note here that if the gas conductivity and pressure are known, it is possible, with a few assumptions, to estimate its temperature; the values thus obtained agree, as we shall show later, with the results of other experimental work and theoretical estimates of the temperature. Such estimates show that the temperature of the channel is of the order of $20,000\,°K$.

We also present information on the properties of the matter, which is in a state of dense low-temperature plasma at pressures and temperatures that are typical for channels of underwater spark discharges.

We give estimates of the plasma relaxation times, which prove to be small compared to the typical time scales of the discharge; this means that the plasma may be considered in a state of equilibrium. This fact allows us to calculate the composition of the plasma and its thermodynamic characteristics, such as, in particular, the specific internal energy.

Finally, we also give expressions for the plasma coefficients, the electric conductivity and the temperature conductivity; in doing so, we take into account and compare various mechanisms of heat transfer: gas-kinetic, electron, and radiative. Convective heat transfer is not examined, although it may very well

play an important role. We give an estimate of thermal conductivity in the cooler layers of the vapor and water surrounding the plasma, which allows us to estimate the energy expended in heating these layers.

3.2. Electric characteristics of a discharge

In this section we examine the electric characteristics of the channel, by which we mean the time dependence of the discharge current and voltage in the channel, the time dependence of the channel resistance, and the power and energy released into the channel, i.e., those characteristics that can be determined from electric measurements. The study of the electric properties of the channel plasma, such as conductivity, is deferred until after we examine the channel expansion.

From the oscillograms of the discharge current and voltage in the interelectrode gap it was found that the resistance of the gap at the time of the channel formation was, as a rule, rather large, provided, of course, that the proper initiation method was adopted. In the case of high-voltage discharges with working voltage of several tens of kV, the resistance of gaps of $5-10$ cm is of the order of $10^2\,\Omega$. In low-voltage discharges with working voltage of a few hundred kV and gap separation of several cm, the gap resistance at the moment of the channel formation is about $10\,\Omega$. The channel resistance drops sharply just after the channel formation, reaching a minimum at about the time the current reaches its maximum, and then increases as the current goes to zero. The channel resistance falls, first because of the increase of the plasma temperature under the effect of the discharge current, and second because of the increased crosssection of the channel due to its expansion brought about by the excess pressure in the channel. At the end of the discharge, or at the end of each half-period, if the discharge is oscillatory, the channel resistance increases due to the cooling of the plasma, even though the crosssection of the channel continues to increase.

The behavior of the channel resistance during a discharge is determined by many factors: inductance of the discharge loop, capacitance of the capacitor, initial voltage, interelectrode gap separation, and conductivity of the liquid shunting the channel. The relation between the resistance and the listed factors is a complex one. Let us illustrate it with a few examples.

Let us first note that a discharge can be *aperiodic* if the direction of the current does not change during the discharge, and *periodic* if there occur current oscillation occur. Correspondingly, the concept of *critical discharge* is introduced to indicate the limiting aperiodic discharge, a discharge that becomes a periodic one if the loop resistance is increased any further. For a critical discharge the effective resistance is equal to the wave resistance $R_{eff} = \sqrt{L/C}$.

Let us begin by considering relatively low-power high-voltage discharges. In Table 3.1 are shown the values of the working voltage u, capacitance C, inductance of the discharge circuit L and gap separation l. The setup is as follows: positive high-voltage electrode (end of an $RK-3$ cable with external

insulation and braid removed), and a grounded rod disposed parallel to the cable.

Figure 2.10 shows the oscillograms of current and voltage for the discharges *No.* 1 and 2 (see Table 3.1).

The oscillograms show that the voltage on the electrodes slowly decreases during the breakdown delay that corresponds to the time of growth of the leaders. At the shunting of the interelectrode gap by one of the leaders, the voltage in the gap drops sharply. This jump is caused by the voltage drop in the inductance loop, which is brought about by the sharp increase of the discharge current. After that, the voltage goes aperiodically to zero. The behavior of the channel resistance, calculated as the ratio of the channel voltage to the discharge current, is shown in Fig. 2.11. In the stage of the leader growth the resistance of the interelectrode gap is approximately $10^2\,\Omega$. After the breakdown, the resistance drops to a few Ohms, and tends to increase toward the end of the discharge. For such high channel resistances we may neglect the correction from inductive reactance. As the capacitance of the capacitor increases, the channel resistance takes smaller values. However, this does not change the character of the discharge; the latter stays close to critical. This means that the decrease of the time averaged resistance of the channel follows approximately a behavior inversely proportional to the square root of the capacitance. The duration of the current pulse, if all other parameters are held unchanged, increases as the square root of the capacitance and is approximately equal to $\pi\sqrt{LC}$, provided that the discharge remains in a near-critical regime.

Figure 3.1 shows the plots of the power and energy released into the channel for the case of discharge *No.* 1 (Table 3.1).

Table 3.1

N_0	u [kV]	C [μF]	L [μH]	l [cm]
1	30	0.4	3	4.5
2	30	0.9	3	5
3	30	0.4	55	4.5
4	30	0.9	3	2

The effect of the inductance on the behavior of the discharge can be estimated from the oscillograms in Fig. 3.2, taken for discharge *No.* 3 (Table 3.1). The increase in L does not cause a variation in the breakdown delay, because the voltage drop in inductance during initiation is small. The time dependence of the channel resistance for this case is shown in Fig. 3.3. Two unusial features draw attention: first, the channel resistance falls during the discharge less than at small inductances, and second, it goes through a maximum when the discharge current is zero. As one can see from Fig .3.4

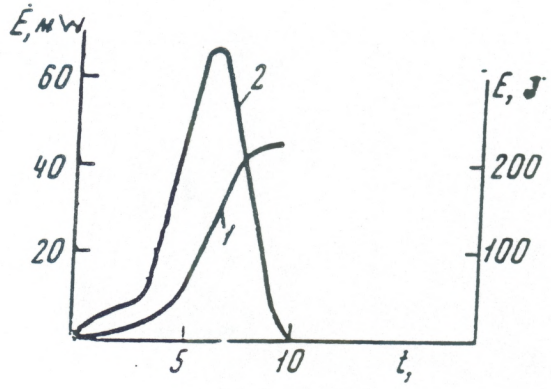

3.1

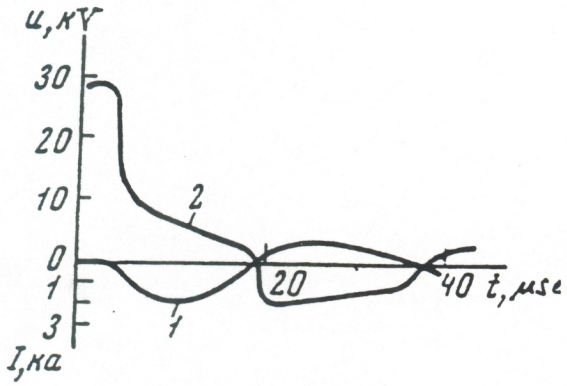

3.2

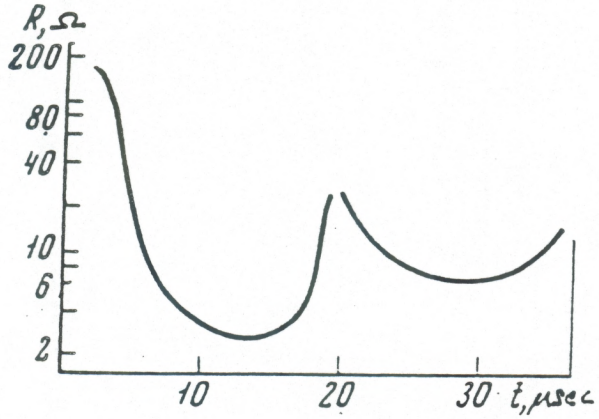

3.3

Fig. 3.1. Energy(1) and power(2) as a function of time for the discharge *No. 1* in Table 3.1.

Fig. 3.2. Oscillograms for the discharge current (1) and voltage (2) for the discharge *No. 3* in Table 3.1.

Fig. 3.3. Channel resistance as a function of time for the discharge *No. 3* in Table 3.1.

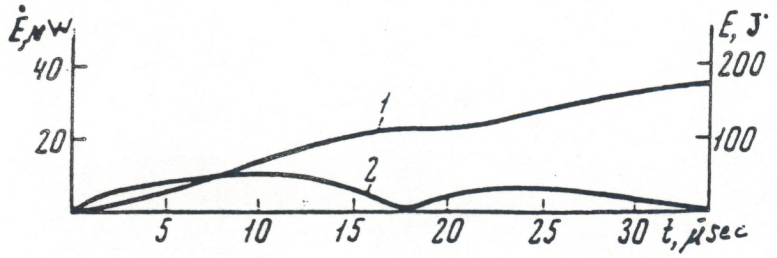

3.4

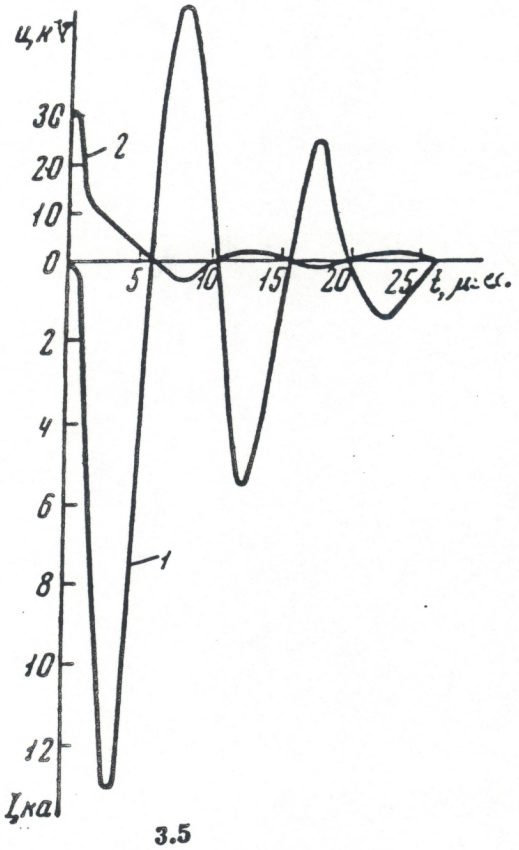

3.5

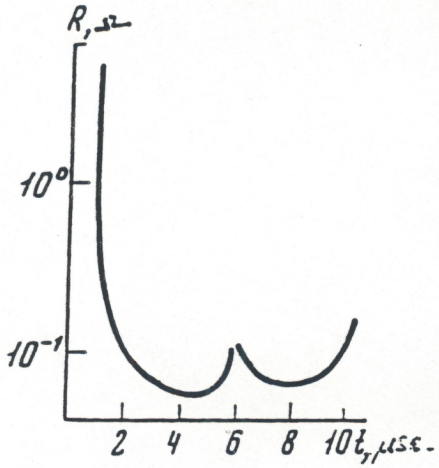

3.6

Fig. 3.4. Energy(1) and power(2) as a function of time for the discharge *No. 3* in Table 3.1.

Fig. 3.5. Oscillograms for the discharge current (1) and voltage (2) for the discharge *No. 4* in Table 3.1.

Fig. 3.6. Channel resistance as a function of time for the discharge *No. 4* in Table 3.1.

the transfer of energy into the channel decreases and electric power drops as inductance increases.

In all the cases considered, the transfer of energy from the capacitor into the channel is practically complete, since the channel resistance is substantially higher than the resistance of the remaining part of the discharge circuit.

The discharge can be brought into a damped oscillatory regime not only by increasing the inductance of the discharge loop, but also by shortening the electrode separation, as in the case of discharge *No.* 4 (Table 3.1). The oscillograms in Fig. 3.5 show that the duration of discharge *No.* 4 increases substantially compared to discharge *No.* 2; as a result, the rate of energy transfer into the channel as a whole decreases. From the behavior of the channel resistance (Fig. 3.6) we can assume that in the stages corresponding to the power minima there occurs, possibly, a possible cooling of the plasma occur. Such an effect sometimes causes the discharge to cease.[1]

Let us examine the role of the initial voltage on the basis of a few discharges with constant capacitor energy equal approximately to 45 J. The other parameters are given in Table 3.2.

Table 3.2

N_0	u [kV]	C [μF]	L [μH]	l [cm]
1	52	0.033	3	5
2	30	0.099	3	5
3	21.2	0.2	3	2.5
4	15	0.4	3	1.2
5	10	0.9	3	0.5

Figure 3.7 shows the oscillogram of the discharge current and voltage for such discharges. As the initial voltage on the capacitor rises, so does the number of leaders. As a result, there is an increase of the leader current, and the voltage drop on the capacitor during the breakdown delay becomes less noticeable. The energy that remains to feed the channel decreases. Contributing to this effect is also the shunting of the channel by streamer currents during the discharge.

As the voltage drops, the breakdown delay increases and becomes unstable. Figures 3.7d,e are the oscillograms pertaining to discharge *No.* 5 (Table 3.2), which show how greatly the breakdown delay can vary from discharge to discharge in low-voltage experiments.

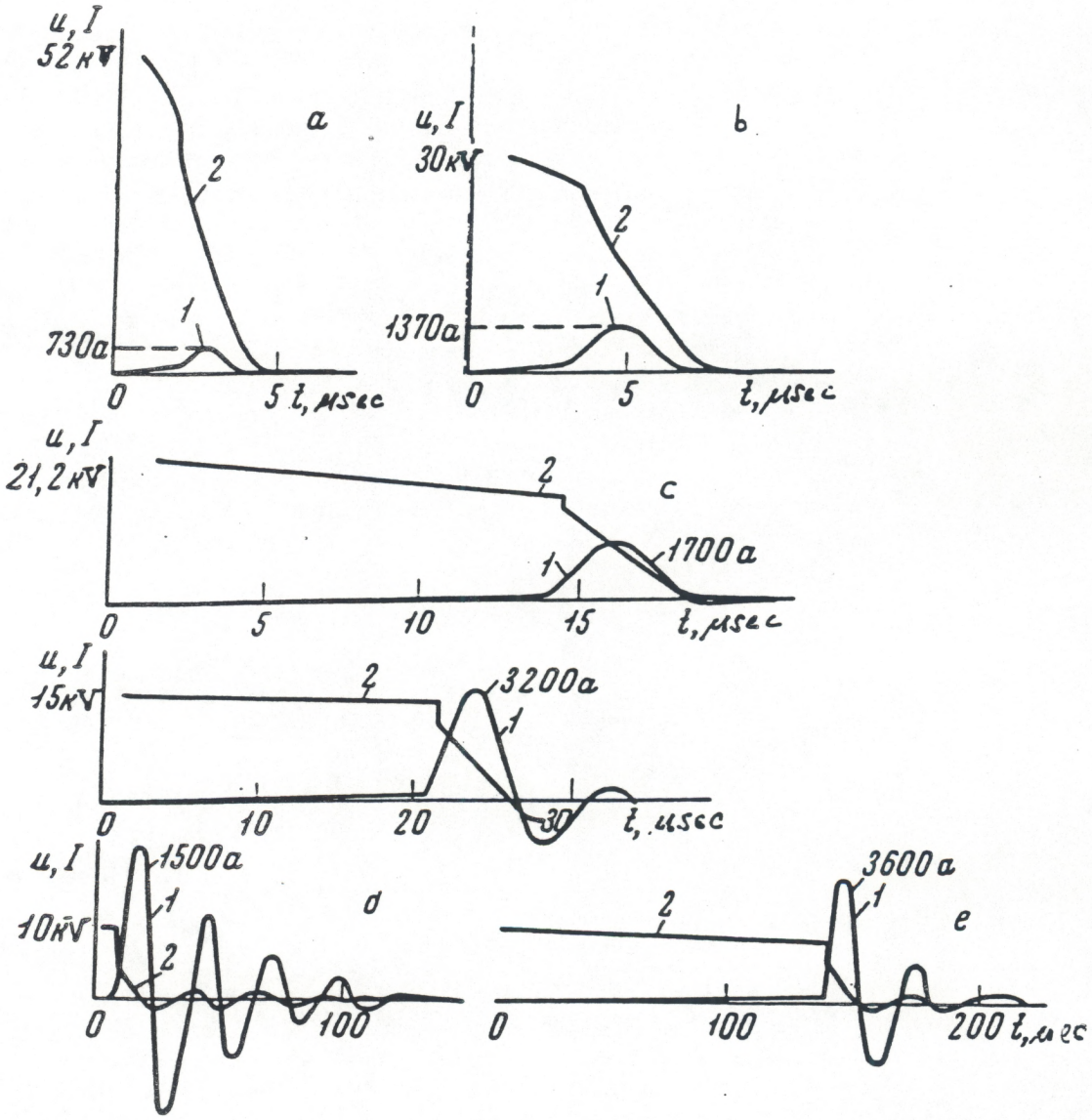

Fig. 3.7. Oscillograms for the discharge currents (lines 1) and voltages (lines 2) for the discharges *No. 1-5* in Table 3.2.

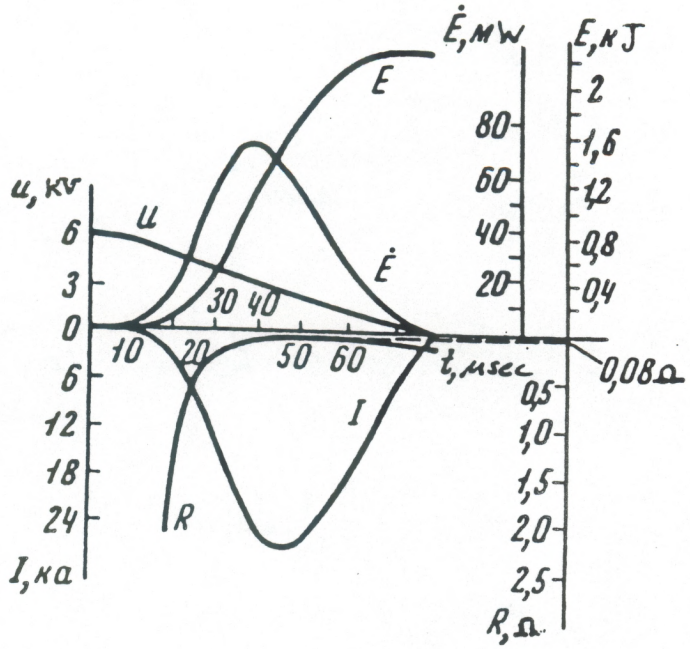

Fig. 3.8. Electric characteristics of discharge *No. 1* in Table 3.2.

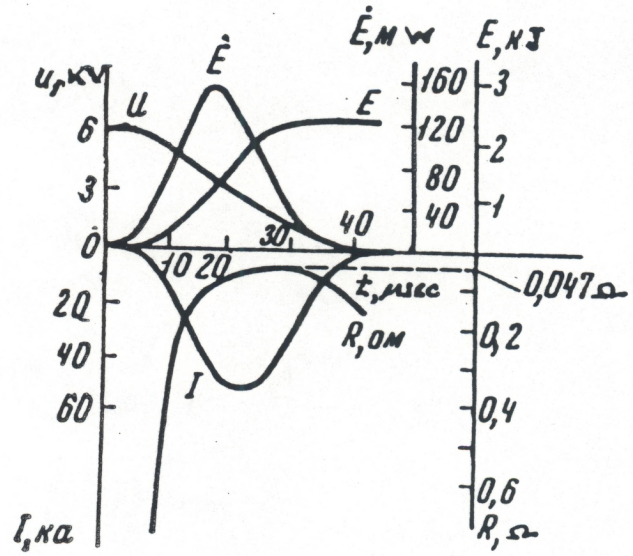

Fig. 3.9. Electric characteristics of discharge *No.* 2 in Table 3.2.

In order to achieve the breakdown of the interelectrode gap, it is necessary to decrease the electrode separation. If the latter is done, the channel resistance drops, and the discharge becomes oscillatory.

Let us examine now the electric characteristics of more powerful discharges with the parameters given in Table 3.3.

Table 3.3

N_0	u $[kV]$	C $[\mu F]$	L $[\mu H]$	l $[cm]$	E $[J]$
1	6	158	1.5	6	2840
2	6	165	0.1	3	2970

These discharges are initiated through an explosion of tungsten wires with a $0.04\,mm$ diameter. Figures 3.8 and 3.9 show the electric characteristics of discharges $No.\,1$ and 2, respectively (Table 3.3). From the diagrams one sees that the channel resistance drops at the time of maximum current to about $0.08\,\Omega$ and $0.05\,\Omega$ respectively. The resistance increases somewhat toward the end of the discharge.

The duration of the first discharge is close to $\pi\sqrt{LC}$, that of the second is noticeably longer. Evidently, the duration of the second discharge could be shortened without transition into an oscillatory regime by shortening the channel length. In fact, the value of the critical resistance $R_c = \sqrt{L/C}$, which corresponds to the maximum energy transfer rate, is equal for the first discharge to $0.1\,\Omega$, a value close to the minimum channel resistance of $0.08\,\Omega$; at the same time, the critical resistance for the second discharge is $0.02\,\Omega$, which is substantially lower than the minimum channel resistance of $0.05\,\Omega$. Therefore, the second discharge is, to a large degree, controlled by the active resistance of the channel.

Higher power discharges were investigated in the work [2]. These discharges occurred in a damped oscillatory regime with several half-periods. The gap separation was $12–15\,mm$, and the electrodes were two opposing coaxial brass rods with 25–30° points. The parameters of the discharges are given in Table 3.4. Also given are the current peak I_m, the maximum current increase rate $\dot{I}_m$, the voltage at the current peak and the duration of the first half-period $\tau/2$.

Table 3.4

N_0	u	C	I_m	$\dot{I}_m$	u at I_m	$\tau/2$
	[kV]	[μF]	[kA]	[kA/sec]	[kV]	[μ sec]
1	40	2.7	12	$3.6 \cdot 10^9$	1.3	15.0
2	40	5.4	61	$2.1 \cdot 10^{10}$	3.2	8.5
3	20	5.4	330	$0.5 \cdot 10^{10}$	5.5	11.0
4	30	130	520	$1.75 \cdot 10^{11}$	6.8	11.0
5	40	130	650	$2.1 \cdot 10^{11}$	7.3	11.5
6	30	240	720	$1.75 \cdot 10^{11}$		15.5

Figures 3.10 and 3.11 show the oscillograms of the discharge current and voltage in the interelectrode gap for discharges *No.* 1 and 2 (Table 3.4). In the case of high-power discharges the correction of the inductive component of the voltage plays an essential role ($\dot{I}_m >$ or $\sim 10^{11}\, A/sec$). What probably happened here was that, due to the large electrode surface in the discharges of ref.[2], the breakdown delays were significantly scattered, (from a few tenths to a few tens of microseconds), and because of the smallness of the gap, several channels were immediately formed; subsequently, these channels merged into one single channel. The channel resistance at the time of the current maximum was about $0.01\,\Omega$.

At the beginning of this section we mentioned that the dependence of the electric characteristics of the discharge on the parameters of the discharge circuit is rather complex. However, for the purpose of obtaining estimates, we can use simple relations that give the correct order of magnitude for the basic electric quantities that characterize a discharge. In fact, for a discharge in a near-critical regime (which is the most important one in practice), the duration of the discharge τ turns out to be close to $\pi\sqrt{LC}$, and the minimum channel resistance R_m is close to the critical resistance of the loop, $2\sqrt{L/C}$. Measurements show that the minimum resistance can be estimated also in the following manner: it is approximately equal to the ratio of half the initial voltage to the maximum current, or $Cu \sim I_m\tau/2$. From these relations we find that R_m equals approximately $\tau/4C$. It is easy to convince oneself that all the experimental values agree well with the values calculated using this formula. The maximum power developed during the discharge is given by Cu^2/τ, the maximum current increase rate by $\dot{I} \sim 4Cu/\tau^2$. The values calculated with the help of these relations agree well also with the experiment involving near-critical discharges, as we have already mentioned. If the channel length is too large, then all of the above relations still give correct values, provided that τ is known from the experiment. If there are signs of oscillatory behavior in the discharge, then τ is close to $\pi\sqrt{LC}$.

The oscillograms of the discharge current and voltage in the discharge channel, taken for various discharge circuits, show that spark discharges in water can occur in two modes: the damped oscillation mode, if the time average resistance

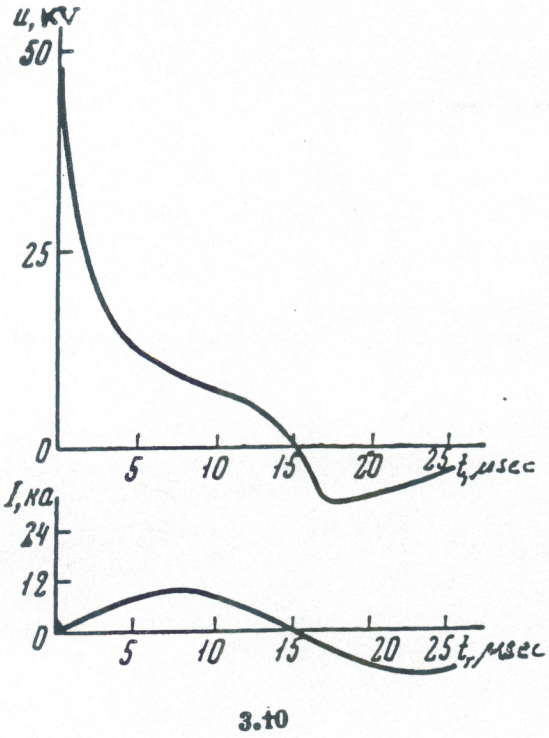

3.10

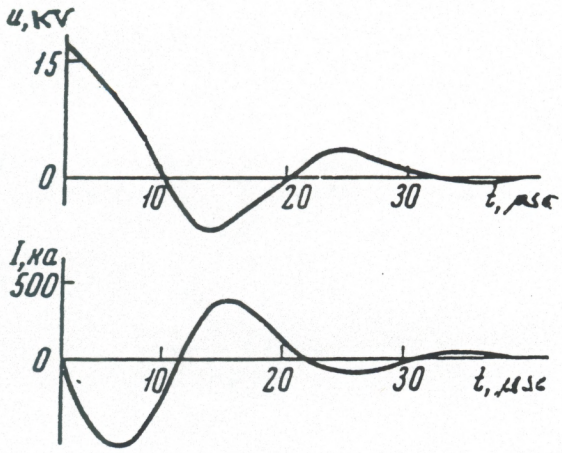

3.11

Fig. 3.10. Oscillograms for the discharge current and voltage for the discharge *No. 1* in Table 3.4.

Fig. 3.11. Oscillograms for the discharge current and voltage for the discharge *No. 4* in Table 3.4.

of the channel is less than $\sqrt{L/C}$, or in a near-critical regime, characterized by the current and power curves nearly symmetric with respect to their peak values. Discharges with channel formation do not occur in a near-aperiodic regime with characteristic exponential decreasing current and voltage. Such a regime takes place only in channel-less discharges which are controlled to a large degree, by the ballast resistance of the water. The absence of a near-aperiodic regime is due to the peculiar behavior of the channel resistance during the discharge, namely, to the fact that the resistance passes through a minimum. For all the discharges in near-critical regimes, the plot of the power as a function of time takes the form of a triangle (Fig. 3.12), as one can see from Figs. 3.8 and 3.9. This suggests that for rough estimates the energy release for all the discharges in near-critical regimes can be approximated by one function. To show this, let us introduce the following dimensionless quantities: $x = t/\tau$ and $f(x) = E(x)/E$, where τ is the discharge duration determined from the plot 3.12, and E is the total energy released into the channel. Then, the thus normalized function $f(x)$, which characterizes the energy release mode, proves to have a rather universal character; $f(x)$ does not change much from discharge to discharge even in the case of strong variations in the discharge parameters. To corroborate this conclusions, in Fig. 3.13 we show the plot of the normalized energy as a function of time for five different discharges. The parameters for these discharges are given in Table 3.5. The numbers in column 1 serve to identify the discharge. In columns 2, 3 and 4 are given the initial voltage of the capacitor, its capacitance, and separation gap, respectively. Column 5 gives the approximate value of the inductance calculated using the parameter of the discharge circuit. In columns 6 and 8 are reported the discharge duration and total energy released in the discharge; these values are calculated from the electric oscillograms. Column 10 gives the characteristic radius of the discharge channel (defined later), and finally, in column 11, we give the references when appropriate.

The solid lines in Fig. 3.13 are the plots of the simple functions that approximate the real time dependence of the normalized energy. Lines 1 and 2 are respectively, the graphics of the

functions

$$f(x) = \begin{cases} 2x^2, & 0 \leq x \leq \frac{1}{2} \\ 4x - 2x^2 - 1 & 1_{\overline{2 \leq x \leq 1}} \\ 1 & 1 \leq x. \end{cases} \tag{3.1}$$

and

$$f_1(x) = \begin{cases} 3x^2, & 0 \leq x \leq \frac{1}{3} \\ 3x - \frac{3}{2}x^2 - \frac{1}{2} & 1_{\overline{3 \leq x \leq 1}} \\ 1 & 1 \leq x \end{cases} \tag{3.2}$$

The function $f_1(x)$ corresponds to the approximation of the power by a scalene triangle of unit area with the perpendicular from the vertex dividing the base in the ratio 1 : 3.

Table 3.5

Table 3.5

N_0	u	C	l	L	$\pi\sqrt{LC}$	E	$Cu^2/2$	τ	R_0	Re
	[kV]	[μF]	[cm]	[μH]	[μsec]	[J]	[J]	[μsec]	[cm]	
1	1.2	816	0.3	-	-	510	590	50	1.09	
2	1.6	321	0.1	0.2	25	375	412	30	0.84	
3	1.6	321	0.1	0.1	18	400	412	30	0.85	
4	15	1500	7.5	-	-	-	169000	400	6.80	[20]
5	4	150	5	1.5	47	1070	1200	100	1.15	
6	6	150	5	1.5	47	2250	3000	80	1.24	
7	6	158	6	1.5	47	2260	2844	53	0.96	
8	6	150	7	1.5	47	2200	3000	95	1.24	
9	6	150	12	1.5	47	2340	3000	160	1.43	
10	6	165	3	0.1	11	2480	2970	30	0.89	
11	40	2.7	1.5	-	15	1990	2160	-	0.66	[2]
12	40	5.4	1.5	-	9	1200	4320	-	0.47	[2]
13	25	5.8	1.5	-	4	840	3625	-	0.29	[15]
14	20	1.35	2.0	5.3	5	-	270	5.3	0.405	
15	30	0.40	2.0	-	3	174	180	-	0.211	
16	30	0.40	4.5	5.0	4	162	180	5	0.166	

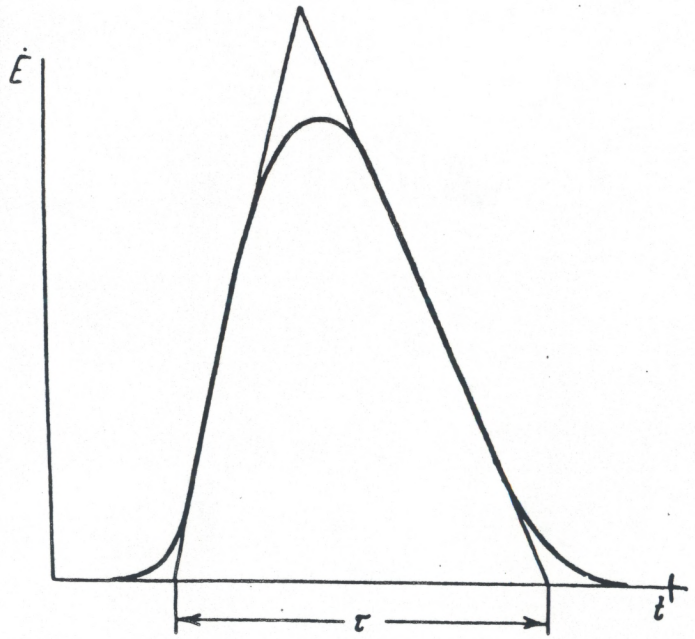

3.12

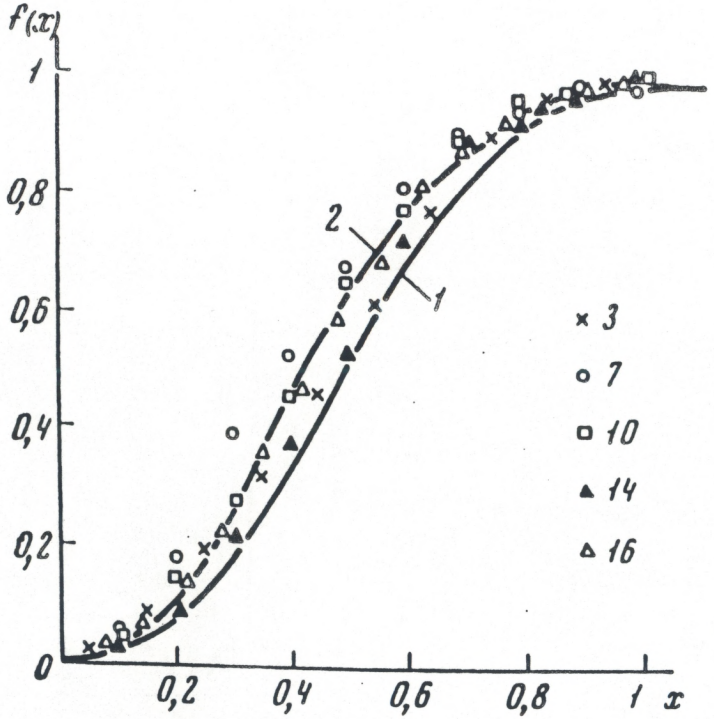

3.13

Fig. 3.12. Approximation of the power curve.

Fig. 3.13. Normalized energy as a function of time. Lines 1 and 2 correspond respectively to Eq. (3.1) and (3.2). The parameters of the discharge are given in Table 3.5. The numbers in the figure correspond to the ordering numbers in the table.

As we can see from Fig. 3.13, the difference in the experimental lines corresponds approximately to the difference between $f(x)$ and $f_1(x)$. Comparing the results of the numerical calculations of the hydrodynamic characteristics obtained using $f(x)$ and $f_1(x)$, we can estimate how accurately the theoretical curve approximates the *actual* law of energy release. Such comparison is carried out in Ch. VI.

3.3. Channel expansion

After the completion of the initiation of a discharge in a liquid, the formation of a channel filled with ionized gas occurs. The initial shape of the channel is determined by the initiation process. If the initiation method used is a high-voltage breakdown of the liquid, the initial shape of the channel is determined by the shape of the leader shunting the interelectrode gap. In such cases, the shape of the channels is almost never a regular geometric figure. The channel usually has both small-scale and large-scale deformations. Fig. 2.2 shows photographs of channels taken using the self-exposure technique. The initial diameter of the channels is of the order of $10^{-2}\ cm$.

In low-voltage discharges, the initial shape of the channel is determined by the gas bubbles that form on both electrodes, if the discharger construction is symmetric, or by the gas bubble that forms on the high-voltage electrode, if the setup is asymmetric. In this case, unlike the the high-voltage breakdown case, the initial diameter and length of the channel are close in value. Channels with regular geometric shapes can be obtained only if the following initiation methods are adopted: (1) wire bridges, (2) breakdown of a gas bubble formed through a preliminary corona discharge in the conductive liquid, and (3) breakdown between parallel electrodes as described in Section 3.4. In the first case, the channel has the form of a straight cylinder with spherical ends; in the second and third cases it has a hemispherical shape, because in both these two cases the discharge usually occurs near the solid reflector onto which the discharger is mounted. In case (1) the initial diameter of the channel is determined by the diameter of the wire, in the second case by the diameter of the bubble and in the third by the electrode separation.

Due to the intensive heating of the plasma by the discharge current, the pressure in the channel increases and an expansion of the channel takes place. During the expansion process the boundary of the channel may be assumed to be impenetrable. This does not mean, however, that in considering the processes taking place inside the bubble we may neglect the evaporation of liquid.

On the other hand, the shift of the boundary caused by the evaporation is practically unnoticeable against the fast hydrodynamic expansion. To see this, let us compare the volume of the evaporated liquid to that of the channel. The energy developed in the channel is expended mainly for the dissociation of water molecules and for the heating of the gas (see Section 3.5). Therefore, if D is the dissociation energy for one molecule, then the energy needed for the dissociation of all the molecules of a mass of water m and the heating of the monoatomic

gas thus formed is given by

$$\frac{m}{\mu}N_0\left(D+\frac{9}{2}kT\right), \tag{3.3}$$

where μ is the molecular weight of the water and N_0 is the Avogadro number.

Assuming that all the energy developed in the channel goes to the formation of the heated gas, we find that

$$m = E\mu/N_0\left(D+\frac{9}{2}kT\right). \tag{3.4}$$

Setting $E = 10^3 J$, $T = 10^4 K$, we find that $m = 10^{-1}\, g$. Therefore, the volume of the water evaporated in this case is $10^{-1}\, cm^3$, while the volume of the discharge channel is several cm^3.

Judging from the glow of the discharge, the plasma fills the channel rather uniformly during the expansion. High-speed photography through a slit perpendicular to the channel axis with strong lighting shows that the separation of the plasma from the walls of the channels occurs only toward the end of the discharge. Figures 3.14 and 3.15 show photographs of the discharge channels taken using a flash lamp and with the lightening provided by a second discharge, identical to the discharge under investigation. In these photographs there is no sign of intralayers of cold gas between the luminescent plasma and the water during the entire discharge. The intralayer formation becomes visible only after the discharge has ended, when the plasma,starting from the peripheral region

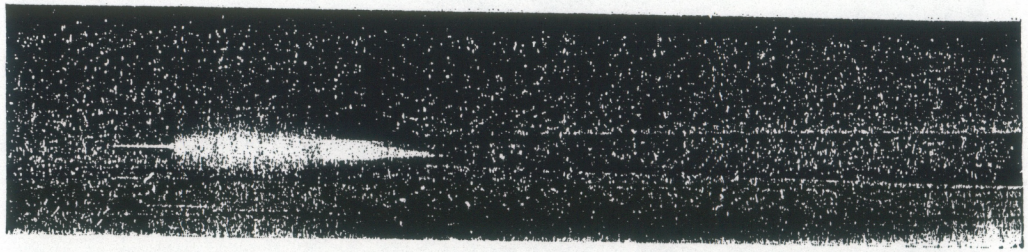

Fig. 3.14. Expansion of the discharge channel (photo).

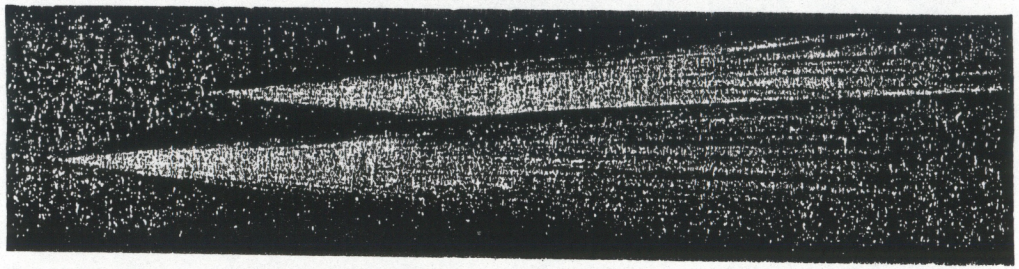

Fig. 3.15. Expansion of the discharge channel (photo).

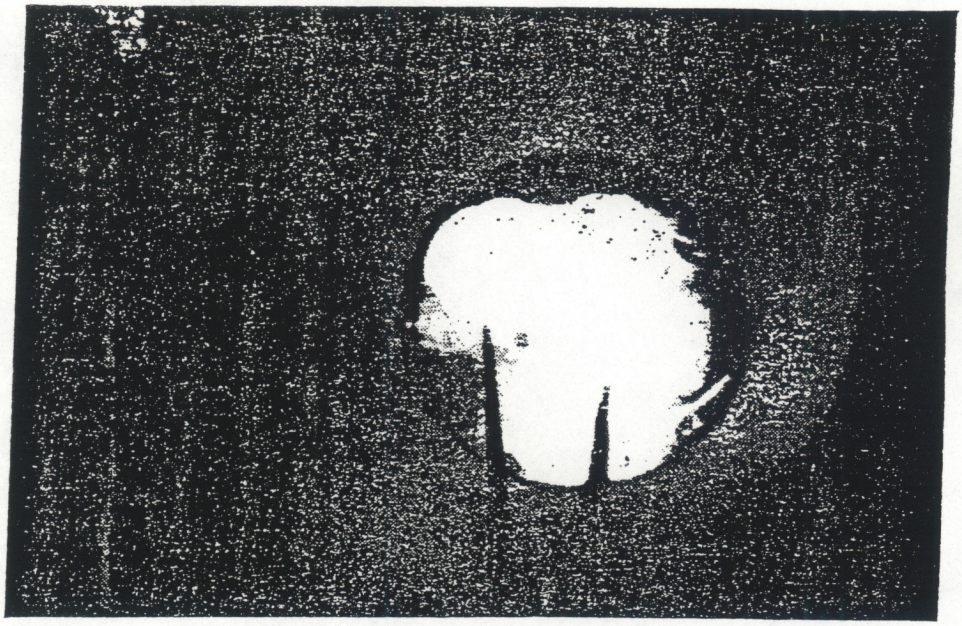

Fig. 3.16. Discharge channel (photo).

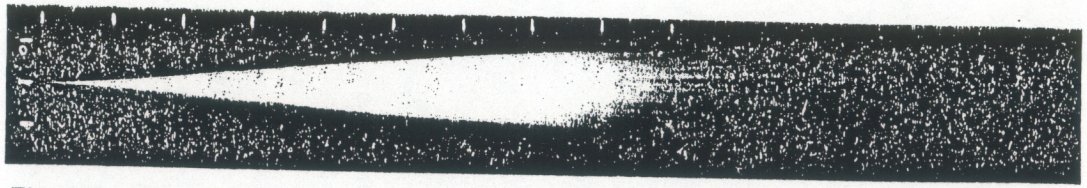

Fig. 3.17. Channel expansion for discharge *No. 7* (photo).

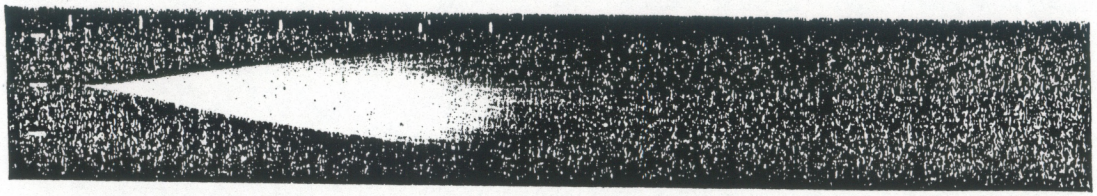

Fig. 3.18. Channel expansion for discharge *No. 10* (photo).

of the channel, cools down. In this stage, the regions with decreased luminosity, and thus with decreased temperature, become visible, even inside the channel. It is possible that the apparent homogeneity of the plasma in the initial stage of the discharge is due to the overall high brightness.

The onset of nonhomogeneity can be attributed to the flow of cold gas from the channel walls. Such flows can be originated by the non-uniformity of the transition layer between hot plasma and water. To take this fact into account in the calculation is difficult. Therefore, hereafter we shall assume, when choosing the discharge model, that the plasma is homogeneous.

The form of the channel and its diameter at the end of the discharge are determined, for a given interelectrode gap, by the discharge duration and by the energy transferred into the channel. The longer the discharge takes and the more energy is transferred, the larger the channel radius becomes and the closer to a sphere the shape of the channel becomes, even if its starting shape was close to a cylinder. If the initial shape of the channel is spherical, then the final shape naturally retains that symmetry. The dependence of the channel radius R_0 on the discharge duration τ and transferred energy E can approximately be found from the following considerations.

Let R_0 be the characteristic radius reached by the channel during the time interval τ. Then the channel expansion rate $\dot{R} = U$ is of the order $U = R_0/$, and, according to the results of Ch. IV, the pressure exerted by the liquid on the walls of the expanding channel can be approximated, for subsonic and near-sonic expansion speeds, by the formula $P \sim \rho_0 R_0^2/\tau^2$. Furthermore, the specific internal energy of the plasma in the discharge channel is given, as discussed in the following section, by the expression $P/(\gamma - 1)$, where γ is the effective adiabatic index, equal for the discharge in water to $\gamma = 1.26$. Then, for discharges in which the initial form of the channel is close to spherical, the internal energy of the plasma in the discharge channel is given by the expression

$$PV/(\gamma - 1) = \frac{4}{3}\pi R_0^3 \rho_0 (R_0^2/\tau^2)/(\gamma - 1).$$

The internal energy is of the order of magnitude of the total energy E transferred into the channel by the end of the discharge. From the above expression, we find that the channel radius at the end of the discharge is

$$R_0 \approx \left[(3/4\pi\rho_0)(\gamma - 1)\tau^2 E\right]^{1/5} \qquad (3.5)$$

.For a cylindrical channel the internal energy of the plasma is given by

$$\pi R_0^2 l \rho_0 (R_0/\tau)^2/(\gamma - 1) \approx E.$$

From this expression we find that the channel radius at the end of the discharge is

$$R_0^{1/4} \approx [\frac{(\gamma - 1)}{\pi\rho_0}\tau^2 \frac{E}{l}]^{1/4}. \qquad (3.6)$$

Let us remark here that both formulas (3.5) and (3.6) will be derived in a more rigorous manner in Ch. V, when discussing the hydrodynamical models of the discharge.

Using Eqs. (3.5) and (3.6), we can estimate the characteristic expansion rate and the order of magnitude of the pressure in the discharge channel, provided that the internal energy E liberated in the channel and the time τ are known. For example, for the discharges whose parameters are given in Table 3.5, the characteristic expansion rate of the channel agrees with the experiment, which gives values of the order of $10^4\, cm/sec$; similarly ,the channel pressure is of the order of a few hundred to a thousand atm .

Experimental investigations of the expansion of channels 5–10 cm long during high-voltage discharges show that the ratio between the channel radius and its length at the end of the discharge remains less than unity if the discharge duration does not exceed a few tens of μsec, and that the energy released per unit of length does not exceed a few kJ. These results are in good agreement with the estimates obtained using Eq. (3.6). The expansion rate of the channel in discharges of this kind remains practically unchanged along the channel. However, if the length of the channel is small, substantial variations of the expansion rate can be observed along the channel axis. Figure 3.16 shows a photograph of a channel at the end of the discharge of a $150\,\mu F$ capacitor at $6\,kV$. The length of the wire used for the discharge initiation is about $3\,cm$ (tungsten wire, diameter $0.04\,mm$). The inductance of the discharge circuit is approximately $0.1\,H$. In the photograph we can see that the near-electrode regions of the channel have expanded more strongly, giving it the shape of a dumbbell. One possible cause of this effect might be that the liberation of energy occurs predominantly in the near-electrode regions due to the increased resistance of these regions. As a result, the picture is the same as if two closely situated point discharges occurred.

The time dependence of the channel radius during the discharge is, in first approximation, approximately linear. This can be seen, e.g., in the photographs of discharges $No.\,7$ and 10, shown in Figs. 3.17 and 3.18.

3.4. Conditions of gas equilibrium in the discharge channel

. The fast release of energy in the channel during a spark discharge in a liquid leads to strong heating of the matter in the channel and to evaporation of the liquid from the channel walls.

The number of particles in the channel increases noticeably during the discharge. The new molecules formed through evaporation undergo heating, dissociatiation and ionization. As a result, in the discharge channel a dense low-temperature plasma forms, whose temperature, as the experimental and theoretical values given later in Sec. 7 show, corresponds to the region of first atomic ionization ($15000-30000\,^\circ K$), and the particle concentration reaches $10^{20}/cm^3$. Keeping the short duration of the discharge in mind (the current flow is usually present for about 10^{-4}–$10^{-6}\,sec$), a problem that must be considered is

that of the equilibrium of the gas in the channel. In other words, we need to clarify whether the equilibrium distribution of the energy among the degrees of freedom has time to establish itself. A detailed discussion of the relaxation processes in gas is presented in ref. [3]. We shall estimate, following ref. [3], the time needed to attain a Maxwell distribution in a gas of electrons, atoms and ions, as well as the relaxation times of the dissociation and ionization processes. All the numerical estimates given pertain to discharges in water.

The time τ_{ee} necessary for the electrons to attain the Maxwell distribution of speeds, i.e., the time that characterizes the attainment of the temperature in an electron gas, is determined by the time during which the electron kinetic energy varies by an amount on the order of the electron kinetic energy itself as a result of Coulomb electron-electron scattering.

As shown, e.g. in [3], τ_{ee} is determined by the formula

$$\frac{1}{\tau_{ee}} = \frac{3.8 n_e \ln \Lambda}{T_e^{3/2}} \; [sec^{-1}] \tag{3.7}$$

where n_e is the number of electrons per cm^3, and the so-called "Coulomb logarithm" is given as

$$\ln \Lambda = \ln \frac{3(kT_e)^{3/2}}{2\sqrt{4\pi} e^3 n_e^{1/2}} \approx \ln 0.62 \cdot 10^4 \left(\frac{T_e^3}{n_e} \right)^{1/2} . \tag{3.8}$$

For typical electric discharges, $T \approx 15,000\,^\circ K$, $n_e \approx 4 \cdot 10^{18} cm^{-3}$, $\tau_{ee} \sim 10^{-12} sec$, i.e., the Maxwell distribution of the electrons in the spark discharge channel is attained very fast compared to the duration of the discharge.

We must emphasize that Eq. (3.7), like all the other expressions used hereafter for the description of collisions between charged particles, is suitable only for estimates of the order of magnitude of the characteristics of the dense low-temperature plasma that forms in the channel of an electric discharge in a liquid.

The time necessary to attain the equilibrium distribution in a gas of atoms (or ions) can be estimated by means of the formula [3]

$$\frac{1}{\tau} \sim n \bar{v} \sigma_{aa} \; , \tag{3.9}$$

where n is the number of particles per unit volume,

$$\bar{v} = \sqrt{\frac{8kT}{\pi m}} = 1.45 \cdot 10^4 \sqrt{\frac{T}{A}} \; [cm/sec] \tag{3.10}$$

is the mean thermal speed, and σ_{aa} is the effective gas-kinetic crosssection, which is on the order of $10^{-15} cm^2$.

For $n = 10^{20} cm^{-3}$, $T = 20,000\,^\circ K$, $A = 16$ (oxygen), and $\bar{v} \cong 4 \cdot 10^5 \; cm/sec$, we have $\tau \sim 10^{-10} sec$, i.e. the (equilibrium) Maxwell distribution is attained in a small amount of time l compared to the duration of the discharge.

A much slower process is the equalization of the electron and ion (or gas-kinetic) temperatures. Because of the large mass difference between electrons and atoms (or ions), the amount of energy they exchange in elastic collision is proportional to the ratio of their masses; such an amount constitutes a very small part of the kinetic energy. Thus, for a noticeable exchange of energy between particles with different mass, such particles need to experience a large number of collisions, a number of the order of m_a/m_e (m_a is the atom mass and m_e the electron mass).

Taking this factor into account, we obtain, as shown in [3], the following expression for the time needed to attain the equilibrium between an electron gas and a gas of heavy particles, such as atoms or ions:

$$\frac{1}{\tau_n} = \frac{1}{\tau_{ei}} + \frac{1}{\tau_{ea}}\,, \tag{3.11}$$

$$\frac{1}{\tau_{ei}} = \frac{n_i Z^2 \ln\Lambda}{250 A T_e^{3/2}} \tag{(3.12)}$$

where n_i is the number of ions per cm^3, A is the atomic weight, Z is the ion charge, and the Coulomb logarithm is given by Eq. (3.8);

$$\frac{1}{\tau_{ea}} = n_a \bar{v}_e \sigma_{ea} 2\frac{m_e}{m_a} = 6.8 \cdot 10^2 \frac{n_a \sigma_{ea}}{A}\sqrt{T_e}\,, \tag{3.13}$$

where n_a is the number of atoms per cm^3,

$$\bar{v}_e = \sqrt{\frac{8kT}{\pi m}} = 6.21 \cdot 10^5 \sqrt{T}\ [cm/sec] \tag{3.14}$$

is the mean thermal speed of the electrons, σ_{ea} is the effective cross-section of electron-atom collisions , and m_a is the atomic mass.

For $T_e = 15{,}000°K$, $n_a = 10^{20} cm^{-3}$, $n_e = 4 \cdot 10^{18} cm^{-3}$, formulas (3.12) and (3.13) give equal values for the relaxation time: $\tau_{ei} \approx \tau_{ea} \sim 10^{-10} sec$ for hydrogen and $\tau_{ei} \sim 10^{-9} sec$, $\tau_{ei} \sim 10^{-8} sec$ for oxygen. The cross section for the scattering of electrons on ions is

$$\sigma'_{ei} = 1.2 \cdot 10^{-5} \frac{Z^2 \ln\Lambda}{T_e^2} \approx 10^{-13} cm^2.$$

The values for the scattering cross sections of electrons on atoms, for the same values of I, n_0 and n_2, were taken from the data of ref. [4], and are

$$\sigma_{ea} \approx 2 \cdot 10^{-15}\ \text{cm}^2, \quad \text{(hydrogen)}, \quad \sigma_{ea} \approx 0.4 \cdot 10^{-15}\ \text{cm}^2 \quad \text{(oxigen)}.$$

Let us consider now the slower processes of attainment of the equilibrium ionization and dissociation. As indicated in the book [3], at electron concentrations higher than $10^{16} cm^{-3}$, the ionization of atoms from the ground state

takes place mainly as a result of inelastic collisions with electrons. The rate of the process is characterized by the relaxation time $\tau_e = \frac{1}{\alpha_e n_a}$, where α_e is the constant of ionization rate and n_a is the number of atoms per cm^3.

Simple considerations lead to the following expression for the constant α_e [3]:

$$\alpha_e = \sigma_e \bar{v}_e \left(\frac{I}{kT_e} + 2\right) \exp -\frac{I}{kT_e},$$

where $\sigma_e = CkT_e$ is a certain value for the crosssection; the constant $C \sim 10^{-17} cm^2/eV$; $\bar{v}_e$ is the mean thermal speed of the electrons given by Eq. (3.14), and I is the atomic ionization potential. For $n_a = 10^{20} cm^{-3}$, $I = 13.6\, eV$ (hydrogen) and $T_e \simeq 15,000°K$ we obtain: $\sigma_e \approx 1.3 \cdot 10^{-17} cm^2$, $\bar{v}_e \approx 7.7 \cdot 10^7 cm/sec$, $\alpha_e \approx 3.3 \cdot 10^{-14} cm^3/sec$ and $\tau_e \sim 3 \cdot 10^{-7} sec$.

Let us examine now how fast the dissociation of molecules evaporating from the channel walls occurs. As will be shown later, at temperatures of $10^4\,°K$ the water molecules are practically totally dissociated. (See also [5,6].) As shown in ref. [3], the order of magnitude of the time necessary to attain the equilibrium dissociation (for $1 - \alpha \ll 1$) can be estimated using the formula

$$\frac{1}{\tau_d} \approx \frac{8}{1-\alpha} n^2 k_r \,, \tag{3.15}$$

where $\alpha = n_a/(n_a + n_m)$ is the degree of dissociation; $m = n_a + n_m$ is the total number of particles in the unit volume, and k_r is the constant of recombination rate.

Simple considerations [3] give the following formula for an estimate of this constant:

$$k_r \sim \bar{v}\sigma \frac{4\pi r^3}{3},$$

where $\bar{v}$ is the mean thermal speed of the atoms given by Eq. (3.10); σ is the scattering gas-kinetic crosssection, and r is a distance on the order of the molecular size. For water we have $\bar{v} \simeq 3.4 \cdot 10^3 cm/sec$, $\sigma \sim 10^{-15} cm^2$ and $r \sim 2.6 \cdot 10^{-8} cm$. Using these values, we obtain $k_r \approx 2.4 \cdot 10^{-34} cm^6/sec$.

Keeping in mind that during the dissociation process there may occur a preliminary dissociation of the water molecule into hydrogen and oxygen molecules, which in turn themselves undergo dissociation, let us obtain an estimate of the

reaction rates for hydrogen and oxygen molecules. For the hydrogen molecule we obtain:

$$\overline{v} = 1.45 \cdot 10^4 \sqrt{T} \text{ cm/sec}, \sigma \sim 10^{-15} \text{ cm}^2, \quad r = 2.5 \cdot 10^{-8} \text{ cm},$$

$$k_r = 9.4 \cdot 10^{-34} \sqrt{T} \; cm^6 / \sec .$$

For the oxygen molecule we obtain :

$$\overline{v} = 0.36 \cdot 10^4 \sqrt{T} \text{ cm/sec}, \sigma \sim 10^{-15} \text{ cm}^2, \quad r = 3.0 \cdot 10^{-8} \text{ cm},$$

$$k_r = 3.7 \cdot 10^{-34} \sqrt{T} \; cm^6 / \sec .$$

Now, using Eq. (3.15) and taking into account that a near-total dissociation (say 90%; see following section) is attained at temperatures of at least several thousand degrees, for $n \approx 10^{20} cm^{-3}$ we find $\tau_d \leq 10^{-8} sec.$

In conclusion, we have obtained that the rates of dissociation and ionization, attainment of a Maxwell distribution of the velocities , and attainment of the electron and ion temperature equilibrium are large compared to the rates of change of the state of the matter in the discharge channel. Such a result allows us to consider the plasma in the channels as being in equilibrium.

3.5. Composition of the gas in the discharge channel

The state of equilibrium of the plasma makes it easy to determine its composition. Let us consider first the dissociation process. The dissociation of a water molecule can occur in different ways. For example, a water molecule can break up first into hydrogen and oxygen molecules, which, in turn, can themselves dissociate at higher temperatures, or, the molecule can directly disintegrate into atoms, etc.

Let us estimate the conditions for the total dissociation of a water molecule by considering one concrete dissociation scheme. Namely, let us examine the breakup of a water molecule into hydrogen and oxygen molecules. The dissociation energy in this process is $D \approx 2.48 eV/molecule \approx 57 \, kcal/mol$,the characteristic temperature $D/k \approx 38,800 \, ^\circ K$. The hydrogen and oxygen molecules have large binding energies. For H_2: $D \approx 4.48 ev/molecule = 103 \, kcal/mol$,

$D/k = 52,000\,°K$; for O_2: $D \approx 5.11\,ev/molecule = 118\,kcal/mol$, $D/k = 59,400\,°K$.

Let us note also that the energy of dissociation of the H_2O molecule into three atoms equals $D \approx 10eV/molecule \approx 230.5\,kcal/mol$; $D/k = 116,000\,°K$.

In the breakup of the water molecule according to the scheme under consideration, its dissociation is determined by the dissociation of the hydrogen and oxygen molecules. Let us, therefore, examine these processes.

The degree of dissociation of a gas of diatomic molecules can be determined from the condition of a minimum of free energy.[1] The formula obtained from this condition can be conveniently written as [3]

$$\frac{\alpha_m^2}{1-\alpha_m} = \frac{\rho_d}{\rho} e^{-\frac{D}{kT}}\,, \tag{3.16}$$

where $\alpha_m = n_a/(n_a + 2n_M)$ is the mass concentration of the atom component; n_a,n_M are, respectively ,the number of atoms and molecules per cm^3; for hydrogen $\rho_d = 1.80\,g/cm^3$ and for oxygen $\rho_d = 150\,g/cm^3$; D is the dissociation energy. As an example, in Table 3.6 the results are given of the calculation of the degree of dissociation for hydrogen and oxygen at a pressure $p = 500\,atm$. As one can see, a noticeable dissociation already takes place at temperatures $T \ll D/k$ (see also the calculation of the plasma composition reported in ref. [6]).

Table 3.6

T $[°K]$	$\alpha_m = \frac{n_a}{n_a+n_m}$	
	D/k=52000 $°K$ (hydrogen)	D/k=59000 $°K$ (oxigen)
4000	0.074	0.077
5000	0.250	0.260
6000	0.560	0.620
9000	0.945	0.975
12000	0.985	0.995

This is due to the large statistical weights of the dissociated states, which reflect the fact that at $kT \ll D$ the molecules "are broken up" in collisions with the fast particles belonging to the far tail of the Maxwell velocity distribution [3].

For these same reasons, a gas is already ionized at small temperatures l compared to the characteristic ionization temperature I/k, where I is the ionization potential.

In the temperature range that interests us, when only the primary atom ionization is essential, the degree of ionization is determined by the Sach formula (see [3])

$$\frac{n_e n_i}{n_a} = A\frac{\Sigma_i}{\Sigma_a} T^{3/2} e^{-\frac{I}{kT}} . \tag{3.17}$$

Here, n_e, n_i, n_a are, respectively, the number of electrons, ions, and atoms per cm^3;

$$A = 2\left(\frac{2\pi m_e k}{h^2}\right)^{3/2} = 4.85 \cdot 10^{15} cm^{-3} \cdot degree^{-3/2} = 6.06 \cdot 10^{21} cm^{-3} \cdot eV^{-3/2}.$$

Σ_i, Σ_a are the statistical sums for ions and atoms; I is the ionization potential; T is the temperature. For hydrogen and oxygen in the considered temperature range, the ratio Σ_i/Σ_a is close to one. In fact, for temperatures not too high that are Σ_i/Σ_a is approximately equal to the ratio of the statistical weights of the free states of ions and atoms; this ratio is $1/2$ for hydrogen and $4/9$ for oxygen. The ionization potentials for hydrogen and oxygen are also close to each other; they are approximately equal to $13.6\,eV$. In Table 3.7 we give the results of the calculation of the plasma composition (either hydrogen or oxygen) for typical particle concentrations and temperatures.

Table 3.7

T $[^oK]$	n_a $[cm^{-3}]$	n_e $[cm^{-3}]$	$\alpha_m = \frac{n_e}{n_a+n_e}$	$\ln\Delta$
10000	10^{20}	$1.84 \cdot 10^{17}$	$0.184 \cdot 10^{-2}$	2.67
15000	10^{20}	$3.46 \cdot 10^{18}$	0.034	1.81
20000	10^{20}	$1.60 \cdot 10^{19}$	0.138	1.48
30000	10^{20}	$8.14 \cdot 10^{19}$	0.447	1.27
10000	$3 \cdot 10^{20}$	$3.18 \cdot 10^{17}$	$0.106 \cdot 10^{-2}$	2.40
15000	$3 \cdot 10^{20}$	$5.99 \cdot 10^{18}$	0.0196	1.54
20000	$3 \cdot 10^{20}$	$2.78 \cdot 10^{19}$	0.085	1.20
30000	$3 \cdot 10^{20}$	$1.14 \cdot 10^{20}$	0.319	1.00

As we see, when there is a formation of hydrogen-oxygen plasma, the degree of ionization in the discharge channel in water is usually large. However, due to the large density, the concentration of charged particles proves to be quite high, reaching 10^{18}–$10^{19} \cdot cm^{-3}$.

Let us clarify how strongly an ionized gas with such particle concentrations deviates from an ideal ionized gas. An ionized gas is considered ideal, if the

energy of the Coulomb interaction of neighboring particles is small compared to the their thermal energy, i.e., if the condition $(Ze)^2/r_0 \ll kT$ is satisfied; here , Z is the mean charge of the two particles; $r_0 \approx n^{-1/3}$ is the mean distance between them; and n is the number of particles per cm^3. This inequality can be rewritten as (see [3]) :

$$n \ll 2.2 \cdot 10^2 \left(\frac{T^o}{Z^3}\right)^3 \frac{1}{cm^3} \,. \tag{3.18}$$

In plasmas generated by discharges in liquids we typically have $n_e \sim n_i \sim 10^{18} - 10^{19}$; $T \approx 2 \cdot 10^4\,^\circ K$; $Z = 1$; thus the condition (3.18) is fulfilled: $10^{19} \ll 1.76 \cdot 10^{21}$. The presence of the Coulomb interaction between particles is the source of attractive forces between them, since each ion surrounds itself with a cloud of particles of opposite charge. This attraction exerts an influence on the gas state in two respects (see [3]). On the one hand, it decreases somewhat the pressure and energy of the gas, as in a Van der Waals gas of attracting particles. On the other hand, the presence of an attractive force means that an electron has a certain binding energy in the ionized gas and therefore somewhat less energy is necessary to separate it from the atom; this in turn manifests itself in an increased ionization potential.

The second effect is more perceptible, since even a small correction in the ionization potential leads to a noticeable shift in the ionization equilibrium, due to the fact that it appears in the exponent. Using the Debye-Hückel method we can calculate the corrections introduced by the Coulomb interactions in the thermodynamic functions of the ionized gas.

As was shown in [3], the correction to the pressure for a singly ionized gas is

$$p_e = -\frac{2e^3}{3}\sqrt{\frac{2\pi}{kT}}(n_e)^{3/2} \,,$$

and the correction to the ionization potential is given by the formula

$$\Delta I = 2e^3\left(\frac{2\pi n_e}{kT}\right)^{1/2} \,.$$

These calculations, however, apply only to gas weakly deviating from an ideal gas, when the Debye radius is large compared to the mean distance between particles; this can be expressed by the condition that

$$n << \left(\frac{kT}{4\pi e^2 \bar{Z}^2}\right)^3 = 1.10 \cdot 10^5 \left(\frac{T}{\bar{Z}^2}\right)^3 cm^{-3} \,, \tag{3.19}$$

where Z is the mean charge of the particle.

From this it follows that at $T = 20,000°K$, in order for the Debye-Hückel theory to be applicable, the particle concentration must be less than $10^{18} cm^{-3}$, while we know that the concentration of charged particles in a charged plasma reaches 10^{18}–$10^{19} cm^{-3}$. Thus, this approach is not applicable. We can only say that the values for the degree of ionization for a hydrogen (or oxygen) plasma given in Table 3.7 are somehawt lower as a consequence of the fact that a drop in the ionization potential was not taken into account. This circumstance, however, does not affect in any essential way the hydrodynamic theory of discharges we will to set forth, because the contribution of the ionization energy to the volume energy of the plasma is negligible, as we shall soon see, and therefore the errors in the calculations of the degree of ionization are not reflected in the calculation of the internal energy.

The number n_a^* of atoms and ions that are in an excited state is determined by the Boltzmann formula

$$n_a^*/n_a = g^*/g_a \exp\left(-I_{exc}/kT\right) , \tag{3.20}$$

where g_a and g_a^* are the statistical weights of the ground and excited states of the atom.

The total number of particles in a unit volume of plasma is $n = n_a + n_i + n_e = n_a + 2n_e$, since for single ionization $n_i = n_e$. The internal energy of a unit volume of plasma that forms in a discharge in water is composed of: (i) kinetic energy of the particles $w_k = \frac{3}{2}(n_a + 2n_e)kT$; (ii) evaporation energy $w_{evap} = \frac{n}{3} D_{evap}$, where $D_{evap} = 0.045 eV/molec = 1.05 kcal/mol$ is the evaporation energy of a water molecule; (iii) dissociation energy $w_d = \frac{D_d}{3} n_a$, where D_d is a dissociation energy equal to $10\, eV/molec$; (iv) ionization energy $W_i = n_e I$, where I is the ionization potential which for hydrogen and oxygen equals approximately $13.6\, eV$; (v) excitation energy of the atoms $w_{exc} = n_a^* I_{exc}$; (vi) excitation energy of the ions $w'_{exc} = n_a^* I'_{exc}$, or

$$w = w_k + w_i + w_d + w_{exc} + w'_{exc} . \tag{3.21}$$

The contributions of the various terms of this sum as a function of the temperature are plotted in Fig. 3.19 for the case $p = 500\, atm$. The negligible values of the excitation energy are not plotted. As we can see, the energy of a unit volume of plasma is mainly composed of the kinetic energy of the particles and the dissociation energy. The ionization energy does not contribute significantly. The contribution from the other terms is negligible. In conclusion, the internal energy of a unit volume of water plasma in a temperature range

corresponding to the primary atom ionization can, practically, be calculated with the formula

$$w = \frac{3}{2}nkT + n\frac{D_d}{3} + n_e I\,, \tag{3.22}$$

where $n = n_a + 2n_e$ is the total number of particles in the unit volume; D_d is the dissociation energy per molecule, and I is the ionization energy.

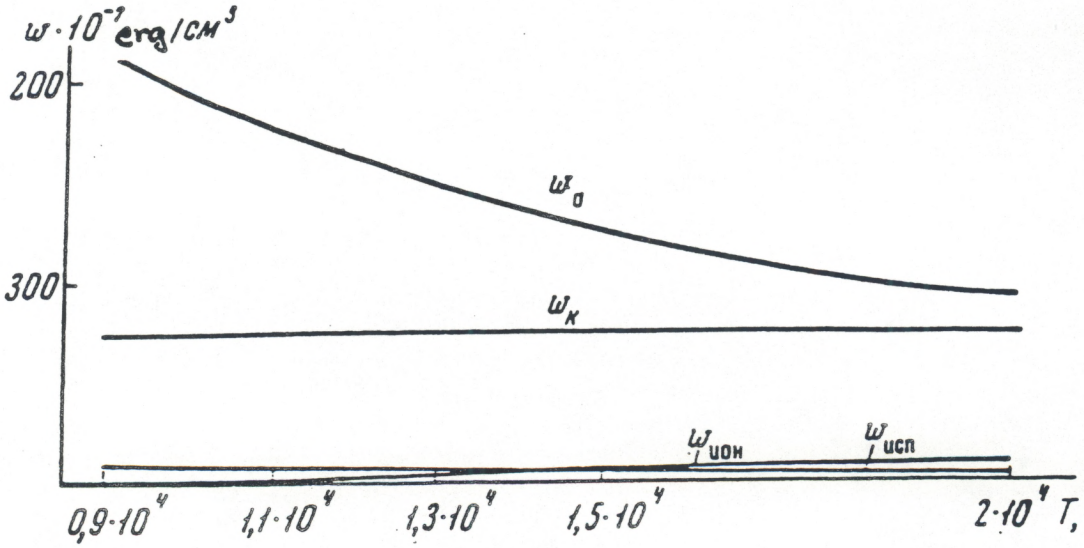

Fig. 3.19. Plasma energy density as a function of the temperature.

For an ideal gas, the internal energy of a unit volume is given by

$$w = \frac{p}{\gamma - 1} , \tag{3.23}$$

where $\gamma = c_p/c_v = 1.66$ for a monoatomic gas.

In the case of a plasma, this ratio varies, but the variations within the pressure and temperature ranges that interest us are small. This allows us to introduce, as usually done[3], an effective constant γ that approximates the actual value of this quantity. The value of this effective γ was chosen to be equal to the mean values of $\gamma's$ in the pressure range from 50 to $1500\,atm$, and temperature range from $15,000$ to $25,000°K$. These values are given in the last column of Table 3.8.

From this table we see that the value of γ proved to be about 1.26, which is the value that we shall be using in the following. It is interesting to note that at $\gamma = 1.26$, the energy of a unit volume of plasma is more than three times greater than the energy of a unit volume of monoatomic ideal gas at the same pressure.

3.6. Kinetic coefficients of gas in the discharge channel

We shall now give estimates of the kinetic coefficients, i.e., the coefficients of electric and thermal conductivity of the plasma in the discharge channel, as well as the coefficients of thermal conductivity in the transition layer between plasma and water. The plasma resistance is due to the collisions of electrons with ions and neutral atoms. The time between collisions can be estimated using the formulas [3]

$$\frac{1}{\tau'_{ei}} \approx 3.6 \frac{n_i Z^2 \ln \Lambda}{T_e^{3/2}} \tag{3.24}$$

and

$$\frac{1}{\tau'_{ea}} \approx n_a \bar{v}_e \sigma_{ea} , \tag{3.25}$$

where n_i and n_a are the number of ions and atoms per cm^3; Z is the ion charge; $\bar{v}_e = (8kT/\pi m_e)^{1/2}$ is the mean thermal electron velocity; σ_{ea} is the electron-atom scattering cross section. Let us note that the formulas (3.24) and (3.25) differ from Eqs. (3.12) and (3.13) only in the absence of the factor equal to the ratio of electron mass and atom mass, which takes into account the fact that a large number of collisions is necessary for a noticeable exchange of energy between particles to occur.

In Table 3.9 the times are given , calculated using these formulas, between particle collisions for typical temperatures and plasma concentrations for a discharge channel in a liquid.

There, we also give the cross sections for Coulomb collisions which can be written as .

$$\sigma_{ei} \approx 1.2 \cdot 10^{-5} \frac{\ln \Lambda}{T_e^2} \,. \tag{3.26}$$

In deriving Eq. (3.26) use has been made of Eq. (3.24) and of the usual relation

$$\frac{1}{\tau'_{ei}} \sim n_i \bar{v}_e \sigma_{ei} \,.$$

In the same table the crosssections for electron-atom scattering are also reported, taken from ref. [4]. We want to emphasize once again that the values given in this table are rough estimates which provide only the order of magnitude of the calculated quantities. Nevertheless, these values give some idea of the collision time of the electrons (and thus of the electrons' mean free path). Furthermore, we can conclude that if the frequencies of the collisions of electrons with atoms and hydrogen ions are comparable within the concentration and temperature ranges that interest us here, then electrons in oxygen will collide with ions more frequently than with atoms.

Knowing the collision frequencies, it is easy to determine the electric conductivity of the plasma. The general formula for the conductivity has the form [8]

$$\eta \approx \frac{n_e e^2 \tau'}{m_e} \,, \tag{3.27}$$

where n_e is the number of electrons per cm^3; e is the electron charge; m_e the electron mass; τ' the time between collision of electrons with ions and neutral atoms

$$\frac{1}{\tau'} = \frac{1}{\tau'_{ei}} + \frac{1}{\tau'_{ea}} \,. \tag{3.28}$$

If $\tau'_{ei} \ll \tau'_{ea}$, i.e., the resistance is determined by the electron-ion collisions, then an expression for the conductivity that is somewhat more accurate than that obtained by direct substitution of (3.24) into (3.27) (taking into account the electron-electron collisions) was obtained by Spitzer [9] (see also ref. [3]). Such expression has the form

$$\eta_{ei} = 2.63 \cdot 10^4 \gamma(Z) \frac{T^{\frac{3}{2}}}{Z \ln \Lambda} \frac{1}{\Omega \cdot cm} = 2.38 \cdot 10^8 \gamma(Z) \frac{T^{\frac{3}{2}}}{Z \ln \Lambda} sec^{-1} \,, \tag{3.29}$$

where Z is the particle charge and 1 ohm·cm^{-1} =9·10^{11} sec^{-1} .

$$\Lambda = \frac{3(kT)^{3/2}}{2\sqrt{(4\pi)}Z^2e^3\sqrt{n_e}}$$
$$\gamma(1) = 0.58; \quad \gamma(2) = 0.68; \quad \gamma(4) = 0.78.$$

If, on the other hand, $\tau'_{ea} \ll \tau'_{ei}$, i.e., the plasma resistance is determined by the collisions of electrons with neutral atoms, then the expression for the conductivity is [10]

$$\eta_{ea} = 0.51\frac{e^2n_e}{\sqrt{m_ekT}}\frac{1}{n\sigma_{ea}} . \tag{3.30}$$

In a general case, as we can see from Eqs. (3.27) and (3.28), the inverses of the conductivity sum up

$$\frac{1}{\eta} = \frac{1}{\eta_{ei}} + \frac{1}{\eta_{ea}} .$$

The plot of η as a function of the temperature at pressures of 500 and 700 atm is shown in Fig. 3.20.

A magnetic field affects the kinetics of the electron if the electron gyration frequency $\omega = eH/mc$ is comparable with the collision frequency $1/\tau$, i.e., if $\omega\tau \sim 1$, or in other words, if during the time between collisions the electron can cover a significant part of the orbit. If, on the other hand, $\omega\tau \ll 1$, i.e., the collisions disturb the gyration motion, then the effect of the magnetic field is not important. This is usually the case in plasmas generated by electric discharges in liquids. In fact, using $\omega = eH/mc$, one obtains for the magnetic field $H = 2I/rc$, and setting $I \approx 3 \cdot 10^4\, A$, $r \approx 1\, cm$, we obtain $H \approx 6 \cdot 10^3$ Oe and $\omega \approx 10^{11} sec^{-1}$. From the data of Table 3.9, $\tau \approx 10^{-14} sec$, and therefore $\omega\tau \approx 10^{-3}$.

The effect of the magnetic field manifests itself also in the formation of the skin-layer. The penetration depth of the magnetic field is

$$\delta^2 \approx \frac{c^2t}{2\pi\eta} , \tag{3.31}$$

where c is the speed of light.

The conductivity of the plasma in discharge channels is usually about $10^{14} sec^{-1}$. Thus, the ratio of the thickness of the skin-layer to the radius of the channel, which is on the order of of $1\,cm$, is

$$\delta^2/R_0^2 \sim \frac{c^2 t}{2\pi\eta R_0^2} \sim 10^2 \gg 1 \ .$$

Let us note that the possibility of neglecting the skin-effect also means that the magnetic pressure is small compared to the gas-kinetic pressure in the channel (see ref. [11]).

In fact, since a sizeable part of the energy liberated in the channel in the form of Joule heat goes to increasing the internal energy of the gas and the density of the internal energy is of the same order of magnitude as the gas-kinetic pressure, we have

$$p \sim \frac{j^2}{\eta} t \sim \frac{I^2 t}{(\pi R_0^2)^2 \eta} \sim \frac{H^2}{8\pi} \frac{\delta^2}{R_0^2} \ ,$$

whence

$$\frac{p}{\frac{H^2}{8\pi}} \sim \frac{\delta^2}{R_0^2} \tag{3.32}$$

and therefore the effect of the magnetic pressure may be neglected when the skin-effect is not important.

Indeed, a direct estimate of the magnetic pressure gives

$$p_m \sim \frac{H^2}{8\pi} \ , \qquad H \sim \frac{2I}{cR_0} .$$

Setting $I \sim 4 \cdot 10^4 A$, $R_0 \sim 1\,cm$ and $H \sim 8 \cdot 10^3 Oersteds$, we obtain $p_m \sim 2.0\,atm$, which is indeed small compared to the gas-kinetic pressure which is equal to $10^3\,atm$.

The energy transport in the discharge channel is accomplished by atoms (or ions), electrons, and photons. These processes are characterized by the coefficients of gas-kinetic, electron and radiative thermal conductivity, respectively [3,10]. The coefficient of gas-kinetic thermal conductivity is

$$\kappa_{\text{g-k}} = \frac{1}{3} l_a \bar{v} \rho c_v \ , \tag{3.33}$$

where $l_a = (n\sigma_a)^{-1}$ is the mean free path; $\bar{v} = \sqrt{9kT/\pi m}$ is the mean thermal speed of the atoms; ρ is the gas density; c_v is the specific heat at constant volume so that ρc_v is the heat capacity of a unit volume; n is the number of particles per cm^3; σ_a is the scattering crosssection of the atoms.

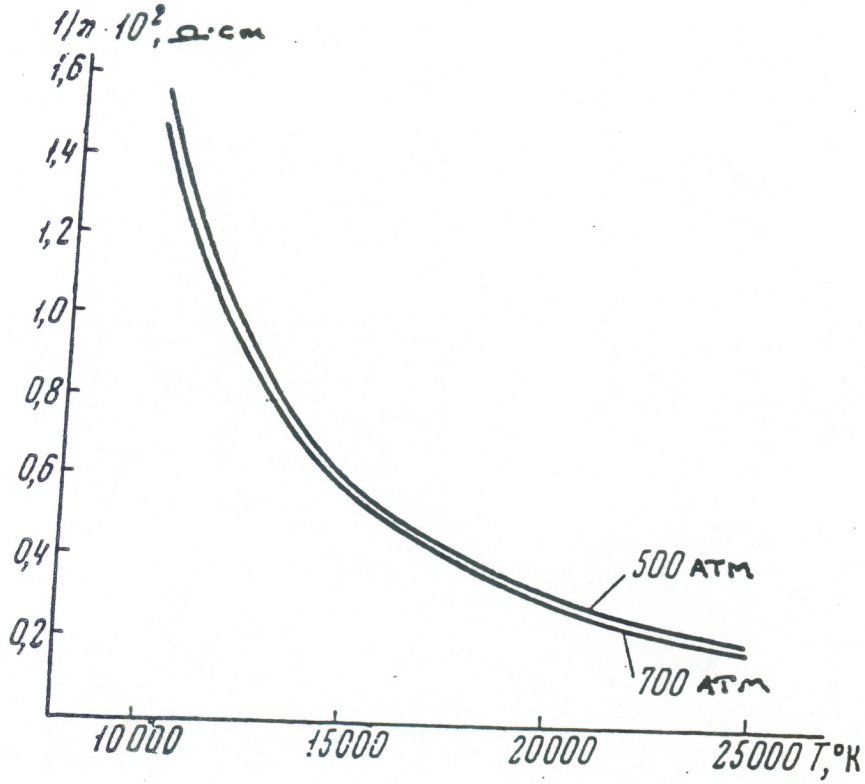

Fig. 3.20. Plasma conductivity as a function of the temperature.

The coefficient of electron thermal conductivity is given by

$$\kappa_{el} = \xi \cdot 1.93 \cdot 10^{-5} \frac{T^{5/2}}{Z \ln \Lambda} erg/sec \cdot cm \cdot degree \,, \tag{3.34}$$

where Z is the ion charge; $\ln \Lambda$ is the Colulomb logarithm; $\xi(Z)$ is a function with a weak dependence on Z: $\xi(1) = 0.95$, $\xi(2) = 1.5$, $\xi(4) = 2.1$. Finally, the coefficient of radiative thermal conductivity is given by

$$\kappa_{rad} = \frac{1}{3} l_c 16 \sigma T^3 \,, \tag{3.35}$$

where l_c is the radiation light mean free path, and $\sigma = 5.67 \cdot 10^{-5}\, erg/cm^2 \cdot sec \cdot degree^4$ is the Stefan-Boltzmann constant.

We need to stress that the radiation transfer has a heat conduction nature if the radiation energy density is at every point close to the equilibrium value. For this to occur, the light mean free path l_c must be small compared to the size of the heated region. The free mean path is given by the formula [3]

$$l_c = 0.9 \cdot 10^7 \frac{T^3}{nZ^2} e^{\frac{I}{kT}} \,, \tag{3.36}$$

where n is the number of atoms per cm^3, I is the atom ionization potential , and $Z = 1$.

If, on the other hand, the mean free path l_c is comparable to or larger than the size of the heated region, then the radiation is not in an equilibrium state, and freely escapes from the volume of the heated region.

The mean free path l_c has a strong dependence on the temperature. In hydrogen or oxygen ($I = 13.6\, eV$), for example, $T = 1.5 \cdot 10^{4\circ} K$ and $n = 10^{20} cm^{-3}$ and $l_c = 1\, cm$, while at $T = 2 \cdot 10^4$ and $n = 10^{20} cm^{-5}$, $l_c \sim 10^{-1}\, cm$. The characteristic size of a discharge channel is usually about $1 cm$, and thus the radiatiative heat transfer can occur in it.

Let us compare the coefficients of thermal conductivity for the three heat transfer mechanisms discussed above. In hydrogen, at $T \approx 20 \cdot 10^3\, ^\circ K$, $n = 10^{20} cm^{-3}$, $\kappa_{\text{g-k}} \approx 1.5 \cdot 10^5 erg/cm \cdot sec \cdot degree$, $\kappa_e \approx 5 \cdot 10^5 erg/cm \cdot sec \cdot degree$ and $\kappa_r \approx 2.8 \cdot 10^8 erg/cm \cdot sec \cdot degree$. The heat conduction leads to the temperature equalization in the channel. This process, as it is well known [3], is characterized by the length scale $\delta \sim 2\sqrt{\chi t}$, which is a measure of the size of the region heated during the time t; χ is the coefficient of temperature conductivity.

In a gas, the coefficient of temperature conductivity is approximately equal to the atomic diffusion coefficient

$$\chi_{\text{g-k}} = \frac{1}{3} l_a \bar{v} \,, \tag{3.37}$$

where l_a is the atom mean free path and $\bar{v}$ is mean thermal speed.

Similarly, the coefficient of electron temperature conductivity can be estimated using the formula

$$\chi_{el} \approx \frac{1}{3} l_e \bar{v}_e \ , \tag{3.38}$$

where l_a is the electron mean free path and $\bar{v}_e$ its mean thermal speed.

The coefficient of radiative temperature conductivity χ_{rad} is

$$\chi_{rad} = \frac{1}{3} l_c c \frac{c_{rad}}{\rho c_v} \ . \tag{3.39}$$

As we can see, unlike the temperature conductivity in gases, where the energy carriers are molecules, the radiative temperature conductivity is not simply equal to the radiative diffusion coefficient $l_c c/3$, but it contains an extra factor equal to the ratio of heat capacities of radiation and matter. The reason for the presence of this factor is that, in this case, radiation plays the role of energy carrier from one gas region to the other, thus causing the heating (or the cooling) of the matter [3].

Below, we give the values of the coefficients of temperature conductivity and of the length scales of the heated region for typical conditions in a discharge channel: $T = 20,000°K$, $n = 10^{20} cm^{-3}$. We also assume that the discharge duration equals $10^{-4} sec$. Using Eqs. (3.37)–(3.39) for a hydrogen gas we obtain:

$$\begin{aligned} \kappa_{g-k} &\approx 6 \text{ cm}^2/\text{sec}, \delta_{g-k} \approx 5 \cdot 10^{-2} \text{ cm}, \kappa_e \approx 25 \text{ cm}^2/\text{sec}, \qquad (3.40) \\ \delta_e &\approx 10^{-1} \text{ cm}, \quad \kappa_{rad} \approx 10^4 \ cm^2/\text{sec}, \quad \delta_{rad} \approx 2 \cdot 10^{-2} \text{ cm}. \qquad (1) \end{aligned}$$

As we can see, the radiative heat transfer provides a fast temperature equalization inside the channel, which allows us to consider the channel plasma approximately homogeneously.

A strongly heated gas in the channel is separated from the surrounding water by a transition layer in which the temperature drops from several tens of thousand to several hundred degrees. The transition layer is where the dissociation of the newly evaporated molecules takes place. The gas in the transition layer is relatively cold and therefore transparent to radiation. The heat release in it is due to the heat conduction from the hotter central part of the channel. Together with the usual gas-kinetic heat conduction mechanisms, in the transition layer another peculiar mechanism works that is connected with the transfer of the dissociation energy by molecules. Atoms arriving into cold layers undergo a recombination, thus releasing dissociation energy, while molecules that come into layers of higher temperatures undergo dissociation, thus absorbing energy.

For a diatomic gas, the coefficient of thermal conductivity due to such a mechanism was calculated in the work of refs. [5,12], and is approximately given as

$$\kappa_d = \frac{3}{16}\left(\frac{1}{\pi m_a}\right)^{1/2}\frac{D^2(\alpha-\alpha^2)}{d_{12}^2\sqrt{kT^3}}, \quad d_{12} = \frac{d_1+d_2}{2}, \quad \alpha = \frac{n_a}{n_a+n_M}. \qquad (3.41)$$

Here, m_a is the atom mass, D the dissociation energy, α the degree of dissociation, and d_1 and d_2 the diameters of the atom and molecule, respectively.

The coefficient of dissociation thermal conductivity reaches a maximum at a temperature at which half of the molecules are dissociated. The coefficient value in the peak region is a few times larger than the gas-kinetic heat conductivity.

For example, in hydrogen, at $T \approx 7000\,°K$, $p = 5000\,atm$, $n = 5\cdot 10^{20} cm^{-3}$, where n is the total number of particles per cm^3, we have $\kappa_d = 7\cdot 10^4 erg/cm\cdot sec\cdot degree$ and $\kappa_{\text{g-k}} \approx 10^4 erg/cm\cdot sec\cdot degree$. In oxygen, at $T = 6000\,°K$, $p = 500\,atm$ and $n = 6\cdot 10^{20}$, we have $\kappa_d = 1.6\cdot 10^5 erg/cm\cdot sec\cdot degree$ and $\kappa_{\text{g-k}} \approx 3\cdot 10^4 erg/cm\cdot sec\cdot degree$. In water steam, according to the data of [6], the maximum value is $\kappa_d = 3.5\cdot 10^5 erg/cm\cdot sec\cdot degree$.

The relation between dissociation and gas-kinetic thermal conductivity becomes more clear if we take into account that the value of the dissociation thermal conductivity coefficient can be estimated with the usual formula $\kappa = (1/3)l\bar{v}c_{vd}$, where c_{vd} must here be understood as the specific heat capacity including the energy loss on dissociation. With this in mind, the ratio $\kappa_d/\kappa_g \sim c_{vd}/c_v$, where c_{vd} and c_v are, respectively, the specific dissociation and gas-kinetic heat capacities.

Taking into account that $c_v = \left(\frac{\partial w}{\partial T}\right)_p$, and $a \sim \frac{D}{3}n_a$, where the temperature dependence of n_a is given by Eq. (3.16), we obtain $\kappa_d/\kappa_g \sim 10^{-1}(D/kT_D)$, where T_D is the temperature at which the degree of dissociation is close to $1/2$. As we have already mentioned above (see Table 3.6), such temperature is small compared to D/k, which is in fact why the coefficient of dissociation thermal conductivity is larger than that of gas-kinetic thermal conductivity.

The value of the temperature conductivity coefficient, both in the case of gas-kinetic and dissociation heat conduction, is determined by the diffusion coefficient of the molecules (see Eq. (3.37)) and is equal to $0.4\,cm^2/sec$ at $T = 6000°K$, $p = 500\,atm$ and $n = 6\cdot 10^{20} cm^{-3}$.

In concluding this section, let us examine even cooler channel layers, where the water vapors are not dissociated. In such layers the coefficient of temperature conductivity is lower than for the hotter ones. Thus, for example, using the data of [13], the temperature conductivity of water vapor at $T = 2500\,°K$, $p = 300\,atm$, $\rho = 0.175\,g/cm^3$, $c_p = 3\cdot 10^7 erg/g\cdot degree$ is $\chi = 0.7\cdot 10^{-3} cm^2/sec$; at $T = 700\,°K$, $p = 300\,atm$, $\rho = 0.33\,g/cm^3$ for the same coefficient we have $\chi = 0.7\cdot 10^{-3} cm^2/sec$. Finally, in water, in a temperature range from 623 to $293\,°K$ (room temperature), $\chi = 1.4\cdot 10^{-3} cm^2/sec$, $c_p = 4.18\cdot 10^7 erg/g\cdot degree$.

3.7. Plasma temperature in the discharge channel. Equation of energy balance

The temperature of the plasma in the channel is usually determined experimentally by optical methods. Assuming that the channel radiates as a blackbody, it is possible to determine the temperature of the matter in it by the relative intensity of various regions of the radiation spectrum. In practice, such measurements are carried out in the visible part of the spectra that corresponds to the transparency region of the water.

Measurements carried out in [14–16] show that in liquid discharges in which an energy release of several kilojoules occurs in a few tens of microseconds, the temperature in the channel lies in the first atom ionization region and amounts to about 15,000–25,000 $°K$. The radiation spectrum proves to be a Plank spectrum, i.e. it corresponds to that of a blackbody radiation.

The temperature of the plasma can be estimated also from measurements of the electric resistance of the channel, if the channel radius and the pressure in it are known. In fact, knowing the resistance and the radius of the channel, it is possible to determine the conductivity, which, according to Eq. (3.29), is mainly determined by the channel temperature and which depends only weakly (logarithmically) on the electron concentration.

The plot of the conductivity as function of temperature is shown in Fig. 3.20 for various values of the pressure in the channel. Using this plot, it is not difficult to solve the inverse problem, i.e., to determine the temperature of the channel from its conductivity at a given pressure. Estimates of this kind were obtained in ref. [17] and led to results in agreement with the data mentioned above obtained using optical methods. For example, for discharge $No.8$ (see Table 3.5), for which in a channel $l = 7\,cm$ long and in a time $\tau = 10^{-4}\,sec$ an energy release of $3 \cdot 10^3\,J$ occured, the temperature proved to be about $15,000\,°K$.

Due to the high particle density, the hot plasma in the discharge channel serves as an intense, blackbody, source of light. This occurrence introduces the possibility of using electric discharges as sources of light with high brightness [18,19].

The portion of energy carried out by light radiation depends strongly on the channel temperature. Such a portion is not large at $150,000°K$, but it becomes noticeable at temperatures around $20,000\,°K$. Thus, for example, for discharge $No.8$ (see Table 3.5), the experimental data and the theoretical estimates (see Sec. 3.2) show that the characteristic radius R_0 of a channel, whose shape is close to a cylinder, is on the order of $1cm$. Assuming that the temperature of the channel plasma is $T_{eff} = 15,000\,°K$ and that the channel mean radius is $R_0/2$, we obtain that the energy of the light radiation is

$$\Delta E_{rad} \approx 2\pi\left(\frac{R_0}{2}\right) l\sigma T_{eff}^4 \sim 600J.$$

At $T_{eff} = 20,000\,°K$, the radiation energy amounts already to abut $1800\,J$. However, not all the light radiation escapes from the channel. At temperatures on the order of $15,000\,°K$ and higher, the wave length corresponding to the peak value in the Planck distribution is given by Wien's law $\lambda_m = A/T \approx 2000$, i.e.,

lies in the ultraviolet region of the spectrum, and the water strongly absorbs light in this region. Thus, for example, at 1500 the absorption coefficient of light in water is about $10^4 cm^{-1}$. Therefore, only the visible part of the radiation escapes from the channel, while a significant portion of it remains "trapped".

This gives us a justification for neglecting the energy carried out of the channel in the form of light radiation when calculating the discharge energy balance. On the other hand, the assumption that radiation is "trapped" allows us to derive a rough estimate of the temperature in the discharge channel. However, such estimate is only as "guide" , helpful in clarifying the qualitative picture of the phenomenon.

In fact, assuming that the radiation is absorbed in the channel shell and is used up for the evaporation and dissociation of water particles, the number for particles that evaporate from a unit surface in a unit of time is

$$\sigma T_{eff}^4 / D = \sigma T^4 l_c / D R_0,$$

where $T_{eff}^4 = (l_c/R_0)T^4$ [3]; D is the dissociation energy for a water molecule per atom; R_0 is the characteristic radius of the channel. In discharge plasmas $(l_c/R_0)^{1/4} \approx 1$, and thus $T_{eff} \approx T$. The total number of particles transferred from the water into the channel is equal to

$$N = \sigma T^4 \tau S l_c / D R_0 \ ,$$

where S is the area of the channel surface; R_0 the channel radius; and τ is the discharge duration. Using this relation we can express the internal energy of the plasma in the discharge channel as a function of the temperature

$$W = \frac{pV}{\gamma - 1} = \frac{NkT}{\gamma - 1} = \frac{kTl_c}{\gamma - 1} \frac{\sigma T^4}{D R_0} \tau S. \tag{3.42}$$

The internal energy of the plasma is of the same order of magnitude as the total energy E liberated in the channel in a time τ

$$\frac{l_c k \sigma T^5}{R_0 (\gamma - 1) D} \tau S \sim E \ ,$$

whence

$$T \sim \left[\frac{E(\gamma - 1) D l_c}{\sigma l \tau S R_0} \right]^{1/5}. \tag{3.43}$$

The area of the channel surface S can be determined on the basis of theoretical estimates or experimental data; for cylindrical discharges $S = 2\pi R_0 l$, where

$$R_0 \approx \left(\frac{(\gamma - 1)}{\pi \rho} \tau^2 \frac{e}{l} \right)^{1/4};$$

for spherical $S = 4\pi R_0^2$, where

$$R_0 = \left(\frac{3}{4\pi}\frac{(\gamma-1)}{\rho}\tau^2 E\right)^{1/5}.$$

(See section 3.3.)

Let us give an example of the temperature estimate obtained using fomula (3.43). For discharge *No.* 8 (Table 3.5) with $l = 7\,cm$, $E \approx 3\cdot 10^3\,J$, $\tau = 10^{-4} sec$, $R_0 \approx 1\,cm$ and $S = 2\pi l R_0$, Eq. (3.43) gives $T \sim 1.5 \cdot 10^4\,°K$. It is interesting to note that, as we can see from Eq. (3.43), the temperature depends weakly on the value of the energy and on the time needed to release such energy. This peculiarity is in qualitative agreement with the experimental data.

On the basis of what has been said, we may approximately assume that the energy released in the channel is expended mainly for heating the matter in the discharge channel and to do the work of expanding the channel against the surrounding liquid.

The energy used up to heat the matter ruling this process is concentrated in the main, rather homogenenously heated part of the channel, while the energy stored in the thin transition layer is relatively small. Its value ΔE can be estimated with the formula $\Delta E \approx wS\delta$, where w is the energy of a unit volume; S is the area of the channel surface; and $\delta \sim 2\sqrt{\chi t}$ is the thickness of the transition layer. The value of the coefficient of temperature conductivity in the transition layer varies .

Let us examine first the temperature region corresponding to the molecule dissociation, i.e., $T \sim 6000\,°K$. For $p = 500\,atm$ and $n = 6\cdot 10^{20}$, the coefficient of temperature conductivity in this region is $0.4 cm^2/sec$ (see the end of the previous section), and the energy of the unit volume is about

$$w \sim \frac{D}{3} n \approx 3 \cdot 10^9 erg/cm^3.$$

Then, for discharge *No.* 8 (Table 3.5): $l = 7cm$, $E = 3 \cdot 10^3\,J$, $\tau = 10^{-4} sec$, so that we obtain: $\delta \approx 10^{-2} cm$ and $\Delta E = 70\,J$.

The quantity of energy stored in the cooler regions of the transition layer is not too large. Corresponding estimates, carried out for the discharge just mentioned and using the results of the previous section and information on the thermodynamic properties of water vapors [13], show that in the temperature region $T \approx 2500\,°K$, $\delta \approx 5 \cdot 10^{-3} cm$, $\Delta E \approx 10\,J$; at temperatures $T \approx 700\,°K$, $\delta \approx 5 \cdot 10^{-4} cm$, $\Delta E \approx 5\,J$. Finally, in the warm layer of water at temperatures $T \approx 350\,°K$, $\delta \approx 7 \cdot 10^{-4} cm$, $\Delta E \approx 10\,J$.

As a result, we may assume that the internal energy of the matter in the channel, taking the increase in the particle number into account, is determined by the energy of the plasma filling the channel. The energy density of such plasma is, according to Eq. (3.23), $w = p/(\gamma - 1)$ with $\gamma = 1.26$.

The work on the channel expansion is given by the expression $\int pdv$, since the expansion caused by the heating is negligible compared to the expansion

due to purely hydrodynamic process; in this sense the channel wall may be considered impermeable.

The equation for the energy balance in a discharge process can therefore be written in the form

$$\frac{d}{dt}\frac{pv}{\gamma - 1} + p\frac{dv}{dt} = N(t), \tag{3.44}$$

where $N(t)$ is the energy release rate in the channel. This equation will be studied more in detail in the following chapters.

REFERENCES to Chapter III

[1] Kuzhekin I. P. ,"Current cut-off and restrike in electrical discharges in a liquid," J. Tech. Phys, **36** (20, 338-444 (1966).

[2] Komel'kiv V.S., Kuznetzov N.A., Skvortzov Ju. V., "Expansion of a spark channel in a liquid," J. Tech. Phys. **30** .(10), 1165-1172 (1960).

[3]Zel'dovich Ja. B., Raizer Ju. P. *Physics of shock waves and high-temperature hydrodynamic phenomena* (Moscow, Nauka, 1966).

[4] MacDaniel I., *Collision processes in ionized gasses* (Moscow, MIR, 1967).

[5] Lighthill M. J. "Dynamics of a dissociating gas equilibrium flow," Fluid Mech. **2** (1), 1-32 (1957).

[6] Grekov L.I., Moskvich Ju. V., Romanychev V. S., Favorskij, *Basic properties of certain gasses at high temperatures* Moscow, IL(1960).

[7] Allen K. U. *Astrophysical quantitites* (Moscow, IL, 1960).

[8] Artzimovich L.A., *Controlled thermonuclear reactions* (Moscow, Fizmatgiz, 1961).

[9] Spitzer L. *Physics of completely ionized gasses,* (Moscow, IL, 1956).

[10] Zhdanov V.M., "Electrical conductivity of a partially ionized gas mixture in a magnetic field," J. Appl. Mech. Tech. Phys. (USA) **4** , 47-53 (1965).

[11] Braginskij S.I., "Theory of the development of a spark channel," J. Theor. Exp. Phys.**34** (6), 1548-1552 (1958).

[12] Butler N. and Brokay R., *Thermal conductivity of gas mixtures in chemical equilibrium.* In *Problems on the motion of the head of long-action rockets* (Moscow, IL, 1959).

[13] *Heat Engineering Handbook* (Manual for politechnical Institutes), (Moscow, Gosenergoizdat, 1957).

[14] Bopp G.A., "Estimates of the temperature of the puse discharge in liquids," *Optics and Spectroscopy*, **18,** 529-531 (1965).

[15] Martin E.A., "Experimental investigation of high-energy density, high pressure arc plasma,"J. Appl.Phys. **31**, 255 267 (1960).

[16] Kutzenko A. N., Kortnev A.V., "On the temperature of the spark discharge in liquid," Izvestije Vuzov, Phys. **1**, 112-114 (1963).

[17] Joffe A. I., Naugolnykh K.A. and Roj N.A., "Initial stage of electrical discharge in water," Zh. Priklad. Mekh. Tekh. Fiz. **4**, 108-112 (1964).

[18] Early H.C., Martin E.A., "The underwater spark; a photographic light source of high intrinsic brilliance," Trans. Amer. Inst. Elect. Engrs. I **74,** 788-790 (1956).

[19] Ogurtzova N.N., Podmoshenskij I.V., Shelemina V.M., "Characteristics of the plasma jet of a powerful capillary discharge," Optics and spectrosc. , **15** (6), 404-406 (1963).

[20]*Electric explosion of conductors,* (Moscow, Nauka, 1965).

Chapter IV

HYDRODYNAMICAL ASPECTS OF BUBBLE EXPANSION IN A LIQUID

4.1. Introduction

From the point of view of hydrodynamics, a spark discharge in a liquid may be regarded as the process of expansion of a bubble. The hydrodynamic characteristics of such a process depend on the relations between the three scale parameters of the phenomenon: the width l of the discharge gap, the characteristic radius R_0 of the channel and the characteristic wavelength $\lambda = c_0\tau$, where τ is the discharge duration. In this respect we can divide the possible cases into two classes.

In the first class we have the cases where $R_0 \ll \lambda$, i.e., situations in which the rate of expansion R_0/τ is small compared with the speed of sound c_0, and in which the perturbations in the fluid density caused by the channel expansion are insignificant. Among these cases we can further distinguish three cases that allow us to adopt a simple model for the channel form but differ among themselves for the relations between the gap width l and the other two scale parameters R_0 and λ.

If $l \ll R_0 \ll \lambda$ (Fig. 4.1,a), then the channel shape is obviously nearly spherical, which allows us to use the simplest spherical model for the calculations . When $R_0 \ll l \ll \lambda$ (Fig. 4.1,b), it is necessary to take into account the extension of the channel in the calculation of the hydrodynamic quantities near the discharge, while from the point of view of acoustics, the source can be considered, as before, close to being point-like. In such a case a cylindrical model is applicable. If $R_0 \ll \lambda \ll l$ (Fig. 4.1,c) we may apply the cylindrical model with the cylinder length being comparable to the wavelength.

To the second class belong regimes in which $R_0 \sim \lambda$ or $R_0 > \lambda$, which correspond to channel expansions at rates close to or higher than the speed of sound; in this case, the perturbations in the fluid density generated by the channel expansion become strong and it is then necessary to take into account the compressibility of the fluid. For this second group we can also distinguish two simplest cases, in which either the spherical model ($l \ll \lambda \leq R_0$) or the cylindrical model ($\lambda \leq R_0 \ll l$) may be applied (Figs. 4.1, d, e).

In the present chapter we examine certain aspects of the hydrodynamic problem of the expansion of spherical and cylindrica bubbles, in a fluid, remembering that we will be making use of these results in the study of the hydrodynamic phenomena generated by discharges.

We will be interested, in particular, in the pressure exerted by the fluid on the expanding bubble, as well as in the characteristics of the compression wave emitted by the expanding bubble. Furthermore, we will solve the problem of the pulsation of a gas bubble in a fluid.

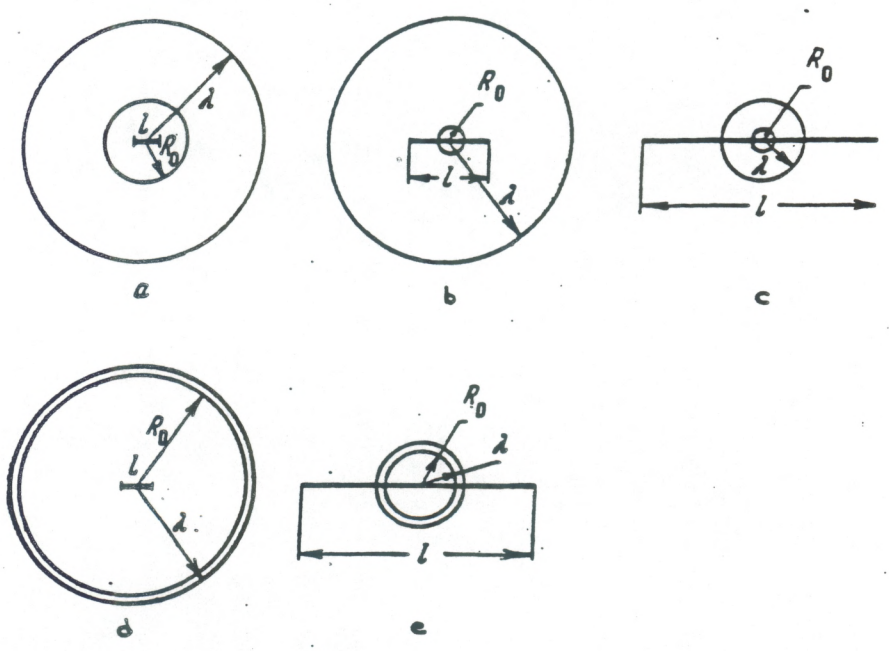

Fig. 4.1. Length parameters in the problem of a bubble expansion.

The motion of the fluid is assumed isentropic and is described by the system of equations of hydrodynamics [1,2] :

$$\frac{\partial \mathbf{v}}{\partial t} + \mathbf{v} \cdot \boldsymbol{\nabla} \mathbf{v} = \frac{\nabla p}{\rho}, \tag{4.1}$$

$$\frac{\partial \rho}{\partial t} + \mathbf{div} \boldsymbol{\rho} \mathbf{v} = 0 \tag{4.2}$$

together with the equation of state

$$p = A \left(\frac{\rho}{\rho_0} \right)^n - B, \tag{4.3}$$

where, for water, $A = 3001\ atm$, $B = 3000\ atm$ and $n = 7$.

For the calculation of pressure in a moving fluid it is convenient to use a relation that represents a generalization of the Bernoulli equation in the non-stationary case and which is the first integral of Euler's equation (4.1) [1],

$$h + \frac{1}{2} v^2 + \frac{\partial \varphi}{\partial t} = f(t) = const, \tag{4.4}$$

where h is the specific enthalpy, v is the hydrodynamic velocity, and ϕ is the velocity potential ($\mathbf{v} = \mathbf{grad} \boldsymbol{\varphi}$).

If the excess pressure in the fluid generated by the bubble expansion is relatively small and it does not change the fluid density significantly, then $h \approx p/\rho_0$, and instead of (4.4) we obtain

$$\frac{p}{\rho_0} + \frac{1}{2} v^2 + \frac{\partial \varphi}{\partial t} = const. \tag{4.5}$$

This relation allows us to determine the pressure at any given point provided that the fluid flow is known, i.e., that the velocity distribution and the variation of the velocity with time are given. The effect of the fluid viscosity is irrelevant for the problem we are considering here and will be disregarded.

4.2. Expansion of a Sphere at Small Expansion Rates

Let us assume that we have a spherical bubble with radius R_1 at rest inside a fluid. The pressure in the surrounding fluid is p_0. At the initial instant $t = 0$, the sphere begins to expand according to a given law $R(t)$. Let us find the pressure on the surface of the sphere whith the assumption that the speed of expansion of the sphere is small, so that the fluid may be considered incompressible.

From the equation of continuity with $\rho = \rho_0 = const$, for the velocity we obtain the following expression which satisfies the boundary condition for the velocities on the sphere surface

$$v = \frac{R^2}{r^2}\dot{R} \tag{4.6}$$

,where r is the radial coordinate.

The radial dependence of the velocity potential of the fluid can be easily obtained from Eq. (4.6)

$$\varphi = -\frac{R^2\dot{R}}{r}. \tag{4.7}$$

Inserting the expression (4.6) for the velocity and (4.7) for the velocity potential into Eq. (4.5), we find the distribution of the pressure in the fluid

$$p - p_0 = \rho_0 \frac{R^2\ddot{R} + 2\dot{R}^2 R}{r} - \rho_0 \frac{\dot{R}^2}{2}\frac{R^4}{r^4}. \tag{4.8}$$

Note that the constant in Eq. (4.5) has been determined from the boundary condition at infinity. This relation can also be rewritten in the form

$$p - p_0 = \rho_0 \frac{\ddot{V}}{4\pi r} - \frac{1}{2}\rho_0 \frac{\dot{V}^2}{(4\pi r^2)^2}, \quad V = \frac{4\pi}{3}R^3 \tag{4.9}$$

Setting $r = R$ in Eq. (4.8), we obtain the expression for the pressure P on the surface of a sphere expanding according to a given law

$$P - p_0 = \rho_0 \left(\frac{3}{2}\dot{R}^2 + R\ddot{R}\right). \tag{4.10}$$

Let us note that in proximity of the sphere, at distances $r \approx R$, the last term in the rhs of Eq. (4.8), which is related to the presence of the non-linear Bernoulli term in Eq. (4.5), proves to be of the same order of magnitude as the other terms in this formula for any arbitrarily small rates of expansion of the sphere.

Let us now take into account the compressibility of the fluid. The expansion of the bubble generates a perturbation in the density, which then propagates in the form of an outgoing spherical wave. If the rate of expansion of the sphere is small compared to the speed of sound in the perturbed medium, then the density perturbations will also be small. Therefore, the propagation of the outgoing wave can be described by a linear acoustics solution, satisfying in an approximate way the boundary conditions of velocity continuity at the surface of the sphere[1]:

$$\varphi = -\frac{\dot{V}(t - \frac{r}{c_0})}{4\pi r}, \tag{4.11}$$

where $V = (4/3)\pi R^3$ is the volume of the sphere and c_0 is the speed of sound.

Substituting in Eq. (4.5) the expression of the velocity potential, we find the pressure in the emitted wave

$$p - p_0 = \rho_0 \frac{\ddot{V}(t - \frac{r}{c_0})}{4\pi r} - \frac{1}{2}\rho_0 \frac{\dot{V}(t - \frac{r}{c_0})}{(4\pi)^2 r^4}. \tag{4.12}$$

In the wave zone, the second term in the rhs of this formula is negligible, and thus Eq. (4.12) becomes

$$p - p_0 = \rho_0 \frac{\ddot{V}(t - \frac{r}{c_0})}{4\pi r}. \tag{4.13}$$

Near the sphere, at distances $r \ll c_0 t$, Eq. (4.12) transforms into Eq. (4.9), which was obtained under the assumption of incompressibility of the fluid.

The radiated energy can be determined by integrating the energy flow through the surface enveloping the sphere

$$W_{ac} = 4\pi r^2 \int_0^\infty \frac{(p - p_0)^2}{\rho c_0} dt.$$

Let us apply the results obtained to investigate the problem of the expansion of a sphere under the effect of a compressed gas filling the sphere. Let a sphere with radius R_1 be at rest at the initial instant, and let the pressure P_1 in it be higher than the pressure p_0 of the surrounding medium. Due to the pressure difference, the sphere begins to expand. Let us further assume that during the expansion of the sphere the change of state of the gas occurs adiabatically. Then, we obtain the following relation between the pressure of the gas in the bubble and the bubble radius

$$P = P_1 \left(\frac{R_1}{R}\right)^{3\gamma}, \tag{4.14}$$

where γ is the adiabatic index of the gas, equal to the ratio of the heat capacities at constant pressure and volume.

Substituting Eq. (4.14) for the pressure into Eq. (4.10), we obtain the equation that describes the process of expansion of a bubble

$$R\ddot{R} + \frac{3}{2}\dot{R}^2 = \frac{1}{\rho_0}\left[P_1 \left(\frac{R_1}{R}\right)^{3\gamma} - p_0\right]. \tag{4.15}$$

This differential equation is often called the Rayleigh equation [3]. (Rayleigh was the first to consider the problem of the expansion and deflation of a bubble in a fluid in the approximation of an incompressible fluid.) Eq. (4.5) can be integrated once if R is taken instead of t as the independent variable. We can thus obtain the first integral of Eq. (4.15) [4] :

$$\dot{R}^2 = \frac{2P_1}{3\rho_0}\left\{\frac{1}{\gamma - 1}\left(1 - \frac{R_1^{3\gamma-3}}{R^{3\gamma-3}}\right)\frac{R_1^3}{R^3} - \frac{p_0}{P_1}\left(1 - \frac{R_1^3}{R^3}\right)\right\}. \tag{4.16}$$

This formula can also be derived directly from energy considerations.

Using Eq. (4.14), the internal energy of an ideal gas filling the volume V

$$W = \frac{PV}{\gamma - 1} \tag{4.17}$$

can be expressed as a function of the bubble radius R in the form

$$W = \frac{P_1}{\gamma - 1}\frac{4}{3}\pi R^3 \left(\frac{R_1}{R}\right)^{3\gamma}. \tag{4.18}$$

Let us take the energy of a fluid with no bubbles as a reference point and set it equal to zero. Then, the potential energy of a bubble with radius R equals the work done against the forces of the external pressure by the formation of such a bubble and is given by

$$A = p_0\frac{4}{3}\pi R^3. \tag{4.19}$$

The kinetic energy of the fluid intertia can be expressed, with the help of Eq. (4.7), by the formula

$$W_\kappa = \int_R^\infty 4\pi r^2 \frac{\rho_0 v^2}{2} dr = 2\pi\rho_0 R^3 \dot{R}^2. \tag{4.20}$$

The law of energy conservation in the process of bubble expansion can then be written as:

$$2\pi\rho_0 R^3\dot{R}^2 + \frac{4}{3}\pi p_0 R^3 + W(R) = \frac{4}{3}\pi p_0 R_1^3 + W(R_1) = E, \tag{4.21}$$

where E is the initial energy of the bubble.

This equation (which, if W is replaced with the rhs of (4.18), coincides with Eq. (4.16)) describes the motion of a bubble filled with gas inside a liquid and it can be integrated numerically for a given set of initial conditions.

In the case under consideration, if the initial pressure of the gas inside the sphere exceeds the equilibrium value, the integration of Eq. (4.16) shows that, at first, the bubble expands, reaching dimensions larger than the equilibrium value, then shrinks into the initial state. This process repeats, thus generating a sequence of pulsations. The variation of the radius of the sphere during a pulsation is shown in Fig. 4.2. Within the adopted approximation, which does not take into account the energy dissipation, the pulsation amplitude does not vary. Analyzing Eq. (4.21), we can derive a series of approximate relations that describe the pulsation process of a bubble [4].

Because of the fast drop of the pressure in the bubble as the radius increases, the internal energy in the equation (4.21) is relatively small during most of the pulsation period, and may be neglected.

Hence, from Eq. (4.21) we obtain the following approximate equation

$$2\pi\rho_0 R^3\dot{R}^2 + \frac{4}{3}\pi p_0 R^3 = E. \tag{4.22}$$

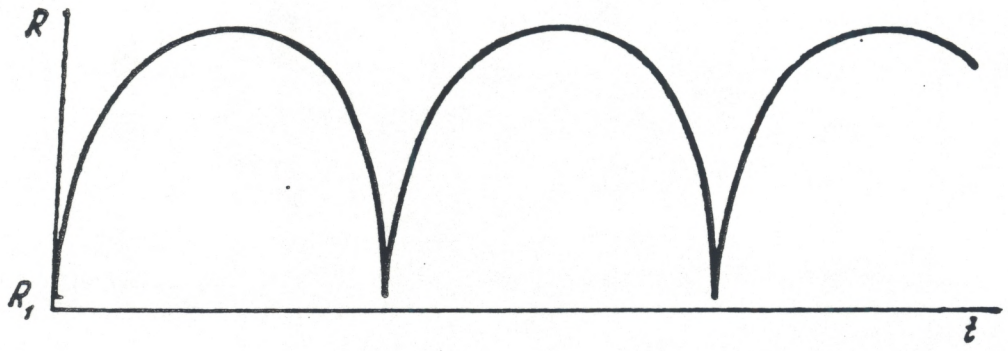

Fig. 4.2. Radius of a pulsating sphere as a function of time.

When the bubble reaches the point of maximum expansion, the speed of the bubble surface is zero. From Eq. (4.22) we can thus express the maximum radius through the total pulsation energy as follows

$$\frac{4}{3}\pi p_0 R_{\max}^3 = E. \tag{4.23}$$

Eliminating now E from Eq. (4.22) and using the relation (4.23), we obtain

$$\dot{R}^3 = \frac{2p_0}{3\rho_0}\left(\frac{R_{\max}^3}{R^3} - 1\right). \tag{4.24}$$

This equation was studied by Rayleigh (see [3]) in his investigation of the collapse of an empty bubble in a fluid under the effect of the hydrostatic pressure.

Eq. (4.24) can be integrated, leading to the relation

$$t = \sqrt{\frac{3\rho_0}{2p_0}} \int \frac{dR}{\sqrt{\frac{R_{\max}^3}{R^3} - 1}} + const. \tag{4.25}$$

The expression appearing in this integral cannot be expressed in terms of elementary functions, although is can be reduced to a sum of incomplete $\beta - functions$.

Choosing as limits of integration in (4.25) $R = 0$ and $R = R_{max}$, we can find the time necessary for the bubble to expand from zero to the maximum radius. Since in the cases of interest $R_1 \ll R_{max}$, such a time interval equals approximately half the pulsation period [4] :

$$\frac{\tau_0}{2} = \sqrt{\frac{3\rho_0}{2p_0}} \int_0^{R_{\max}} \frac{dR}{\sqrt{\frac{R_{\max}^3}{R^3} - 1}}, \tag{4.26}$$

whence,

$$\tau_0 \approx 1.83 R_{\max}\left(\frac{\rho_0}{p_0}\right)^{\frac{1}{2}}. \tag{4.27}$$

Using the relation (4.23), we can express the pulsation period through the total energy of the pulsating bubble as [5]:

$$\tau_0 = 1.14 \frac{\rho_0^{\frac{1}{2}} E^{1/3}}{p_0^{5/6}}. \tag{4.28}$$

This expression is sometimes called the Willis formula.

As we can see, the pulsation period increases as the cubic root of the total pulsation energy and decreases as the hydrostatic pressure increases to the power of $5/6$. We must remark, however, that this formula is not applicable if the pulsating bubble is near the fluid boundary, due to the different nature of the fluid inertia there.

To neglect the pressure of the gas inside the bubble is correct for most of the pulsation period, but is not admissible in the initial stage of the bubble expansion. This is related to the fact that at the initial instant the pulsation energy is completely in the form of internal energy of the compressed gas, whose pressure is the factor determining the motion. In this stage, however, we may neglect the effect of the external pressure and drop the second term in braces in Eq. (4.15).

The equation thus obtained

$$\dot{R}^2 = \frac{P_1}{\rho_0}\frac{2}{3(\gamma-1)}\left[\left(\frac{R_1}{R}\right)^3\left(1-\frac{R_1^{3\gamma-3}}{R^{3\gamma-3}}\right)\right] \tag{4.29}$$

together with the equation (4.15), in which p_0 has been dropped, form a system that, with the condition that $\ddot{R} = 0$, allows us to determine the value of the maximum expansion rate $\dot{R}_{max}$ and the value of the bubble radius at the moment of maximum rate

$$\dot{R}^2_{\max} = \frac{2}{3}\frac{P_1}{\rho_0}\gamma^{-\frac{\gamma}{\gamma-1}} \qquad \text{at} \qquad \left(\frac{R_1}{R}\right)^{3-3\gamma} = \gamma. \tag{4.30}$$

Furthermore, in the particular case of $\gamma = 4/3$, Eq. (4.29) can be integrated giving an approximate expression for the radius as a function of time, valid in the initial stage of the expansion, when $P \gg p_0$[4] :

$$t = \sqrt{2}\frac{R_1}{\sqrt{\frac{P_1}{\rho_0}}}\sqrt{Y}\left(1+\frac{2}{3}Y+\frac{1}{5}Y^2\right), \tag{4.31}$$

where

$$Y = \frac{R}{R_1} - 1.$$

From the relations (4.30) and (4.31) we can see that in the initial stage of the expansion, when the internal pressure is the determining factor of the process, the expansion rate is on the order of magnitude of

$$\dot{R} \sim \sqrt{P_1/\rho_0}\,, \tag{4.32}$$

and the time τ_1 necessary for the radius of the sphere to increase by one order of magnitude with respect to its initial value equals $\tau_1 \sim R_1\sqrt{P_1/\rho_0}$.

Let us give an example. Let $P_1 = 10^3\,atm$, $R_1 = 1\,cm$ and $\gamma = 1.4$. Then the maximum rate of expansion of a bubble, reached at $R = 1.3R_1$, equals approximately $1.4 \cdot 10^4\,cm/sec$; correspondingly, the bubble radius increases to $2R_1$ in a time interval $\tau \sim 10^{-4}sec$.

The velocity distribution in the fluid surrounding the sphere is described by relation (4.7), and the pressure distribution is given by formula (4.8). With the help of Eqs. (4.10) and (4.14), the latter can be transformed and rewritten in the form

$$p - p_0 = \frac{R}{r}\left[P_1\left(\frac{R_1}{R}\right)^{3\gamma} - p_0 + \frac{1}{2}\rho_0\dot{R}^2\left(1-\frac{R^3}{r^3}\right)\right], \tag{4.33}$$

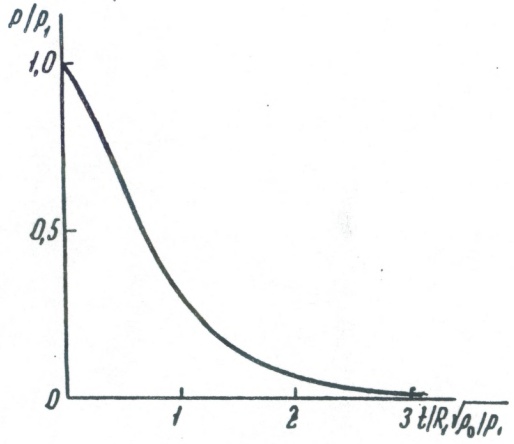

4.3

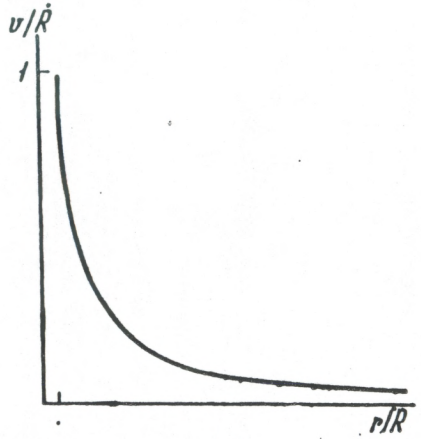

4.4

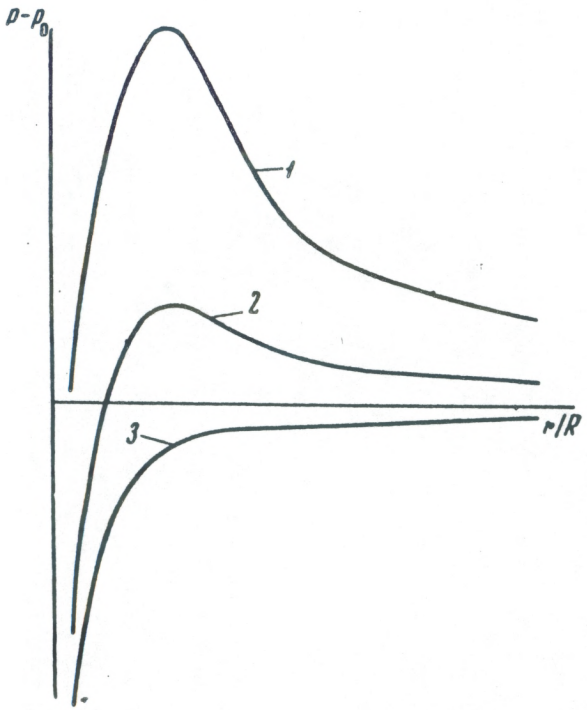

4.5

Fig. 4.3. Pressure inside a bubble during expansion.

Fig. 4.4. Velocity distribution in the vicinity of an expanding sphere.

Fig. 4.5. Pressure distribution in the vicinity of an expanding sphere.

which is convenient to elucidate the relation between the pressure in the bubble and the pressure at a given point r in the fluid.

From Eq. (4.33) we see that the pressure at a point sufficiently far away from the bubble($r \gg R$) differs from the pressure inside the bubble at a given instant in time not only by the factor $1/r$, but also by an additional term proportional to $\rho_0 \dot{R}^2$. This term, which has the effect of decreasing the pressure in the region near the bubble where the fluid speed is high, is sometimes conventionally called the Bernoulli term.

In Fig. 4.4 a velocity profile is schematically shown , and in Fig. 4.5 the profiles of the pressure in the vicinity of the expanding bubble are plotted . Line 1 in Fig. 4.5 corresponds to the instant when the pressure inside the bubble still exceeds the hydrostatic pressure, while lines 2 and 3 represent the pressure distribution at later times, when $P < p_0$. The sharp variation in the value of the pressure in the vicinity of the bubble at distances of a few R is due to the effect of the Bernoulli term; at large distances, the main reason for the pressure variation is its decrease according to the spherical law $1/r$.

Let us clarify the boundaries of applicability of the obtained solution which is based on the assumption of incompressibility of the fluid. Namely, let us determine the condition under which the variations in the fluid density are indeed small.

From the equation of state (1.3) we have

$$\frac{\Delta\rho}{\rho_0} \sim \frac{p}{nA} . \tag{4.34}$$

From this expression, for example, we obtain that, for water, the compressibility may be neglected if

$$\frac{\Delta\rho}{\rho_0} \sim \frac{p}{21000} \ll 1 , \tag{4.35}$$

.Rewriting Eq. (4.35) with the help of formula (4.32), which determines the order of magnitude of the bubble expansion rate, in the form

$$\frac{\Delta\rho}{\rho_0} \sim \frac{p/\rho_0}{nA/\rho_0} \sim \frac{\dot{R}^2}{c_0^2} \ll 1 , \tag{4.36}$$

we notice that the compressibility of the fluid in the problem of bubble expansion may be neglected if the rate of expansion of the sphere is small compared with the speed of sound in the fluid.

The compressibility, however, has to be taken into account in the problem of the compression waves emitted by the sphere, to which we now turn. At small expansion rates, this calculation may be carried out in the approximation of linear acoustics.

We may remark here that in the case under consideration , there is no inconsistency in disregarding the fluid compressibility in the calculations of sphere expansion and including it in the calculations of radiation. In the case of the small expansion rates under consideration, the fluid compressibility factor does not affect in any important way the process of expansion of the sphere.

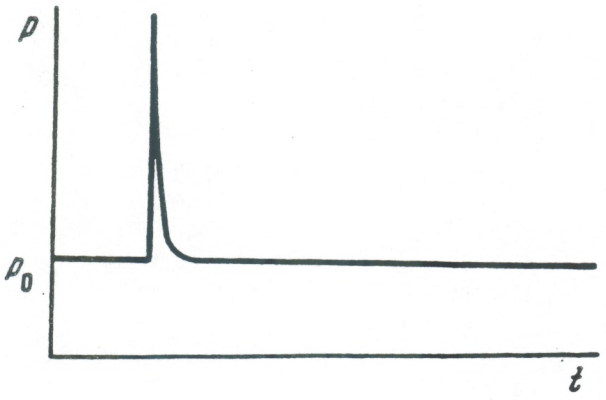

Fig. 4.6. Schematic profile of a compression wave radiated by an expanding sphere.

Fig. 4.7. To the calculation of the potential in a cylindrical problem.

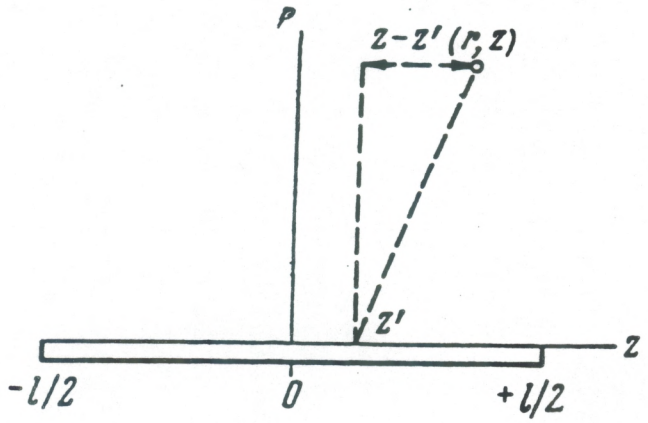

We may say that the radiation energy is small compared with the kinetic energy of the fluid inertia and thus it may be disregarded in the equation of energy balance (4.21). Hence, in this case, the radiation problem is divided into the calculation of the sphere expansion, which can be carried out in the approximation of an incompressible fluid, and the calculation of the radiation of a sphere expanding according to a known law in a compressible fluid.

The solution to the first problem is given by the formula (4.16). Substituting the result of the integration of Eq. (4.16) into Eq. (4.12), we find the profile of the pressure of the wave radiated by the sphere.

In practice, for the calculation it is convenient to rewrite Eq. (4.12) by using (4.10) and (4.14) in the form

$$\begin{aligned} p - p_0 &= \frac{R}{r}[P_1(\frac{R_1}{R(\bar{t})})^{3\gamma} - p_0 + \frac{1}{2}\rho_0 \dot{R}^2(\bar{t})(1 - \frac{R^3(\bar{t})}{r^3})], \qquad (4.37) \\ \bar{t} &= t - \frac{r}{c_0}. \end{aligned}$$

Calculations show that the bubble, which at the initial time contains gas under high pressure, during the process of expansion radiates a wave consisting a relatively short compression pulse and a longer rarefaction pulse. Schematically, the form of the wave is shown in Fig. 4.6. The compression pulse is emitted in the initial stage of the expansion, when the pressure in the bubble is still large. Then, during that segment of the pulsation period when the pressure in the bubble is lower than the hydrostatic pressure, the rarefaction pulse is radiated. When the bubble collapses, a compression pulse is again emitted, and the whole process is repeated.

We can give a simple estimate of the parameters of the compression pulse. In the initial stage of the expansion, according to Eq. (4.32), $R \sim R_1$ and $\dot{R}^2 \sim P_1/\rho_0$. Hence, $\ddot{V}/4\pi \sim R_1\dot{R}^2 \sim R_1 P_1/\rho_0$, and, from Eq. (4.13), the pressure in the compression pulse is $p \sim P_1 R_1/r$, and the pulse duration is $\tau_1 \sim R_1\sqrt{P_1/\rho_0}$.

The radiated energy is concentrated mainly in the compression pulse and its numerical value is given by the expression

$$W_{ac} \approx 4\pi r^2 \frac{p^2\tau}{\rho_0 c_0},$$

.This allows us to determine what fraction of the energy initially stored in the form of potential energy of the gas in the bubble

$$W = \frac{P_1}{\gamma - 1}\frac{4}{3}\pi R_1^3$$

is carried away by the compression wave

$$\frac{W_{ac}}{W} \sim 3(\gamma - 1)\frac{R_1}{c_0\tau}. \qquad (4.38)$$

As we see, at expansion rates R/τ small compared with the speed of sound, the fraction of energy carried away by the wave is not large.

4.3. Expansion of a Cylindrical Bubble in a Liquid

Let us examine a cylindrical bubble expanding in an ideal fluid according to given law $R(t)$. The pressure in the surrounding fluid equals p_0. We will assume that the rate of expansion is not large compared to the speed of sound, and correspondingly, the radius of the cylinder is small compared with the characteristic wavelength. The velocity potential of a fluid set in motion by the expansion of the cylinder can be obtained, for small expansion rates, by summing the potentials of elementary sources. The potential at a point with coordinates r and z created by one of such elementary source located, say, at a point z' is given as

$$d\varphi = -\frac{\dot{S}\left(t - \frac{\sqrt{r^2+(z-z')^2}}{c_0}\right)}{4\pi\sqrt{r^2+(z-z')^2}}dz', \tag{4.39}$$

where $S = \pi R^2$ is the cross-section area of the cylinder. The meaning of the other quantities is evident from Fig. 4.7.

The potential created by a cylinder of length l is given by the integral

$$\varphi = -\frac{1}{4\pi}\int\limits_{\frac{-l}{2}}^{\frac{l}{2}} \frac{\dot{S}\left(t - \sqrt{\frac{r^2+(z-z')^2}{c_0}}\right)}{\sqrt{r^2+(z-z')^2}}dz'. \tag{4.40}$$

Formula (4.40) can be employed also to calculate the potential of a cylinder with infinite length. To this end, we set $z = 0$ and introduce the new variable $\bar{t} = t - \sqrt{r^2+z'^2}/c_0$, whence $c_0^2(\bar{t}-t)^2 = r^2 + z'^2$, and

$$dz' = -\left[c_0^2(\bar{t}-t)\Big/\sqrt{c_0^2(\bar{t}-t)^2 - r^2}\right]d\bar{t}.$$

Changing the limits of integration to 0 and $l/2$, we can rewrite formula (4.40) in the form:

$$\varphi = \frac{c_0}{2\pi}\int\limits_{\alpha}^{\beta} \frac{\dot{S}(\bar{t})d\bar{t}}{\sqrt{c_0^2(\bar{t}-t)^2 - r^2}}, \tag{4.41}$$

where

$$\alpha = t - \frac{r}{c_0}; \qquad \beta = t - \frac{\sqrt{r^2+(l/2)^2}}{c_0}.$$

Letting $l \to \infty$, we obtain

$$\varphi = -\frac{c_0}{2\pi} \int_{-\infty}^{t-\frac{r}{c_0}} \frac{\dot{S}(\bar{t})d\bar{t}}{\sqrt{c_0^2(\bar{t}-t)^2 - r^2}}, \tag{4.42}$$

which coincides with the well-known expression for the potential of an infinite cylinder.

If we confine ourselves to considering the hydrodynamical quantities in the proximity of the cylinder in the region where the ratio $r/c_0 t$ is small, then instead of the relations written above, we can obtain simpler, approximate expressions by expanding the exact formulas with respect to the smallness parameter $r/c_0 t$. Let us consider first a cylinder with a small length compared with the characteristic wavelength. In the case of the small expansion rates that we consider here, the expression (4.40) for the potential can be simplified in the following manner. Expanding the integrand expression in a Taylor series with respect to the small phase "lead" $\sqrt{r^2 + (z-z')^2}/c_0$, at sufficiently later times, when $t > \sqrt{l^2/4 + r^2}$, we obtain

$$\dot{S}\left(t - \frac{\sqrt{r^2 + (z - zl^2)}}{c_0}\right) \approx \dot{S}(t) - \ddot{S}(t)\frac{\sqrt{r^2 + (z-z')^2}}{c_0}. \tag{4.43}$$

Integrating by parts, we find

$$\varphi = -\frac{1}{2}\frac{\dot{S}(t)}{2\pi} \ln \frac{z + \frac{l}{2} + \sqrt{\left(z + \frac{l}{2}\right)^2 + r^2}}{z - \frac{l}{2} + \sqrt{\left(z - \frac{l}{2}\right)^2 + r^2}} + \frac{\ddot{S}(t)l}{4\pi c_0}. \tag{4.44}$$

In the plane normal with respect to the cylinder and passing through its middle point ($z = 0$), Eq. (4.44) becomes

$$\varphi = -\frac{\dot{S}(t)}{4\pi} \ln \frac{\frac{l}{2} + \sqrt{\frac{l}{4} + r^2}}{\frac{-l}{2} + \sqrt{\frac{l}{4} + r^2}} + \frac{\ddot{S}(t)l}{4\pi c_0}. \tag{4.45}$$

Let us consider two limiting cases of this formula. Let $l \ll r$. Then

$$\varphi = -\frac{\dot{S}(t)l}{4\pi r} + \frac{\ddot{S}(t)l}{4\pi c_0} + \cdots \tag{4.46}$$

.In the opposite case, when $r \ll l$, we have

$$\varphi = -\frac{\dot{S}(t)}{2\pi} \ln \frac{l}{r} + \frac{\ddot{S}(t)l}{4\pi c_0} + \cdots. \tag{4.47}$$

Substituting (4.47) into (4.5) and setting $r = R$, we find the pressure on the surface of a short (compared to the wavelength) cylinder

$$p - p_0 = \rho_0 \frac{\ddot{S}(t)}{2\pi} \ln \frac{l}{R} - \frac{1}{2}\rho_0 \frac{\dot{S}(t)^2}{4\pi^2 R^2}. \tag{4.48}$$

Let us now consider a cylinder of infinite length. Making the substitution $\cosh\zeta = c_0(t-\bar{t})/r$ in Eq. (4.42), we obtain

$$\varphi = -\frac{1}{2\pi}\int_0^{\operatorname{arcosh}\frac{c_0 t}{r}} \dot{S}\left(t - \frac{r}{c_0}\cosh\zeta\right) d\zeta. \tag{4.49}$$

Taking into account that for $r/c_0 t \ll 1$we have $\operatorname{arcosh}\frac{c_0 t}{r} \approx \ln\frac{2c_0 t}{r}$ and that in the cases that interest us here $S(t) = 0$ for $t < 0$, we can rewrite the expression (4.49) in the form

$$\varphi = -\frac{1}{2\pi}\int_0^{\ln\frac{2c_0 t}{r}} \dot{S}\left(t - \frac{r}{c_0}cosh\zeta\right) d\zeta. \tag{4.50}$$

Expanding the integrand expression in a series and integrating by parts we obtain

$$\varphi \approx -\frac{\dot{S}(t)}{2\pi}\ln\frac{2c_0 t}{r} + \frac{S(t)t}{2\pi}. \tag{4.51}$$

In the particular case of a cylinder expansion at constant rate, from Eq. (4.51) we obtain the relation

$$\varphi = -U^2 t\ln\frac{r}{2c_0 t} + U^2 t + \cdots. \tag{4.52}$$

Whence, making use of the general relation (4.5) between pressure and velocity potential, we find

$$p - p_0 = \rho_0 U^2\left(\ln\frac{2c_0}{U} - \frac{1}{2}\right). \tag{4.53}$$

It is interesting to note that Eq. (4.53), within the framework of the adopted approximation (small expansion rates), satisfies the exact auto-model equations of the problem of a cylinder expansion at the constant rates reported in ref. [6].

Substituting formula (4.51) into the relation (4.5) and setting $r = R$, we obtain for the pressure exerted on the expanding cylinder by the medium the expression

$$p - p_0 = \rho_0\frac{\ddot{S}(t)}{2\pi}\ln\frac{2c_0 t}{R} - \frac{1}{2}\rho_0\frac{\dot{S}^2}{4\pi^2 R^2}. \tag{4.54}$$

This formula is applicable if the rate of expansion of the cylinder is small ($R/c_0 t \ll 1$) and its length is much larger than the characteristic wavelength ($l \gg c_0\tau$).

Let us turn to the calculation of the acoustic radiation of a cylindrical bubble expanding in a fluid. We will regard the cylinder as an ensemble of point-like sources. With this in mind, the general expression of the potential of the field created in the fluid

by an expanding cylinder is given by Eq. (4.40). If we consider the field only at sufficiently large distances from the discharge, in the Fraunhofer zone, then this formula, as is well known, can be approximately rewritten in the form

$$\varphi = -\frac{1}{4\pi r}\int_{-l/2}^{+l/2} \dot{S}\left(t - \frac{r(\zeta)}{c_0}\right) d\zeta\,, \tag{4.55}$$

where $r = r_0 - \zeta\cos\theta$ is the distance to the point of observation, and the meaning of θ and ζ is clear from Fig. 4.8.

From (4.55) it is not difficult to find the pressure in the radiated wave

$$p - p_0 = \frac{\rho_0}{4\pi r}\int_{-l/2}^{+l/2} \ddot{S}\left(t - \frac{r}{c_0}\right) d\zeta = \frac{\rho_0 c_0}{4\pi r\cos\theta}\int_{\alpha}^{\beta} \ddot{S}(\xi)d\xi\,, \tag{4.56}$$

where

$$\alpha = t - \frac{r_0}{c_0} - \frac{l\cos\theta}{2c_0}, \quad \beta = t - \frac{r_0}{c_0} + \frac{l\cos\theta}{2c_0}.$$

In the direction normal to the channel axis $\theta = \pi/2$ and $\cos\theta = 0$. Hence, using the first equality of Eq. (4.56) we readily obtain

$$p - p_0 = \frac{\rho_0 l}{4\pi r}\ddot{S}\left(t - \frac{r_0}{c_0}\right). \tag{4.57}$$

In the case of a short cylinder, the maximum phase difference l/c_0 of the signals emitted from the opposite ends of the cylinder is small compared with the pulse duration τ, $l/c_0\tau \ll 1$. This allows us to obtain from (4.56) a simple approximate formula. To this end, we need to expand the expression in series

$$\ddot{S}\left(t - \frac{r}{c_0}\right) = \ddot{S}\left(t - \frac{r_0}{c_0}\right) + \dddot{S}\left(t - \frac{r_0}{c_0}\right)\frac{\zeta\cos\theta}{c_0} + \cdots.$$

Integrating and dropping the now superfluous subscript from the coordinate, we obtain

$$p - p_0 = \rho_0\frac{l}{4\pi r}\ddot{S} + \rho_0\frac{l^2\cos\theta}{8\pi r c_0}\dddot{S}\,. \tag{4.58}$$

Using (4.58), it is now easy to calculate the radiated acoustic energy by integrating the energy flux over the spherical control surface and the time

$$W_{ac} = 2\oint_0^{\frac{\pi}{2}}\int_0^t \frac{(p-p_0)^2}{\rho_0 c_0} dt 2\pi r^2\sin\theta d\theta. \tag{4.59}$$

In the case of a cylinder that is long compared with the wavelength, the phase difference between the signals radiated from the two ends of the cylinder is large and formula

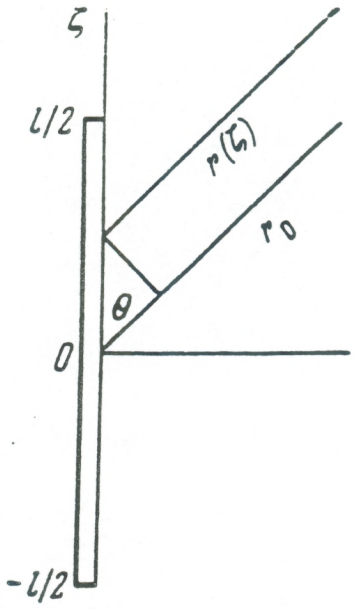

Fig. 4.8. To the calculation of the radiation by a cylinder.

Fig. 4.9. Formation of a shock wave in the propagation of a compression wave emitted by an expanding sphere.

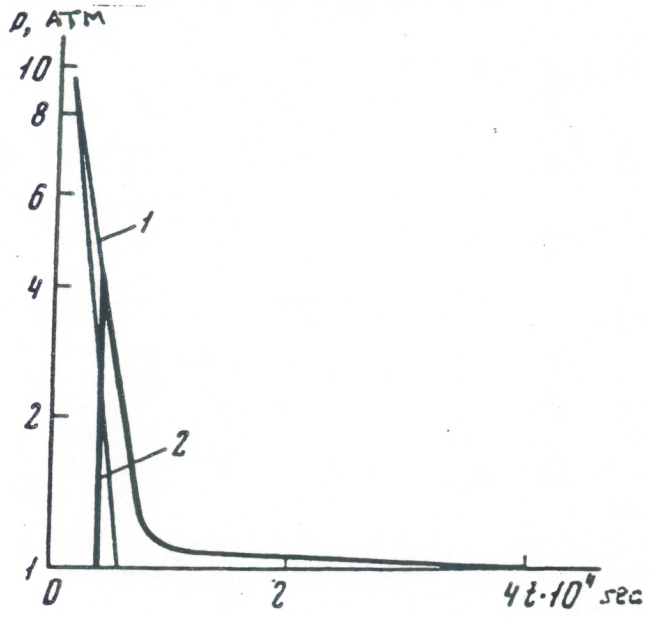

.(4.58) becomes inapplicable. In its place it is necessary to use the exact formula (4.56). Naturally, the transversal signal is described, as before, by the expression (4.57).

The total acoustic energy radiated by a long cylinder can be calculated with the formula (4.59), using in the process the Parceval equality

$$\int_{-\infty}^{+\infty} (p - p_0)^2 dt = \frac{1}{\pi} \int_0^{\infty} | s(\omega, \theta) |^2 \, d\omega, \tag{4.60}$$

where $s(\omega, \theta)$ is the spectrum of the signal radiated by the discharge in the direction θ with respect to the channel axis. The spectrum is given by the formula

$$s(\omega, \theta) = s(\omega) \frac{\sin n\omega \frac{\Delta t}{2}}{\sin \omega \frac{\Delta t}{2}}, \tag{4.61}$$

where $\Delta t = \frac{\Delta \zeta}{c_0} \cos\theta$, $n = \frac{l}{\Delta \zeta}$. Formula (4.61) describes the spectrum of the signal of a system of n point-like sources arranged at a distance of $\Delta\zeta$ from each other. Letting $\Delta\zeta$ go to zero, we can use a continuous distribution of sources over a length l. The quantity $s(\omega)$ in Eq. (4.61) represents the spectrum of an elementary signal and coincides, up to a constant, with the spectrum of the signal radiated by the channel in the normal direction

$$s(\omega) = \frac{\Delta \zeta}{l} \int_{-\infty}^{\infty} p_\perp(t) \exp(-i\omega t) dt, \tag{4.62}$$

where $p_\perp = p - p_0$ for $\theta = \pi/2$ and at a distance r from the channel.

If we assume, for example, that $p_\perp(t)$ has a square form , amplitude $p_\perp$ at a distance r and duration τ, from Eq. (4.62) we obtain

$$s(\omega) = 2\tau \frac{\Delta \zeta}{l} p_\perp \frac{\sin \omega\tau/2}{\omega\tau/2}. \tag{4.63}$$

Substituting (4.63) into (4.61), after integration we find

$$\int_0^{\infty} | s(\omega_1 \theta) |^2 \, d\omega = \frac{32 p_\perp^2 c_0^2}{\pi l^2 \cos^2 \theta}. \tag{4.64}$$

Returning now to the formula (4.59), let us determine the acoustic energy radiated by a cylinder with length $l \gg c_0\tau$, assuming that the cylinder expansion is such that in a direction normal to the channel axis a square pulse is emitted having duration τ and amplitude $p_\perp$ at a distance r from the channel [12]:

$$W_{ac} = \frac{4\pi r^2 p_\perp^2 \tau^2}{\rho_0 l} \left[\frac{1}{8} \frac{c_0\tau}{l} + \frac{1}{2} - \ln \frac{c_0\tau}{l} \right]. \tag{4.65}$$

Let us note that within the square form approximation, calculation of the radiation can be carried out in a relatively simple manner also by performing a direct summation of the elementary signals radiated in a given direction.

Finally let us consider the case in which the form of the compression and rarefaction pulse emitted in the direction normal to the channel axis is approximated by a Gaussian distribution with decay constant τ_0, i.e., the form of the signal at a distance r from the discharge is described by the expression

$$p - p_0 = p_\perp e^{-\pi(\frac{t}{\tau_0})^2}. \tag{4.66}$$

Then, a calculation similar to the one carried out for the previous case gives for the radiated energy the expression

$$W_{ac} = \frac{4\pi r^2 p_\perp^2 \tau_0^2}{\rho_0 l}\left[\frac{1}{4}\frac{c_0\tau_0}{l} + 0.42 + \ln\frac{l}{c_0\tau_0}\right]. \tag{4.67}$$

4.4. Effect of Fluid Compressibility on Bubble Expansion

Let us now consider the cases in which the rate of expansion of the bubble is large ($R_0 \approx \lambda$) and the perturbations in the density generated by the bubble expansion are significant. We shall first examine the case of a spherical bubble.

An exact solution of the problem of the expansion of a spherical bubble in a fluid by direct integration of the hydrodynamics equations is impossible to obtain. Hence, we must use numerical or approximate methods. Quite an effective approximate method for solving the problem of spherical (and cylindrical) flows is the Kirkwood-Bethe method (see [5]), devised for research on underwater explosions.

Replacing the velocity potential φ with the quantity $\Phi = r\varphi$, we can combine Eqs. (4.1) and (4.2) in one single equation of the form [5]:

$$\frac{\partial^2\Phi}{\partial t^2} - c^2\frac{\partial^2\Phi}{\partial r^2} = \left[\frac{v}{2}\left(\frac{\partial v}{\partial r}\right)^2 - \left(\frac{\partial v}{\partial t}\right)^2\right], \tag{4.68}$$

where

$$c(\rho) = \left(\frac{\partial p}{\partial \rho}\right)_s.$$

For small perturbations, when quadratic terms may be neglected, Eq. (4.68) reduces to the wave equation. This means that in this case the values of Φ are being "mixed" with the velocity c_0, where $c_0 = c(\rho)$ is the velocity of sound propagation in the unperturbed fluid.

For arbitrary perturbations, it is not possible to obtain a solution to Eq. (4.68) in the form of a travelling wave. Nevertheless, Kirkwood and Bethe [5] made the assumption that the Φ is propagated in this case with speed $\bar{c} = c + v$, in very much the same way as fixed values of pressure and speed are propagated in a Riemann wave. This means that the quantity $-r\frac{\partial\varphi}{\partial t}$ is also propagated with velocity $\bar{c}$. From Eq. (4.4) it follows that

$$-\frac{\partial\varphi}{\partial t} = h + \frac{v^2}{2}, \tag{4.69}$$

where h is the specific enthalpy, which, in the case of isentropic flows, is determined by the formula

$$h = \int_{p_0}^{p} \frac{dp}{\rho}. \tag{4.70}$$

Thus, according to the Kirkwood-Bethe theory, it is assumed that the function

$$G(t,r) = -r\frac{\partial\varphi}{\partial t} = r\left(h + \frac{v^2}{2}\right) \tag{4.71}$$

propagates with speed $\bar{c}$, i.e., the equation

$$\frac{\partial G}{\partial t} + \bar{c}\frac{\partial G}{\partial r} = 0 \tag{4.72}$$

remains valid. Eq. (4.72) gives the fundamental equation of the theory. Let us stress that Eq. (4.72) does not follow from the equations of hydrodynamics; we may regard it simply as a "lucky guess", justified *a posteriori* by the good agreement of its solutions with the results of numerical calculations. This equation can be rewritten in a different form, more convenient for the calculation of the pressure on the surface of an expanding sphere in a compressible fluid [5]. From (4.71) we have

$$dG = \left(h + \frac{v^2}{2}\right)dr + r\frac{dp}{\rho} + rvdv. \tag{4.73}$$

Substituting (4.73) into (4.72) and eliminating the partial derivatives with respect to the time and the coordinate using the relations (which were obtained from Eqs. (4.1) and (4.2))

$$\begin{aligned} \frac{\partial p}{\partial t} &= \frac{dp}{dt} + \rho v\frac{dv}{dt}, \quad \frac{\partial v}{\partial t} = \frac{dv}{dt} + v\left(\frac{1}{\rho c^2}\frac{dp}{dt} + \frac{2v}{r}\right), \\ \frac{\partial p}{\partial r} &= -\rho\frac{dv}{dt}, \quad \frac{\partial v}{\partial r} = -\frac{1}{\rho c^2}\frac{dp}{dt} - \frac{2v}{r}, \end{aligned} \tag{4.74}$$

and the expression for the total derivative

$$\frac{d}{dt} = \frac{\partial}{\partial t} + v\frac{\partial}{\partial r},$$

we obtain, after simple transformations,

$$\frac{dv}{dt}\left[\bar{c}-2v\right]+\frac{3}{2}\frac{v^2}{r}\left[\bar{c}-\frac{4}{3}v\right]=\frac{\bar{c}h}{r}+\frac{dh}{dt}\left[1+\frac{v^2}{c^2}-\frac{\bar{c}v}{c^2}\right]. \tag{4.75}$$

On the surface of the sphere $r = R$, $v = U$ and $h = H$; taking into account also that $\bar{c} = c + v$, we finally obtain

$$\frac{du}{dt}1-\frac{U}{c})+\frac{3}{2}\frac{U^2}{R}(1-\frac{U}{3c})=(1+\frac{U}{3c})\frac{H}{R}+(1-\frac{U}{c})\frac{1}{c}\frac{dH}{dt}. \tag{4.76}$$

If the law of expansion of the sphere $R(t)$ is known, Eq. (4.76) allows us to determine the value of the enthalpy on the sphere surface as a function of time, and also the pressure exerted by the compressible fluid on the expanding sphere.

The relation of the pressure to the enthalpy is given by an expression that follows from the equation of state (4.3) and the definition of enthalpy (4.70),

$$p=A\left[1+\frac{n-1}{c_0^2}H\right]^{\frac{n}{n-1}}-B. \tag{4.77}$$

The relations (4.76) and (4.77) may be regarded as a generalization of the formula (4.10), applicable for incompressible fluids.

As can be infered from Eqs. (4.76) and (4.77), the effect of the compressibility leads to an increase of the pressure on the surface of the expanding sphere if the pressure decreases with time, $dp/dt < 0$, and to a decrease of the pressure if the pressure increases with time. In other words, the fluid compressibility has a damping effect, as expected.

Let us notice that Eq. (4.76) can be somewhat simplified if we take into account that the hydrodynamic velocity U remains small compared with the local speed of sound c even for high rates of expansion of the sphere, i.e. rates comparable with c_0. This fact allows us to neglect the quantities U/c compared to unity and to rewrite Eq. (4.76) in the form

$$\frac{dU}{dt}+\frac{3}{2}\frac{U^2}{R}=\frac{h}{R}+\frac{1}{c}\frac{dh}{dt}. \tag{4.78}$$

Still another simplification of Eq. (4.76) can be obtained by expanding this equation with respect to the smallness parameter U/c and using the approximate expression for the enthalpy $h \approx \frac{P-p_0}{\rho_0}$,

$$\frac{dU}{dt}\left(1-\frac{2U}{c}\right)+\frac{3}{2}\frac{U^2}{R}\left(1-\frac{4}{3}\frac{U}{c}\right)=\frac{U}{\rho c}\frac{dP}{dR}+\frac{P}{\rho R}. \tag{4.79}$$

This relation coincides with the equation obtained in ref. [7].

Let us examine now the radiation problem at large rates of expansion, when it becomes necessary to take into account the compressibility of the medium even in the calculations concerning the expansion of the sphere.

A method suitable for the solution of this problem is based on the assumption that the function

$$G = r\left(h + \frac{v^2}{2}\right) \tag{4.80}$$

is propagated with a velocity $\bar{c} = c + v$. (In the presentation of this method we shall follow ref. [8].) Hence, if the value of this function on the boundary is known, the function can be evaluated at any other point in space.

The problem can thus be broken down into two steps:
1) determination of the function $G(\bar{t})$ on the surface of the expanding sphere ($\bar{t}$ denotes the retarded time measured on the surface of the sphere);
2) determination of the function $G(t, r)$ and of all the other hydrodynamic quantities at any point of observation.

If the motion of the sphere is given, $R = R(\bar{t})$, then we know also that $U = \dot{R}$, and the enthalpy h on the surface can be found from the relation (4.76). This concludes the determination of $G(\bar{t})$ on the surface of the sphere.

According to the basic assumption of the Kirkwood-Bethe theory [5], the value of the function $G(t, r)$ at an arbitrary point in space is determined by the relation

$$G(t, r) = G(R, \bar{t}) = G(\bar{t}), \tag{4.81}$$

with

$$t = \bar{t} + \int_R^r \frac{dr}{c}. \tag{4.82}$$

Near the wave front, at small distances compared with the distance to the signal source, the following relations hold :

$$G = rc_0 v(1 + \beta v), \tag{4.83}$$

$$\bar{c} = c_0(1 + \beta v), \tag{4.84}$$

$$\beta = \frac{n+1}{4c_0}.$$

Expressing dr from (4.83) and taking into account that the function G stays constant during the propagation, we obtain

$$\int \frac{dr}{\bar{c}} = -\frac{G}{c_0^2} \int_U^v \frac{dv}{v^2(1 + \beta v)^2}, \tag{4.85}$$

where $U = U(R)$. Expressing $\bar{t}$ as a function of G from Eq. (4.81), carrying out the integration in formula (4.85) and substituting the results into (4.82), we finally determine t as a function of G, r and R

$$t = \bar{t}(G) + \frac{G}{c_0^2}\beta\left[\frac{1+2\beta v}{\beta v(1+\beta v)} - \frac{1+2\beta U}{\beta U(1+\beta U)} - 2\ln\frac{(1+\beta v)\beta U}{\beta v(1+\beta U)}\right], \tag{4.86}$$

where, according to Eq. (4.83),

$$\beta v = \frac{1}{2}[(1+\frac{n+1}{rc_0^2}G)^{1/2} - 1], \tag{4.87}$$

$$\beta U = \frac{1}{2}[(1+\frac{n+1}{Rc_0^2}G)^{1/2} - 1]. \tag{4.88}$$

Let us analyze the solution we have obtained.

If the perturbations are small and βv may be neglected compared with unity in formula (4.85), then Eq. (4.86) is replaced by the following well- known results of linear acoustics

$$t = \bar{t} + \frac{r-R}{c_0}. \tag{4.89}$$

In this case the retarded time $t-\bar{t}$ in the propagation of the perturbation from the surface of the radiating sphere of radius R to the observation point r is independent of G.

Taking into account the next term in the expansion series of the denominator in Eq. (4.85) with respect to βv, we obtain the solution

$$t - \bar{t} = \frac{r-R}{c_0} - \frac{G}{c_0^2}2\beta\ln\frac{r}{R}. \tag{4.90}$$

In this approximation the retarded time $t - \bar{t}$ is a linear function of G. Consequently, such a solution, unlike formula (4.89), describes a wave with a profile varying during propagation.

It is interesting to note that solution (4.90) coincides exactly with the result obtained by direct integration of the hydrodynamics equations in the second approximation with respect to βv [9,10].

In the general case of an arbitrary perturbation, formula (4.86) allows us to determine t as a function of G, R and r, and thus to find the fields of the hydrodynamics quantities, i.e., velocity (given by Eq. (4.86)) and pressure, which can be expressed as

$$p(r,t) = A\left[\frac{2}{n+1} + \frac{n-1}{n+1}\left(1+\frac{n+1}{rc_0^2}G\right)^{\frac{1}{2}}\right]^{\frac{2n}{n-1}} - B. \tag{4.91}$$

To illustrate this method, let us give the results of the calculations of the radiation of a compression wave by a sphere expanding under the effect of the pressure exerted

by the gas filling it. The solution to this problem is obtained with the Kirkwood-Bethe theory (see [8]). The variation in the state of the gas inside the bubble is assumed to be adiabatic. Correspondingly, the value of the function $G(\bar{t})$ on the surface of the expanding sphere is determined by numerical integration of the system of equations (4.76) and (4.77) and the adiabatic equation

$$\frac{p}{p_1} = \left(\frac{R_1}{R}\right)^{3\gamma}, \tag{4.92}$$

where R_1 and p_1 are the initial values of the sphere and pressure in it. The thus calculated $G(\bar{t})$ is then inserted in Eq.(4.86) to determine the profiles of the pressure at various distances from the sources.

If the initial pressure of the gas is sufficiently high, the calculated pressure profile is non-unique, which indicates the formation of shock waves. The position of the shock waves and the discontinuity are determined from the obtained solution with the help of the Rankine - Hugoniot relations, which in the case of weak shock waves reduce to the simple *equal areas rule* [1].

A typical result of such calculation is show in Fig. 4.9, taken from ref. [8]. Line 1 is constructed from Eqs. (4.86) and (4.91) with $r/R = 10^4$, $R = 0.1\,cm$ and $p_1 = 10^5\,atm$, and line 2 represents the profile of the generated shock wave.

In a similar way we could also approach the problem of the expansion of a cylindrical bubble in a fluid at large expansion rates. We assume that the function $G = r^{1/2}(h + \frac{v^2}{2})$ is propagated at speed $\bar{c} = c + v$, and thus satisfies the equation

$$\frac{\partial G}{\partial t} + \bar{c}\frac{\partial G}{\partial r} = 0. \tag{4.93}$$

In the case of an expanding cylinder, this equation can be rewritten as

$$\frac{dU}{dt}\left(1 - \frac{2U}{c}\right) + \frac{3}{4}\frac{U^2}{R}\left(1 - \frac{1}{3}\frac{U}{c}\right) = \frac{1}{2}\frac{H}{R}(1 + \frac{U}{c}) + (1 - \frac{U}{c})\frac{1}{c}\frac{dH}{dt}. \tag{4.94}$$

If the law of expansion $R(t)$ is known, Eq. (4.93) allows us to calculate the enthalpy. Inserting the latter in Eq. (4.77) , we obtain the pressure on the surface of the cylinder as a function of time.

Using the Kirkwood-Bethe method, we can also find the distribution of hydrodynamical quantities in the vicinity of the cylinder, namely, at distances that are small compared with the cylinder length.

In fact, using the condition that the function G is constant during the propagation of the wave, and knowing the values of this function on the surface of the expanding cylinder, we can determine its values at those points in space where the wave may still be considered cylindrical.

In practice, it is more convenient to calculate the inverse of G with the formula

$$t = \bar{t}(G) + 2\frac{G^2}{c_{0^2}}\left[6\beta^2 \ln\frac{(1+\beta v)U}{(1+\beta U)v} + \frac{4\beta^3 v}{1+\beta v} - \frac{4\beta^3 U}{1+\beta U}\right] - \quad (4.95)$$
$$-\frac{\beta^4 v^2}{2(1+\beta v)} + \frac{\beta^4 U^2}{2(1+\beta U)^2} + \frac{(1+\beta v)^2}{2v^2} - \frac{(1+\beta U)^2}{2U^2} -$$
$$-\frac{4\beta(1+\beta v)}{v} + \frac{4\beta(1+\beta U)}{U}]$$

$$\beta = \frac{n+1}{4c_0}.$$

The hydrodynamic quantities are connected with the auxiliary function G through the relations

$$\beta v = \frac{1}{2}[(1 + \frac{4\beta G}{r^{1/2}c_0})^{1/2} - 1] \quad (4.96)$$

$$\beta U = \frac{1}{2}[(1 + \frac{4\beta G}{R^{1/2}c_0})^{1/2} - 1]. \quad (4.97)$$

These relations allow us to find the spatial distribution of these quantities.

At moderate expansion rates formula (4.95) takes the simpler form

$$t - \frac{r-R}{c_0} = \bar{t}(G) - \frac{4\beta}{c_0^2}G(r^{\frac{1}{2}} - R^{\frac{1}{2}}), \quad (4.98)$$

which is in agreement with linear acoustics [11]. At small expansion rates ($\beta v \to 0$), formula (4.95) becomes

$$t - \frac{r-R}{c_0} = \bar{t}(G), \quad (4.99)$$

a well- known result from linear acoustics.

REFERENCES to Chapter IV

[1] Landau L. D., Lifshitz E. M., *Fluid Mechanics*, (Pergamon Press, N.Y., 1975).

[2] Zel'dovich Ja. B., Raizer Ku. P., *Physics of shock waves and high temperature hydrodynamic phenomena*, (Moscow, Pshyizmatgis, 1966).

[3] Rayleigh "On the pressure developed in a liquid during the collapse of a spherical cavity," Philos. Mag. **34**, 94-98 (1917).

[4] Lamb G. *Hydrodynamics*, (Moscow, OGIZ, 1947).

[5] Cole R., *Underwater explosion*, (Princeton UP, Princeton,1948).

[6] Kochina N. N., Mel'nykova N. S., "Expansion of a piston in water," PMM **23** (1), 132-133 (1959).

[7] Trilling L., "The collapse and rebound of a gas bubble," J. Appl. Phys. **23**, 14, 14-17 (1952).

[8] Akylichev V. A., Boguslovskij Ju. A., Ioffe A. I., Naugolnykh K. A., Radiation of finite-amplitude spherical waves," Akust. Zh. **13** (3), 321-328 (1967).

[9] Whitham G. B., "On the propagation of weak shock waves," Fluid Mech. **3** (1), 290-318 (1956).

[10] Naugolnykh K. A., "Compression wave radiated by an expanding sphere," Akust. Zh., **11** (3), 351-358 (1965).

[11] Naugolnykh K. A., Solujan N. G., Khkochlov R. P., "Cylindrical waves of finite amplitude in dissipative media," Vestnik MGU, **3** (4), 65-72 (1962).

[12] Ioffe A. I., Kozhelupova N. G., Naugolnykh K. A., Roy N. A., "Sound radiation from a long spark in water," Akust. Zh. **13** (2), 208-212 (1967).

Chapter V

THEORY OF THE DISCHARGE CHANNEL EXPANSION

5.1. Introduction

The release of energy in the discharge channel leads to an increase of the pressure in it. This in turn causes rapid expansion of the channel, accompanied by radiation of a compression wave and subsequent formation of a pulsating gas bubble.

The walls of the channel during the expansion process may be considered impenetrable to the surrounding fluid. Obviously this does not mean that when considering the processes taking place inside the channel, one may neglect the evaporation of matter on the channel wall. However, because of the great difference between the density of the matter inside the channel and the density of the surrounding fluid, the evaporation of matter on the channel wall is important to the processes taking place inside the channel, but nevertheless , it causes an insignificant shift of the channel boundary with respect to the fast hydrodynamic expansion.

Another important feature of discharges in a liquid is that due to the high density of the plasma, inside the discharge channel there are various effective heat conduction mechanisms, such as radiative and electron conduction, that quickly equalize the temperature along the channel radius. This is in contrast with the peripheral regions of the channel, where there are less effective heat conduction mechanisms that cause consequent slow heating of the matter there. As a result, there is a fast drop in the temperature at the boundary of the channel. The peculiar features just mentioned allow a simple theoretical model that describes the channel expansion in a satisfactory manner.

We shall regard a discharge channel as a bubble filled with homogeneous plasma having a sharp boundary with the external cold fluid. The quantity of plasma increases as the discharge progresses, due to evaporation from the channel wall. Temperature, pressure, and plasma density are considered constant along the bubble radius.

Furthermore, we will confine ourselves to examining discharges with moderate currents, and will therefore neglect also the influence of the skin-effect and the magnetic pressure compared with the gas-kinetic pressure.

As a result of energy release, the pressure in the bubble increases and the bubble expands. During the expansion process, hydrodynamic and electric quantities are related by an equation of energy balance. The solution of such an equation for a given regime of energy release (which is determined by the electric characteristics of the discharge) allows us to find the radius as a function of time, the pressure in the channel, the parameters of the radiated compression wave and of the pulsating bubble [1].

According to the results of Ch. III, neglecting the energy losses on radiation of light and heating of the fluid outside the channel, we may then assume that the energy E released in the form of Joule heat is expended to increase the internal energy W of

the plasma and on the work done by the channel onto the surrounding fluid during the expansion

$$W + A = E \,. \tag{5.1}$$

The actual calculation depends on the relation among three spatial parameters: width of the spark gap l, characteristic radius of the channel R_0 and characteristic wavelength λ. Such a relation determines both the type of approximations made in the investigation of the hydrodynamical phenomena and the choice of the geometric model for the discharge. We will examine several models of discharge.

Within the approximation based on the smallness of the density perturbation (acoustic or incompressible fluid approximation), we shall consider the spherical model ($l \ll R_0 \ll \lambda$), the model of a short cylinder($R_0 \ll l \ll \lambda$) ,and the model of a long cylinder ($R_0 \ll \lambda \ll l$).

We shall also examine the spherical model in a nonlinear approximation, in which the finiteness of the density perturbations is taken into account, ($l \ll \lambda \ll R_0$)

5.2. Spherical Model of Discharge

Let us consider a spark discharge in a fluid in which the discharge gap is small compared with the characteristic radius of the channel, which, in turn, is small compared with the wavelength, i.e., $l \ll R_0 \ll \lambda$.

Since the characteristic radius of the channel R_0 is large compared with the discharge gap, we may assume that during the discharge the shape of the channel is close to spherical. At the same time, the fact that the channel radius is small compared with the length of the radiated wave means that the perturbations of the fluid density generated by the discharge are small. Thus, from the point of view of acoustics, such discharges are similar to a point-like source of sound, which justifies the name of point-like discharges [2].

Let us consider the equation of energy balance (5.1) for the case of a point-like discharge. As shown in Ch. III, the internal energy of the plasma within a finite temperature range is given by the usual formula for the energy of an ideal gas

$$W = \frac{pV}{\gamma - 1} \,, \tag{5.2}$$

where p denotes pressure, V is the volume occupied by the plasma, $V = \frac{4}{3}\pi R^3$, and R is the channel radius. Formula (5.2) may be used if γ is understood to denote an effective value of the adiabatic index, which, for example, for a plasma generated in water, equals 1.26.

The work on the channel expansion is

$$A = \int_{V_0}^{V} p dV \ . \tag{5.3}$$

The energy $E(t)$ released in the channel is determined by the electric characteristics of the discharge, current I and voltage U during the time t, and is given by

$$E(t) = \int_{0}^{t} IU dt \ . \tag{5.4}$$

The pressure inside the channel can be expressed as a function of the channel radius and its time derivatives from the solution of the hydrodynamic problem of the expansion of a spherical bubble in a fluid.

In the case under consideration, $R_0 \ll \lambda$, this problem can be solved in the incompressible fluid approximation, since the perturbations in the fluid density are small.

The solution to this problem was obtained in Sec. 4.2 (Eq. (4.8)). Neglecting in this expression the pressure in the unperturbed fluid compared to the pressure in the channel, we find

$$p = \rho_0 \left(\frac{3}{2} \dot{R}^2 + R\ddot{R} \right) = \rho_0 \frac{\ddot{V}}{4\pi R} - \frac{1}{2} \rho_0 \frac{\dot{V}^2}{8\pi R^4} \ . \tag{5.5}$$

Substituting (5.5) into (5.3), we find the work on the channel expansion

$$A = \frac{\rho_0}{4\pi} \int_{V_0}^{V} \left(\frac{\ddot{V}\dot{V}}{R} - \frac{\dot{V}^3}{8\pi R^4} \right) dt = \rho_0 \frac{\dot{V}^2}{8\pi R} \ , \tag{5.6}$$

with the assumption that $\dot{V}(0) = 0$.

This result can be interpreted as follows: A is the work done on increasing the kinetic energy of the mass adjacent to the expanding sphere,

$$A = \rho_0 4\pi R^3 \frac{\dot{R}^2}{2} \ . \tag{5.7}$$

Substituting (5.2), (5.5) and (5.6) into (5.1), we obtain the equation:

$$\ddot{V}V - \frac{4/3 - \gamma}{2} \dot{V}^2 = \frac{\gamma - 1}{\rho_0} 4\pi R E(t) \ . \tag{5.8}$$

In this equation we may neglect the second term, which has a small coefficient. We can verify the validity of this approximation by comparing the various quantities in Eq. (5.8) using the results of a numerical integration of the simplified equation. Thus, in the following we shall use the equation

$$\ddot{V}V = \frac{\gamma - 1}{\rho_0} 4\pi R E(t) \ . \tag{5.9}$$

Let us introduce the dimensionless variable

$$a = \frac{t}{\tau}; \qquad f(x) = \frac{E(t)}{E}; \qquad y = \frac{R}{R_0}, \tag{5.10}$$

where τ denotes the duration of the discharge, $E = E(\tau)$ is the energy released in the channel during the time τ, R_0 is a still undetermined unit of length.

With the new variables, Eq. (5.9) takes the form

$$y^2 \frac{d}{dx}\left(y^2 \frac{dy}{dx}\right) = \left[\frac{3}{4\pi}\frac{\gamma - 1}{\rho_0}\tau^2 E R_0^{-5}\right] f(x) . \tag{5.11}$$

Let us choose R_0 so that the factor in the rhs of Eq. (5.11) equals unity

$$R_0^5 = \frac{3}{4\pi}\frac{\gamma - 1}{\rho_0}\tau^2 E = 0.062\tau^2 E . \tag{5.12}$$

This relation coincides exactly with the expression (3.5) obtained earlier, which determines the order of magnitude of the channel radius at the end of the discharge. This means that the unit of length introduced by the relation (5.12) has the meaning of the characteristic radius of the channel.

For numerical calculations, the thus obtained equation

$$y^2 \frac{d}{dx}\left(y^2 \frac{dy}{dx}\right) = f(x) \tag{5.13}$$

can be more conveniently written in the form of a system of equations

$$\frac{dz}{dx} = \frac{f(x)}{y^2}, \qquad \frac{dy}{dx} = \frac{x}{y^2}. \tag{5.14}$$

The initial conditions follow naturally from physical considerations and may be chosen in the form

$$x = 0, \qquad y = y_0, \qquad \dot{y} = 0, \tag{5.15}$$

where $y_0 = R_{str}/R_0$ is the initial radius of the channel. From the data given in Ch. II, we may assume that the streamer radius $R_{str} \sim 10^{-2} cm$. An exact determination of the initial radius is unnecessary, because the expansion process is determined mainly by the regime of energy release in the channel, and not by the initial conditions, which are quickly "forgotten" by the system.

Eq. (5.13), together with the initial conditions (5.15), completely describes the process of channel expansion, provided that the function $f(x)$, which characterizes the regime of energy release, is known (e.g., from the experiment). Let us notice that, as a result of the special choice of the units of time, energy, and length, the parameters of the discharge do not appear explicitly in Eq. (5.13); their effect in the equation is mediated by the function $f(x)$. We can, therefore, say that all the discharges, characterized by the same regimes of energy release (i.e., having the same $f(x)$), are similar in the sense that they are described by the same equation.

In particular, as we showed in Ch. III, for all the near-critical discharges, the form of the normalized law of energy release, i.e. the function $f(x)$, is the same, which points to the similarity of these discharges in the sense cited above.

Let us express the fundamental quantities characterizing the homogeneous spherical model of discharge through the solution of Eq. (5.13). For the channel radius we have

$$R = R_0 y \,. \tag{5.16}$$

Substituting (5.16) into (5.5) and using (5.14), we find the pressure in the channel

$$P = \rho_0 \frac{R_0^2}{\tau^2} \zeta(x) \,, \tag{5.17}$$

where

$$\zeta(x) = \frac{f(x)}{y^3} - \frac{1}{2}\frac{z^2}{y^4} \,.$$

From (5.7), the work on the expansion is expressed by the formula

$$A = 2\pi\rho_0 \frac{R_0^5}{\tau^2} y^3 \dot{y}^2 \,, \tag{5.18}$$

and the internal energy of the plasma in the channel is given by

$$W = \rho_0 \frac{R_0^5}{\tau^2} \frac{4\pi}{3(\gamma-1)} \left[f(x) - \frac{z^2}{2y} \right] \,. \tag{5.19}$$

The perturbations of the density of the surrounding fluid generated by the discharge propagate in the form of a spherical compression wave. The profile of such a wave can be determined from the solution of the problem of the radiation of a sphere expanding in a fluid according to a given law. In the case of the small expansion rate we are considering here, this problem can be solved in the approximation of linear acoustics (see Section 4.2), when the velocity potential of the radiated wave is determined simply by the volume velocity of the source (Eq. (4.11)), and the pressure in the wave radiated by the sphere is proportional to the volume acceleration (Eq. (4.13)).

Denoting with p the excess pressure generated by the wave, on the basis of Eqs. (4.11), (4.13), (5.14) and (5.16) we obtain

$$p = \rho_0 \frac{R_0^3}{\tau^2 r} g(\bar{x}) \,, \qquad \bar{x} = \frac{\bar{t}}{\tau} \,, \qquad \bar{t} = t - r/c_0 \,, \tag{5.20}$$

where

$$g(\bar{x}) = \frac{f(\bar{x})}{y^2} \,,$$

$$v = \frac{\partial \varphi}{\partial r} = \frac{R_0^3}{r^2 \tau} y^2 \dot{y} + \frac{R_0^3}{\tau^2 c_0 r} \left(2y\dot{y}^2 + y^2 \ddot{y} \right) . \tag{5.21}$$

Let us stress that these expressions, based on the solution of the equation of energy balance (5.14), describe only the *head* part of the wave radiated during the active stage of the discharge, when an electric current flows along the channel and release of energy occurs.

Knowing the profile of the pressure of the radiated compression wave, we can find the acoustic energy carried away by this wave

$$W_{ac} = 4\pi r^2 \int_0^\infty \frac{p^2}{\rho c_0} = \frac{4\pi\rho_0 R_0^6}{c_0 \tau^3} J \,, \tag{5.22}$$

where

$$J = \int_0^\infty \left(\frac{f(\bar{x})}{y^2}\right)^2 d\bar{x} \,.$$

The integration of the expression for the acoustic energy can be performed easily up to $\bar{x} \approx 1$ because the integrand expression decreases rapidly. Within this range, and with the function $f(x)$ given in Fig. 3.13, we obtain $J \approx 1$.

It may be useful to point out the following peculiarity of the formulas given above for the various hydrodynamic characteristics of a discharge: they consist of a dimensional constant coefficient and of a dimensionless function of time. Furthermore, the result is that the order of magnitude of the quantities described by these formulas is determined, in practice, by the dimensional coefficients .

The dimensionless functions of time are nearly equal to unity in the peak regions. The peculiarities listed are related to the particular choice of the units of time and length that are characteristic of the time and length scales in the processes under consideration.

Formulas (5.16)–(5.19) and (5.20)–(5.22) allow us, in principle, to calculate the hydrodynamic characteristics of a discharge, provided that the function $f(x)$, which determines the energy release regime, is known.

In particular, as was shown in Ch. III, for all near-critical discharges the normalized law of energy release is the same and is described by the function plotted in Fig. 3.13. Correspondingly, for such types of discharges, the same dimensionless function appears in the formulas for the various hydrodynamical quantities.

From that it follows that in order to calculate the characteristics of such discharges it is sufficient to know only two parameters: the duration of the discharge τ and the total energy E released during such time. According to Eq. (5.12), these parameters determine R_0, and with it the dimensional coefficients in the formulas given above. It is even possible to eliminate R_0 and rewrite these formulas directly in terms of the parameters τ and E.

Bearing this in mind, the hydrodynamic characteristic can be written as:

• channel radius:

$$R = a\rho_0^{-\frac{1}{5}} \tau^{\frac{2}{5}} E^{\frac{1}{5}} y \,, \tag{5.23}$$

• pressure in the channel:

$$P = a^3 \rho_0^{\frac{2}{5}} E^{\frac{2}{5}} \tau^{-\frac{6}{5}} \left[\frac{f(x)}{y^3} - \frac{1}{2} \frac{z^2}{y^4} \right] , \tag{5.24}$$

• pressure in the radiated compression wave:

$$p = \rho_0^{\frac{2}{5}} \frac{a^3}{r} E^{\frac{3}{5}} \tau^{-\frac{4}{5}} \frac{f(x)}{y^2} , \tag{5.25}$$

• acoustic energy radiated:

$$W_{ac} = 4\pi \rho_0^{-\frac{1}{5}} a^6 E^{\frac{6}{5}} c_0^{-1} \tau^{-\frac{3}{5}} J , \tag{5.26}$$

where

$$a = \left[\frac{3}{4\pi} (\gamma - 1) \right]^{1/5} .$$

It is interesting to note that the time scale τ appears in Eq. (5.23) with the same power, $2/3$, as in the case of strong explosions or of the bubble collapse in a fluid.

In turn, in near-critical discharges, the parameters τ and E can be approximately expressed as

$$\tau = \pi \sqrt{LC} , \qquad E \approx \frac{CU^2}{2} \tag{5.27}$$

(see Table 3.5), which allows us to calculate the dependence of the hydrodynamical characteristics on the parameters of the electric circuit. For example, the pressure in a compression wave is determined, by order of magnitude, by the formula

$$p \approx 10^{-3} \frac{1}{r} \left(\frac{CU^6}{L^2} \right)^{1/5} atm$$

with r given in *cm*, C in *Faradays*, U in *Volts* and L in *Henrys*.

An important characteristic of a discharge is its electro-acoustic efficiency, defined as the ratio of the acoustic energy radiated during the discharge to the total energy released into the channel

$$\eta = \frac{W_{ac}}{E} = 3(\gamma - 1) \frac{R_0}{c_0 \tau} J = 4\pi \rho_0^{-\frac{1}{5}} a \frac{E^{1/5}}{c\tau^{3/5}} J . \tag{528}$$

We see that the efficiency is proportional to the rate of the channel expansion R_0/τ, depends on the value of the effective adiabatic coefficient for the discharge plasma, is weakly dependent on the release energy E, and increases as the discharge duration decreases. For the discharges of moderate intensity considered here $\eta \sim 10\%$ (typical parameters for these discharges are given in Table 3.5).

In actual experimental setups, it is convenient to generate the discharge near the surface of a solid reflector. The effect of this surface can be taken into account in the

calculation. Let us consider, for example, a discharge occurring directly on a solid plane surface. If, as before, the interelectrode gap is small compared with the characteristic radius of the channel (and the latter is in turn small compared to the wavelength), then the form of the channel is close to being hemispherical. With the accuracy dependent on the effects related to the formation of a boundary layer, such a discharge is equivalent to half a spherical discharge in a free space. Hence, it is clear that the hydrodynamic characteristics of a discharge near a surface coincide with the corresponding characteristics of a free discharge with double the energy.

These quantities can be calculated with the formula for the discharges in a free space, with the *proviso* that in calculating the quantity R_0 one replaces E in Eq. (5.12) with $2E$. Furthermore, the work of the channel, the internal energy of the plasma and the acoustic energy must be divide in half so as to include only the energy in one of the two half-spaces.

5.3. Model of a Short Cylinder

If the width of the interelectrode gap is large compared with the channel radius, but it is small compared with the wavelength, i.e., $R_0 \ll l \ll \lambda$, then during the discharge process the channel has an elongated form, which allows us to adopt for the description of such a discharge the model of a short (compared with the wavelength) homogeneous cylinder. The calculations are similar to those reported in the previous section (see [1],[3]).

The energy $E(t)$ released in the channel is expended mainly to increase the internal energy of the plasma

$$W = \frac{PSl}{\gamma - 1} \tag{5.29}$$

and on the work for the channel expansion

$$A = \int_{S_0}^{S} PldS\,, \tag{5.30}$$

where P is the pressure in the channel, S is the crosssection of the channel, and l its length.

The pressure on the surface of a short cylinder, which is expanding in a fluid at a small rate compared with the speed of sound, was calculated in an approximate way in Ch. IV (See Eq. (4.48)). Neglecting the equilibrium pressure compared with the pressure in the channel, we can rewrite this formula in the form

$$P = \rho_0 \frac{\ddot{S}}{2\pi} \ln \frac{l}{R} - \frac{1}{2}\rho_0 \frac{\dot{S}^2}{4\pi^2 R^2}\,. \tag{5.31}$$

Substituting (5.31) into (5.30), and taking into account that

$$P\frac{dS}{dt} = \frac{d}{dt}\rho_0\frac{\dot{S}^2}{4\pi}\ln\frac{l}{R}\,,$$

we find

$$A = l\rho_0\frac{\dot{S}^2}{4\pi}\ln\frac{l}{R}\,. \tag{5.32}$$

Substituting further Eqs. (5.29), (5.31) and (5.32) into Eq. (5.1), and eliminating l, we obtain the equation of energy balance for unit of channel length

$$2\ddot{S}S\ln\frac{l}{R} + \frac{\dot{S}}{2}\left[(\gamma-1)2\ln\frac{l}{R} - 1\right] = 4\pi\frac{(\gamma-1)}{\rho_0}\frac{E(t)}{l}\,. \tag{5.33}$$

Let us introduce the dimensionless variables

$$x = \frac{t}{\tau}\,, \quad f(x) = \frac{E(t)}{E}\,, \quad y = \frac{R}{R_0}\,,$$

where τ, E and R_0 are, respectively, the discharge duration, the total energy released in the channel during the time τ, and the characteristic unit of length.

With the new variables, Eq. (5.33) takes the form

$$\frac{d}{dx}y\dot{y} + \dot{y}^2\left[(\gamma-1) - \frac{1}{2\ln\frac{l}{R_0 y}}\right] = \frac{(\gamma-1)\tau^2 E}{\pi\rho_0 R_0^4 l}\,\frac{f(x)}{y^2\ln\frac{l}{R_0 y}}\,. \tag{5.34}$$

Choosing the discharge gap separation l as the characteristic length unit R_0, we can rewrite this equation as follows

$$\frac{d}{dx}y\dot{y} + \dot{y}^2\left[(\gamma-1) - \frac{1}{2\ln y}\right] = \bar{l}\,\frac{f(x)}{y^2\ln\frac{l}{R_0 y}}\,. \tag{5.35}$$

The dimensionless coefficient $\bar{l} = \frac{(\gamma-1)}{\rho_0}\frac{\tau^2 E}{\pi l^5}$ can be regarded as the similarity criterion in the sense that discharges characterized by the same $\bar{l}$ and $f(x)$ are described by the same equations.

In practice, however, for the channel expansion calculations it is more convenient to choose for the function of the unit of length R_0 not l, but a quantity that makes the coefficient in the rhs of Eq. (5.34) equal to unity and has the meaning of characteristic radius of the channel

$$R_0^4 = \frac{(\gamma-1)}{\pi\rho_0}\tau^2\frac{E}{l}\,. \tag{5.36}$$

Comparing (5.34) and (5.36), it is easy to establish that the dimensionless similarity criterion $\bar{l}$ is nothing but the fourth power of the ratio between the characteristic radius of the channel and its length. In other words, this is a criterion of geometric similarity of the discharges.

The choice of the length scale according to (5.36) leads to the following form for the equation of energy balance

$$\frac{d}{dx}y\dot{y} + \dot{y}^2\left[(\gamma-1) - \frac{1}{2\ln\frac{l}{R_0 y}}\right] = \frac{f(x)}{y^2\ln\frac{l}{R_0 y}}\,. \tag{5.37}$$

An estimate shows that the second term in the lhs of this equation is small and may be neglected.

The validity of such an approximation can be verified by comparing the terms of Eq. (5.37) after a numerical integration of the equation.Thus, from (5.37) we obtain

$$\frac{d}{dx}y\dot{y} = \frac{f(x)}{y^2\ln\frac{l}{R_0 y}}\,. \tag{5.38}$$

This equation can be rewritten in the form of two first-order equations

$$\frac{dz}{dx} = \frac{f(x)}{y^2\ln\frac{l}{R_0}y} \qquad \frac{dy}{dx} = \frac{z}{y}. \tag{5.39}$$

The boundary conditions are chosen on the basis of physical considerations in the form

$$x = 0\,, \qquad y = y_0\,, \qquad \dot{y} = 0\,, \qquad z = y\dot{y} = 0\,, \tag{5.40}$$

where y_0 is the initial radius of the channel.

If the energy release in the discharge channel , determined by the function $f(x)$, is known, the integration of Eq. (5.38) allows us to determine the law of the channel expansion, and with it other hydrodynamic quantities as well.

The corresponding formulas are:

- channel radius:

$$R = R_0 y\,. \tag{5.41}$$

- pressure in the channel:

$$P = \rho_0\frac{R_0^2}{r^2}\zeta_1(x)\,, \tag{5.42}$$

where

$$\zeta_1(x) = \frac{f(x)}{y^2} - \frac{z^2}{2y^2}\,.$$

- work done by the channel during the expansion:

$$A = l\rho_0\pi\frac{R_0^4}{r^2}z^2\ln\frac{l}{R}\,. \tag{5.43}$$

• internal energy of the plasma in the channel:

$$W = \frac{1}{\gamma - 1}\rho_0 \frac{\pi R_0^4 l}{\tau^2}\left[f(x) - \frac{z^2}{2}\right] . \tag{5.44}$$

For the calculation of the acoustic radiation of the discharge we can use formula (4.58). The first term in this formula, which can be rewritten in the form

$$p = \rho_0 \frac{R_0^2 l}{\tau^2} g_1(\overline{x}), \quad g_1(\overline{x}) = \frac{f(x)}{y^2 \ln \frac{l}{R_0} y} , \qquad \overline{x} = \frac{1}{\tau}(t - \frac{r}{c}) \tag{5.45}$$

describes the form of the wave radiated perpendicularly to the discharge axis ($\theta = \pi/2$).

The second term in (4.58), which gives a correction to the first term for $\theta \neq \pi/2$, is proportional to the small parameter of the model of a short cylinder and is thus small. This reflects the fact that the wave radiated by a short cylinder compared to the characteristic wavelength does not deviate much from spherical symmetry.

The acoustic energy radiated during the time of the discharge can be obtained by integrating the energy flux over the spherical control surface and the time

$$W_{ac} = 2 \oint_0^{\pi/2} \int_0^{\tau} \frac{p^2}{\rho_0 c_0} dt 2\pi r^2 \sin\theta d\theta = \pi \rho_0 \frac{l^2 R_0^4}{c_0 \tau^3}\left[J_1 + \frac{1}{12}\frac{l^2}{c_0^2 \tau^2} J_2\right] dx , \tag{5.46}$$

where

$$J_1 = \int_0^1 \left[\frac{f(x)}{y^2 \ln \frac{l}{R_0 y}}\right]^2 dx , \qquad J_1 = \int_0^1 \left[\frac{d}{dx}\frac{f(x)}{y^2 \ln \frac{l}{R_0 y}}\right]^2 dx .$$

The second term in brackets in Eq. (5.46) takes into account the deviation of the wave form from spherical symmetry. Formula (5.46) is applicable if this term is small compared with the first one.

Using (5.36) and (5.46), we find for the electro-acoustic efficiency of the discharge

$$\eta = \frac{W_{ac}}{E} = \frac{l}{c_0 \tau}(\gamma - 1) J_1. \tag{5.47}$$

To avoid misunderstandings, let us stress once again that all the results of this section, including Eq. (5.47), are valid only under the condition $R_0 \ll l \ll c_0 \tau$.

Let us also notice that, as was done in the case of the spherical model, we can, with the help of the relation (5.36), eliminate R_0 from the expressions of the hydrodynamic quantities, and obtain them in terms of the three parameters of the discharge: total energy released in the channel, time of the energy release and interelectrode gap.

Furthermore, from rough estimates for near-critical discharges, we may say that the energy release in the channel and the discharge duration are determined by formulas

(5.27). Correspondingly, we can obtain estimates for various hydrodynamic characteristics of the discharge. As an example, the peak pressure in the compression wave in the plane normal to the discharge axis and passing through the middle of the channel is determined by the expression

$$p_{\perp} \approx 10^{-4} \frac{U}{r} \sqrt{\frac{l}{L}}\, atm\,, \tag{5.48}$$

with U , r , l , L expressed, respectively, in $Volts$, cm and $Henrys$.

5.4. Model of a Long Cylinder

The approximation based on the smallness of the density perturbations is valid also for the treatment of long discharges, provided that the characteristic radius of the channel stays small compared with the wavelength: $R_0 \ll \lambda \ll l$ [4].

The pressure on the surface of a cylindrical bubble, whose extension is large compared with the wavelength, is approximately determined by Eq. (4.54)

$$P \approx \rho_0 \frac{\ddot{S}^2}{2\pi} \ln \frac{2c_0 t}{R} - \rho_0 \frac{\dot{S}^2}{8\pi^2 R^2}\,.$$

Inserting this expression first into Eq. (5.29) for the internal energy of the plasma and into Eq. (5.30) for the work on the channel expansion, and substituting the thus obtained formulas into the equation of energy balance (5.1), we obtain the following approximate equation

$$\left(\rho_0 \frac{\ddot{S}}{2\pi} \ln \frac{2c_0 t}{R} - \rho_0 \frac{\dot{S}^2}{8\pi^2 R^2}\right) S + \rho_0 \frac{S^2}{4\pi} \left(\ln \frac{2c_0 t}{R}\right) (\gamma - 1) = (\gamma - 1) E/l\,. \tag{5.49}$$

Introducing the dimensionless variables $x = t/\tau$, $y = R/R_0$ and $f(x) = E/E_0$, and neglecting the second and third terms of this equation, which are small, we obtain

$$\frac{dz}{dx} y^2 \ln \frac{2c_0 \tau}{R_0} - \frac{x}{y} = \frac{(\gamma - 1)}{\pi \rho_0} \frac{\tau^2 E}{R_0^4} f(x)\,. \tag{5.50}$$

Choosing as the new length unit the quantity defined by the relation

$$R_0^4 = \frac{(\gamma - 1)}{\pi \rho_0} \tau^2 E \tag{5.51}$$

which represents the characteristic radius of the channel, we arrive at the equation

$$\frac{dz}{dx} = l\frac{f(x)}{y^2 \ln \frac{2c_0\tau}{R_0}\frac{x}{y}}\,, \tag{5.52}$$

where $z = y\dot{y}$.

The initial condition in the case given can be conveniently chosen as

$$x \to 0\,, \quad y \to 0\,, \quad \dot{y} \to 0\ .$$

In practice, since the calculations are unaffected by the initial values of the various quantities, it is possible to choose as initial conditions values of channel radius and expansion rate that are sufficiently small compared with their characteristic values.

The hydrodynamic characteristics can be expressed through the solution of this system as follows:

• channel radius:

$$R = R_0 y\ . \tag{5.53}$$

• pressure in the channel:

$$P = \rho_0 \frac{R_0^2}{\tau^2}\zeta_1(x)\,. \tag{5.54}$$

• work on the channel expansion:

$$A = \pi\rho_0 l \frac{R_0^4}{\tau^2} \cdot \ln \frac{2c_0\tau}{R_0}\,\frac{x}{y}\,. \tag{5.55}$$

• internal energy of the channel plasma :

$$W = \pi\rho_0 \frac{R_0^4 l}{\tau^2}\left[f(x) - \frac{z^2}{2}\right]\,. \tag{5.56}$$

The acoustic radiation can be found, as in the case of a short cylinder, by totaling the signals from the elementary sources using Eqs. (4.56) and (4.57).

Along the direction normal to the channel axis ($\theta = \pi/2$, Fig. 4.8), we immediately obtain

$$p_\perp = \rho_0 \frac{R_0^2}{2\tau^2 r}\, g_2(\bar{x})\,, \tag{5.57}$$

where

$$g_2(\bar{x}) = \frac{f(\bar{x})}{y^2 \ln \frac{2c_0\tau}{R_0}\,\frac{x}{y}}\ .$$

In the longitudinal direction ($\theta = 0$), formula (3.46) gives

$$p_{\|} = \frac{\rho_0 c_0 R_0^2}{2r\tau} \int_{x_1}^{x_2} \frac{dz}{dx}\, dx\ ; \qquad x_{1,2} = x - \frac{r_0}{c_0\tau} \pm \frac{l}{2c_0\tau}\ . \tag{5.58}$$

Taking into account that the integrand function is not vanishing only on the interval $0 \leq x \leq 1$ (the duration of the signal is small compared with its *traveling* time along the cylinder length l/c_0), it is not difficult to establish that the maximum value of the longitudinal signal is determined by the expression

$$p_{\|} = \frac{\rho_0 c_0 R_0^2}{2r\tau} \int_0^1 \frac{dz}{dx}\, dx\ = \frac{\rho_0 c_0 R_0^2}{2r\tau} z(1)\ . \tag{5.59}$$

The ratio between the amplitudes of the transverse and longitudinal signals $p_\perp / p_{\|} = l/c_0\tau z(1)$, is, up to the factor $\frac{1}{z}$ (1) (which is close to 1, see Ch. VI), equal to the ratio between the channel length and the pulse length. This reflects the simple fact that the transverse signal is obtained by totaling the amplitudes, while the longitudinal one is obtained by totaling the durations of the elementary pulses, the number of which is proportional to the length l of the emitter.

The total energy radiated by the channel during the time of the discharge

$$W_{ac} = \frac{4\pi r^2}{\rho_0 c_0} \int_0^{\pi/2} \sin\theta d\theta \int_0^{\tau} p^2 dt \tag{5.60}$$

can be calculated using the results of Ch. IV, namely Eqs. (4.65) and (4.67).

Assuming, rather roughly, that an elementary pulse has a rectangular form, and assuming also, on the basis of Eq. (5.57), that $p_\perp = \rho_0 R_0^2 l / 2\tau^2 r$, from Eq. (4.65) we obtain, using (5.51)

$$W_{ac} = (\gamma - 1) E \left[\frac{1}{8} \frac{c_0\tau}{l} + \frac{1}{2} - \ln \frac{c_0\tau}{l} \right]\ , \tag{5.61}$$

whence, without difficulty we can determine also the electro-acoustic efficiency of the discharge

$$\eta = (\gamma - 1) \left[\frac{1}{8} \frac{c_0\tau}{l} + \frac{1}{2} - \ln \frac{c_0\tau}{l} \right]\ . \tag{5.62}$$

Let us consider now the case in which the form of the compression pulse emitted in a transverse direction with respect to the channel axis is approximated by a Gaussian distribution with decay constant $\tau_0 = 0.7\tau$, and amplitude given, according to (5.57), by

$$p_\perp = \frac{\rho_0 R_0^2 l}{2\tau^2 r}. \tag{5.63}$$

(In other words, we are considering the case in which the dimensionless function of (5.57) is approximately replaced by the error function.) As it will be seen later in the calculation of the hydrodynamical characteristics of a discharge, the Gaussian approximation for the pulse is the closest to the experimental situation. Formulas (4.67), (5 51) and (5.63) lead to the following expressions for the acoustic energy and electro-acoustic efficiency

$$W_{ac} = (\gamma - 1)\left(\frac{\tau_0}{\tau}\right)^2 E\left[0.25\frac{c_0\tau}{l} + 0.42 + \ln\frac{l}{c_0\tau}\right], \tag{5.64}$$

$$\eta = (\gamma - 1)\left(\frac{\tau_0}{\tau}\right)^2 \left[0.25\frac{c_0\tau}{l} + 0.42 + \ln\frac{l}{c_0\tau}\right]. \tag{5.65}$$

Let us note that the hydrodynamic characteristics can be expressed as a function of the fundamental discharge parameters E, τ and l by eliminating R_0 from the appropriate formula with the help of the relation (5.51).

These quantities, in turn, can be expressed, as before, in terms of the parameters of the discharge loop. By doing so, we would obtain a formula to estimate the pressure in the compression wave exactly coinciding with Eq. (5.48).

5.5. Spherical Model : Case of High Channel Expansion Rates

The channel expansion rate of a point-like electric discharge is determined, on order of magnitude, by the expression

$$\frac{R_0}{\tau} \sim \frac{E^{1/5}}{t^{3/5}},$$

which follows from Eq. (5.12).

As we see, the rate is proportional to the energy density in the discharge channel and increases as the time of energy release decreases. If a sufficiently large amount of energy is introduced into the discharge channel in a small time interval , then the expansion of the channel can occur at rates close to, or even exceeding the speed of sound in the fluid. The density perturbations are considerable and the fluid compressibility must to be taken into account in the investigation of such discharges.

We shall restrict ourselves to the case of a point-like discharge, characterized by the following relations among the three length parameters [5]:

$$l \ll R_0 \ll \lambda .$$

As previously, we will neglect the effect of the magnetic pressure, which is assumed to be small compare with pressure of hydrodynamic origin. The motion of the fluid

caused by the channel expansion will be considered isentropic, which allows us to use the equation of state (4.3)

$$p = A\left(\frac{\rho}{\rho_0}\right)^n - B \ ,$$

where $A = 3001\, atm$, $B = 3000\, atm$ and $n = 7$ (for water).

In practice, it is convenient to divide the calculation of the hydrodynamical characteristics of a discharge into two problems to be solved in succession: 1) calculation of the channel expansion for a given energy release law; 2) calculation of the radiation of a compression wave by the channel which is expanding according to a given law.

The process of channel expansion is described in an approximate way by the system of equations

$$\begin{aligned} P\frac{dV}{dt} + \frac{1}{\gamma - 1}\frac{d}{dt}PV &= \dot{E}(\bar{t}), \qquad (5.66) \\ R\frac{d^2R}{d\bar{t}^2}(1 - \frac{U}{c}) + \frac{3}{2}(1 - \frac{U}{c})U^2 &= (1 + \frac{U}{c})H + \frac{R}{c}(1 - \frac{U}{c})\frac{dH}{d\bar{t}} \\ H &= \int_{p_0}^{p}\frac{dP}{\rho} = \frac{c_0^2}{n-1}[(\frac{P+B}{A})^{\frac{n-1}{n}} - 1] \ . \end{aligned}$$

The first of these equations describes the law of energy conservation in the discharge. The second and third ones may be regarded as relations determining the pressure on the surface of the expanding sphere, which equals the pressure P inside the channel, as a function of the channel radius and its time derivatives. The last two equations are derived from the hydrodynamic equations and the equation of state for the fluid is obtained within the Kirkwood-Bethe approximation (see [6] and Eq. (4.76)).

In writing Eq. (5.66), we have introduced additional notations not used before: $\dot{E}$ is the power released in the channel; H is the enthalpy of the fluid near the surface of the expanding sphere; and $c = c(\rho)$ is the local speed of sound, which is here, unlike previous cases, a variable quantity.

We choose the initial conditions as follows:

$$\bar{t} \to 0 \ , \quad R \to 0 \ , \quad \dot{R} \to 0 \ .$$

In practice, as previously noted, for the channel radius and the channel expansion rate at $\bar{t} = 0$ we may take values sufficiently small compared with their characteristic values. For the purpose of performing numerical calculations, it is convenient to rewrite Eqs. (5.66) in a dimensionless form. Let us introduce the dimensionless variables

$$x = \frac{\bar{t}}{\tau}, \quad y = \frac{R}{R_0}, \quad z = \frac{c}{c_0}, \quad \zeta = \frac{P}{\rho_0\frac{R_0^2}{\tau^2}}, \quad \eta = \frac{H}{\frac{R_0^2}{\tau^2}}, \quad M = \frac{R_0}{c_0\tau}, \qquad (5.67)$$

where τ, R_0 are the new units of time and length; c_0 is the equilibrium speed of sound, and M is Mach's number.

Choosing the duration of the discharge as a time unit, and as a length unit the characteristic radius of the channel determined by Eq. (5.12), from (5.66) we can obtain the following system of equations :

$$\frac{d\zeta}{dx} = \frac{\dot{f}(x)}{y^3} - 3\gamma\frac{\zeta}{y}\frac{dy}{dx} \tag{5.68}$$

$$\frac{d^2y}{dx^2} = \frac{1 + M\frac{\dot{y}}{z}}{1 - M\frac{\dot{y}}{z}}\frac{\eta}{y} + M\frac{1}{z}\frac{d\eta}{dx} - \frac{3}{2}\frac{1 - \frac{1}{3}\frac{\dot{y}}{z}}{1 - M\frac{\dot{y}}{z}}\frac{\dot{y}^2}{y} \tag{5.69}$$

$$\eta = \frac{i}{M^2(n-1)}[(nM^2\zeta + \frac{B}{A})^{\frac{n-1}{n}} - 1] \tag{5.70}$$

$$z = (M^2 n\zeta + \frac{B}{A})^{\frac{n-1}{n}}, \quad \dot{y} = \frac{dy}{dx}, \quad M = \frac{R_0}{c_0\tau}, \tag{5.71}$$

where $y(x)$, $\zeta(x)$, $z(x)$ and $\eta(x)$ are unknown functions, A, B and n are the constants of the equation of the state of the fluid, and $f(x)$ is the dimensionless power function that characterizes the energy release regime in the channel. In dimensionless form, the initial conditions are written as

$$x \to 0, \qquad y \to 0, \qquad z \to 0, \qquad \zeta \to 0, \qquad \eta \to 0.$$

Let us note that the system of equations (5.68)-(5.71), which describes the process of expansion of the channel, contains only one similarity criterion the Mach number M. In the limiting case, as $M \to 0$, this system becomes, as expected, a system of equations describing the expansion of the channel in the spherical model for small expansion rates (see Section 5.2).

The numerical integration of the system (5.68)-(5.71) gives the time dependence of the channel radius, the channel expansion rate, the pressure in the channel, and the value of the functions

$$G(\bar{t}) = R(H + U^2/2) = (R_0^3/\tau^2)y\left(\eta + \frac{1}{2}\dot{y}^2\right) = \frac{R_0^3}{\tau^2}g(x)$$

on the surface of the expanding sphere.

The determination of these functions is the starting point in the solution of the radiation problem in the Kirkwood-Bethe theory. This theory assumes that the values of the

function $G = r\left(h + \frac{1}{2}v^2\right)$, where h is the fluid enthalpy at a given point r, and v is the hydrodynamic speed, stay constant at points *travelling* at speed $c + v$. This assumption allows us to determine the values of G at an arbitrary point in space given its values on the surface of the sphere.

In practice, it is more convenient to calculate the function inverse to $G(t, r)$ [7] using the formulas Eqs. (4.86)–(4.91) rewritten in dimensionless form:

$$\xi = \frac{t}{\tau} = x(g) + M^3\frac{n+1}{4}g[\frac{1+2\beta v}{\beta v(1+\beta v)} - \frac{1+2\beta U}{\beta U(1+\beta U)} - \\ -2\ln\frac{(1+2\beta v)\beta U}{(1+2\beta v)\beta v}] \tag{5.72}$$

$$\beta v = \frac{1}{2}[(1+(n+1)\frac{R_0}{r}M^2 g)^{1/2} - 1], \tag{5.73}$$

$$\beta U = \frac{1}{2}[(1+(n+1)\frac{g}{y}M^2 g)^{1/2} - 1], \qquad \beta = \frac{(n+1)}{4c_0}. \tag{5.74}$$

For small perturbations, when $M \ll 1$ and therefore $\beta U \ll 1$ and $\beta v \ll 1$, these expressions become

$$t - \frac{r-R}{c_0} = \tau x(g)\,, \tag{5.75}$$

which represents the solution corresponding to the approximation of linear acoustics.

The inclusion of the next term in the expansion of Eqs. (5.72)–(5.74) with respect to M leads to the equation :

$$t - \frac{r-R}{c_0} = \tau x(g) - \tau g M^3\frac{n+1}{2}\ln\frac{r}{R}\,, \tag{5.76}$$

This approximate equaion shows the effect of the nonlinear terms on the wave propagation: the points in the wave profile corresponding to large values of g arrive at the observation point in shorter times t, i.e., they *travel* faster than the point with smaller g.

Knowing the values of the function G, we can easily determine the hydrodynamic speed (5.73) and pressure

$$p = A\left[\frac{2}{n+1} + \frac{n-1}{n+1}\left(1 + \frac{n+1}{r}R_0 M^2\right)^{\frac{1}{2}}\right]^{\frac{2n}{n-1}} - B \tag{5.77}$$

and find the profile of the compression wave at an arbitrary point in space.

This formula simplifies in the region where $(n+1)M^2R_0/r \ll 1$ and takes the form

$$p = \rho_0 \frac{R_0^3}{\tau^2 r} g(t)\,. \tag{5.78}$$

As is well known, at large enough distances from the discharge, the solution for the compression wave profile may become non-unique [8]. This fact indicates the formation of shock fronts. The position of the shock fronts and the value of the discontinuity are determined by matching the obtained solution with the Rankine- Hugoniot relations on the shock front. For small intensity shock waves, this reduces to the simple *equal areas* rule [8].

At large distances from the discharge, where nonlinear effects lead to strong distortions of the original wave profile, the shock wave takes a form that depends weakly on the detailed behavior of function G on the surface of the channel. This allows us to derive simple asymptotic expressions describing the shock wave in a region far from the discharge, and, in particular, to explain the character of wave damping. Two situations are possible.

If the rate of channel expansion equals or exceeds the speed of sound, the shock waves are generated in the immediate vicinity of the discharge. In such a case, we can use the asymptotic expressions of the theory set forth by Kirkwood and Bethe to describe shock waves from explosions that are valid at large distances from the point of the explosion.

According to this theory, the wave is assumed to have an approximately exponential form

$$p = p_m \exp\left(-t/\tau_0\right),$$

with p_m and τ_0 given by

$$p_m = \rho_0 G_m / r\,, \quad G_m = \alpha G_0\,.$$

Here G_0 is the maximum value of G on the surface of the sphere, and α is a quantity that characterizes the damping of the shock wave

$$\alpha = \frac{2}{1+\sqrt{1+4\beta\frac{G_0}{c_0^2\tau}\ln\frac{r}{R_0}}}\,, \tag{5.80}$$

where R_0 and τ are the characteristic values of the channel radius and expansion time:

$$\tau_0 = \frac{2\beta G_0}{c_0^2} \ln \frac{r}{R_0}. \tag{5.81}$$

Formulas (5.79)–(5.81) are applicable if the conditions

$$2\beta G_0/\tau c_0^2 > 1, \tag{5.82}$$

$$\ln \frac{r}{R_0} >> 1 \tag{5.83}$$

are satisfied. The first inequality expresses the condition for the formation of the discontinuity near the discharge, and the second one allows us to use the asymptotic formulas of the Kirkwood-Bethe theory. As we can see, the parameters of a shock wave at large distances are determined simply by the maximum values of the function G, provided that the characteristic values R_0 and τ are known.

In turn, for rough estimates we may assume that $G_0 \approx R_0^3/t^2$, i.e., that the maximum value of g is close to unity. As we shall see later, such an assumption agrees with the results of numerical calculations.

Using the estimate for G_0 given above, we can rewrite the inequality (5.82) as

$$\frac{2\beta G_0}{c_0^2 \tau} = 4M^3 = \left(\frac{E/R_0^3}{\rho_0 c_0^2}\right)^{\frac{3}{2}} \approx \left(\frac{E}{\rho_0 c_0^5 \tau^3}\right) > 1\,. \tag{5.84}$$

From this formula it follows, in particular, that the possibility of formation of a shock wave depends on the ratio between the energy density in the channel, which is proportional to the pressure in it, and the characteristic pressure $\rho_0 c_0^2$ in the fluid.

If the rate of the channel expansion is smaller than the speed of sound, which occurs when the condition opposite to (5.84) is realized, i.e.

$$4M^3 = \frac{2\beta G_0}{\tau c_0^2} < 1\,, \tag{5.85}$$

then shock waves may be generated as a result of the accumulation of nonlinear effects at a certain distance from the discharge. Including this inGthe calculations, performed in the nonlinear approximation of ref. [5], leads to the following approximation for p_m

$$p_m = \rho_0 \frac{G_m}{r}\,, \qquad \beta G_m^2/c_0^2 = \frac{5}{4} G_0 \tau \left[\ln \frac{r}{R_0}\right]^{-1}. \tag{5.86}$$

This formula is valid if $\ln \frac{r}{R_0} \gg \frac{c_0 \tau}{2\beta G_0}$. The realization of this conditions means that the shock wave was formed at a distance r.

5.6 Approximate Calculation of Electric and Hydrodynamic Characteristics of a Discharge for Given Parameters of the Electric Loop

The models for an electric discharge in a fluid considered in the previous sections are incomplete in that, in order to calculate the hydrodynamic characteristics of a discharge, the law of energy release must be given, which in turn is determined by the electric characteristics of the process.

If we include the electric loop in our analysis, we can obtain a closed system of equations that describes both the electric and the hydrodynamic phenomena involved in a discharge. An approximate calculation along this line was carried out by A. I. Ioffe in his work [9], which we shall follow in our presentation below.

The main difficulty arising in considering this closed model is related to the determination of the time varying channel resistance, which depends on the particle density and temperature in the channel.

We shall assume that the discharge electric loop consists of an oscillatory circuit with a given inductance L, capacitance C, and resistance determined by the time-varying resistance of the discharge channel.

Then, the electric characteristics of the process are described by the equation of the oscillatory circuit

$$\frac{d^2U}{dt^2} + \frac{R_e}{L}\frac{dU}{dt} + \frac{U}{LC} = 0\,, \qquad R_e = \frac{l}{\eta_{ei} S}\,. \tag{5.87}$$

Here, U is the voltage applied to the capacitor, R_e is the ohmic resistance of the discharge channel, $1/\eta_{ei}$ is the resistivity, and S is the cross-section area of the channel.

We shall assume that, according to what was presented in Ch. III, the conductivity of the plasma is determined solely by the interaction of the electrons with the ions and is described by the expression (3.29) (for $Z = 1$)

$$\eta_{ei} = 1.52 \cdot 10^{-4} \frac{T^{3/2}}{\ln \Lambda} \qquad \left(\frac{1}{\Omega \cdot cm}\right), \tag{5.88}$$

where

$$\Lambda = \frac{3(kT)^{3/2}}{2\sqrt{4\pi} e^3 n_e^{1/2}}\,.$$

In practice, the quantity $\ln \Lambda$, which does not vary much with the electron concentration, is assumed constant in the calculations. Here, e is the electron charge, T the temperature,and $n_e$is the number of elektrons per unit volume.

For definitiveness , let us consider a discharge in the model of a short cylinder. In other words, we assume that the width of the interelectrode gap is large compared

with the characteristic radius of the channel, but much smaller than the characteristic wavelength: $R_0 \ll l \ll \lambda$, $\lambda = c_0\tau$, where τ is the discharge duration.

Then, the equation of energy balance per unit of the channel length can be written in the form

$$P\frac{dS}{dt} + \frac{1}{\gamma - 1}\frac{dPS}{dt} = c^2(\frac{dU}{dt})^2\frac{1}{\eta S} = I^2R_e \tag{5.89}$$

$$I = C\frac{dU}{dt},$$

and the pressure on the surface of the expanding cylinder is determined by Eq. (4.48), which can be conveniently rewritten as

$$P = \frac{\rho_0}{2\pi}\ddot{S}\ln\left(\sqrt{\frac{\pi}{S}}l\right) - \rho_0\frac{\dot{S}^2}{8\pi}. \tag{5.90}$$

Estimates show that the free path of the radiation in plasma at a temperature of $T \approx 2 \cdot 10^{4\circ}K$ and density $n_e \approx 10^{20}cm^{-3}$ equals approximately $l_v \sim 10^{-1}cm$ and is small compared with the characteristic channel radius (see Ch. III). Therefore, channel plasma may be considered a blackbody radiating a flux $q = \sigma T_{eff}^4$ per unit of surface.

Thus, if we assume that the radiation energy flux q is absorbed in the thin water layer and is used only for the evaporation of water in the channel, for the particle density in the channel we can write the following equation:

$$\frac{d}{dt}nS = \frac{2\pi R\sigma T^4}{D}, \tag{5.91}$$

where D is the evaporation energy per molecule.

Together with the equation of state for an ideal gas

$$p = nkT, \tag{5.92}$$

which is approximately applicable for a discharge plasma only weakly ionized, relation (5.91) closes the system of equations, which now consists of the five equations (5.87)–(5.92).

This system can be integrated numerically with suitable initial conditions. Some of these conditions are obvious: at the initial instant the capacitor is charged with a given voltage U_0, and there is no current, which gives the condition $dU/dt = 0$. The remaining conditions are not as definite: in practice, for the calculations we assume that the initial value of the channel crosssection equals $0.1\,cm^2$, the expansion rate is zero, and the initial temperature and particle density are chosen equal to $10^4\,^\circ K$ and

$10^{19}\,cm^{-3}$. A 10–30% variation in the initial values has a small effect on the final results.

The results of calculations describe the electric and hydrodynamic characteristics of a discharge for given values of the four parameters: initial voltage on the capacitor, inductance L, and capacitance C of the discharge loop and discharge gap l. The results are compared with experiments in the next chapter.

5.7. Similarity of Electric Discharges in a Liquid

As stated earlier, the relation among the three length scales, width of the discharge gap l, characteristic channel radius R_0, and characteristic wavelength λ, is an important characteristic of the hydrodynamic phenomena in a discharge. In particular, such a relation determines which of the models previously examined is to be adopted.

This relation is characterized by two dimensionless parameters: $M = R_0/\lambda$ and $N = l/\lambda$. The first parameters equals the ratio between the characteristic rate of channel expansion and the speed of sound, and may, therefore, be called the Mach number. The second one characterizes the channel length with respect to the length of the radiated wave. Different values for these parameters lead to different discharges; conversely, equal values correspond to the same discharges, in the hydrodynamical sense. Hence, these parameters play the role of hydrodynamic similarity criteria.

The meaning of these parameters becomes more clear if we examine the dimensionless equations that describe the various discharge models [see, e.g., Eqs. (5.13), (5.28), (5.38), (5.47), (5.52), (5.62) and (5.69)] . In spite of the differences between these equations, the common feature is that the parameters M and N (or their ratio) appear in all of them.

From this observation it follows that discharges with equal values of M and N are described by equations that may differ only in the form of the dimensionless function $f(x)$ that characterizes the law of energy release in the channel.

It is, however, easy to convince oneself that the character of this function, determined by the time dependence of the power I^2R_{ohm}, depends, besides M, only on one other parameter, namely $Z = R_{eff}\sqrt{L/C}$, which appears as a factor in the equation of the discharge current

$$\frac{d^2I}{dx^2} + \pi Z \frac{d}{dx}\bar{R}(x)I + \pi^2 I = 0.$$

Here, I is the discharge current; R_{ohm} is the active loop resistance, which is supposed to be determined mainly by the channel resistance; R_{eff} denotes the effective value of this quantity, equal to $l/\eta S$ for the cylindrical model and to $1/\eta R$ for the spherical model; L,C are the loop inductance and capacitance, respectively; $\bar{R}(z) = R_{ohm}/R_{eff}$ is a dimensionless resistance, which may be assumed equal for similar discharge functions of x, $x = t/\tau$, $\tau = \pi\sqrt{LC}$.

Thus, we conclude that discharges with equal values of M, N, and Z are described by the same equations, i.e., these parameters provide a similarity criterion.

Let us represent them in a somewhat different form. Let us first consider discharges that may be described by cylindrical models. In this case, the parameter Z, which represents the similarity criterion for the electric (and energy) characteristics of the discharge, can be written as

$$Z = R_{eff}\sqrt{\frac{C}{L}} = \sqrt{\frac{C}{L}}\frac{l}{\eta S} \sim \sqrt{\frac{C}{L}}\frac{l}{\eta_{eff}\frac{R_0^2}{\tau^2 c^2}\tau^2 c^2}, \tag{5.93}$$

where S is the cross-section area of the channel.

The plasma conductivity is determined by the temperature and the pressure in the channel. From Eq. (3.43) for discharges described by a cylindrical model, the temperature is

$$T \sim (E/\tau^2 l)^{3/20} \sim M^{3/5},$$

and therefore it is equal for discharges with equal M; for discharges corresponding to the spherical model,

$$T \sim M^{4/5}\tau^{1/5}$$

i.e.the temperature does not vary much with τ for constant M. The pressure in the channel is $\sim M^2$ and is therefore equal for the similar discharges.

Therfore, both the temperature and the pressure can be considered equal for similar discharges, and therefore dropping η_{eff} as well as the combination of parameters that are constant for similar discharges and equal to M^2 , we obtain

$$Z \sim \sqrt{\frac{C}{L}}\frac{l}{\tau^2 c^2}. \tag{5.94}$$

When considering the similarity of discharges in a given fluid, we may consider the speed of sound c to be constant. Then

$$M \sim R_0/\tau, \qquad N \sim l/\tau, \qquad Z \sim \sqrt{\frac{C}{L}\frac{l}{\tau^2}}. \tag{5.95}$$

Let us now express these similarity criteria in terms of the parameters usually given in an experiment: C, U, L, and l. From (5.36), we have

$$M = R_0/\tau \sim \left(\frac{E}{l\tau^2}\right)^{\frac{1}{4}} \sim \left(\frac{U^2}{lL}\right)^{\frac{1}{4}}, \qquad N \sim \frac{l}{\sqrt{LC}}, \qquad Z \sim \frac{l}{L^{3/2}C^{1/2}}.$$

From these expressions it follows that in order for discharges to be similar, the quantities U^2/lL, $l/\sqrt{LC}$, $l/L^{3/2}C^{1/2}$ must be constant. For the case of cylindrical discharges in a given fluid, this leads to the following similarity criterion

$$\frac{u_1^2}{u_2^2} = \frac{l_1}{l_2} = \sqrt{\frac{C_1}{C_2}}, \qquad L_1 = L_2 . \tag{5.96}$$

Let us note that relations (5.93)–(5.96) coincide with the results of ref. [10], obtained using the general methods of the similarity theory.

Taking into account that the equations of the spherical model do not depend on the parameter N, we obtain that in this case discharges are similar if the parameters

$$M = \frac{R_0}{c\tau}, \qquad Z = \sqrt{\frac{C}{L}}\frac{1}{\eta R_0} \sim \sqrt{\frac{C}{L}}\frac{1}{\eta\frac{R_0}{c\tau}c\tau} \sim \sqrt{\frac{C}{L}}\frac{1}{c\tau} \tag{5.97}$$

are constant. For discharges in a given fluid, these criteria can be rewritten in the form

$$M \sim (E/\iota^3)^{1/2} \sim u^2/L^{3/2}C^{1/2}, \qquad Z \sim \sqrt{\frac{C}{L}\frac{1}{\tau}} \sim 1/L^{3/2}C^{1/2}. \tag{5.98}$$

From these relations we obtain, e.g., that two spherical type discharges are similar if the conditions

$$\frac{u_1^2}{u_2^2} = \frac{L_1^{3/2}}{L_2^{3/2}} = \frac{C_1}{C_2} \tag{5.99}$$

are satisfied.

Discharge similarity means not only that the dimensionless functions appearing in Eqs. (5.16)–(5.19), (5.20)–(5.22) and others are the same, but also that the absolute values of the quantities that characterize the channel expansion process (pressure, expansion rate, etc...) at corresponding moments in time (equal x) are equal. Furthermore, also equal are the characteristics of the compression wave, determined at the corresponding points in space (i.e., at l/r or R_0/r) and corresponding moments in time.

REFERENCES to Chapter V

[1] Ioffe A.I. Naugolnykh K. A., Roi N. A., "On the initial stage of the underwater electrical discharge," Zh. Priklad. Mekh. Tekh. **4** 108-112 (1964)

[2] Naugolnykh K. A., Roi N. A., Point electrical discharge in a liquid, Zh. Priklad. Mekh. Tekh. **4,** 137-140 (1967).

[3] Naugolnykh K. A., Roi N. A., "Connection between hydrodynamical and electrical characteriscitcs of the discharge in a liquid," Doklady Academii Nauk SSSR **168** (3), 556-559 (1966).

[4] Ioffe A. I., Kozhelupova N. G., Naugolnykh K. A., Roi N. A., "Acoustical radiation of a long underwater spark,"Akust. Zh. **13** (2), 208-212 (1967).

[5] Ioffe A. I., Naugolnykh K. A., "On the generation of shock waves by underwater electrical discharge,"Zh. Priklad. Mekh. Tekh. **1,** 134-137 (1968).

[6] Cole R., *Underwater explosion*, (Princeton UP, Princeton,1948).

[7] Akylichev V. A., Boguslovskij Ju. A., Ioffe A. I., Naugolnykh K. A., "Radiation of a spherical wave of finite amplitude,"Akust. Zh. **13** (3), 321-327 (1967).

[8] Landau L. D., Lifshitz E. M., *Fluid Mechanics*, (Pergamon Press, N.Y. 1975)

[9] Ioffe A. I., "Theory of the initial stage of an electrical discharge in water,"Zh. Priklad. Mekh. Tekh., **6,** 69-72 (1966).

[10] Okun' I. Z., *Theoretical and Experimental Investigation of Pulse Discharges in a Liquid*, (Dissertation), Politechnical Institute, Leningrad, (1969).

Chapter VI

HYDRODYNAMIC CHARACTERISTICS OF SPARK DISCHARGES. COMPARISON WITH EXPERIMENT

6.1. Introduction

The theory of electric discharges in fluids allows us to calculate the hydrodynamic characteristics, provided that the law of energy release in the channel is known. The law of energy release may be characterized by the dimensionless function $f(x) = E(t)/E(\tau)$ with $x = t/\tau$, where τ is the discharge duration. Experimental data show that the form of this function is nearly the same for near-critical discharges. This fact lends a certain universality to the calculation of the hydrodynamic characteristics of a discharge performed for one kind of function $f(x)$. Below we give the results of such numerical calculations obtained using expressions (3.1) and (3.2), which approximate the energy release law for near-critical discharges.

Let us remark that these results can by applied in an approximate way for the calculation not only of near-critical discharges, but also of aperiodic and periodic discharges, provided that a correction is introduced. In the first (aperiodic) case, such a correction is needed to take into account the increase of the discharge duration compared to the value $\pi\sqrt{LC}$, and in the second (periodic) case, to compensate for the fact that during the first half-period only part of the stored energy $CU^2/2$ is released .

We need to emphasize that we are discussing only phenomena occurring during the discharge, when electric current flows along the channel. The hydrodynamic phenomena in the subsequent stages of the discharge are not considered at all in the present work. We shall only note that a pulsating bubble that is formed as a result of a discharge is in many aspects similar to a gas bubble generated in an underwater explosion or cavitation.

In particular, the pulsation process of a spherical bubble at large distances from the boundaries is described by the expressions given in Section 4.2, which lead to the simple relation (Eq.4.28) connecting the pulsation period with the pulsation energy.

During the contraction phase of the pulsation, the bubble radiates compression waves, which can be easily detected experimentally. This allows us to determine the pulsation period, and then, using Eq. (4.28), the energy of the pulsating bubble in the spherical model.

Discharges corresponding to cylindrical models generate gas bubbles similar in form to cylinders with hemispherical ends. In the subsequent stages of the expansion, such a bubble progressively takes a form close to spherical. Film records show that the contraction of non-spherical bubbles is accompanied by loss of a stable form. A bubble breaks up into several separate bubbles of various forms, which contract at different times, thus generating several compression pulses. The instability of the contraction process is reflected also in the noticeable fluctuation of the pulsation periods of bubbles generated by discharges with equal electric characteristics. Naturally, the

connection between bubble energy and pulsation period given by Eq. (4.28) is a rather rough approximation in the case of cylindrical type discharges.

The pulsation energy, being equal to the product of the maximum volume of the bubble and the hydrostatic pressure, can be determined also through measurements from photos taken with lightening from the bottom . According to the experimental data, the pulsation energy of a bubble generated in an electric discharge amounts to about 30% of the total energy released in the channel.

Out of the three basic hydrodynamic characteristics of a discharge, namely time dependence of the channel radius, pressure in the channel and pressure in the compression wave, the last two are the most sensitive to the accuracy of the calculation, since they depend not only on the channel radius, but also on its time derivatives.

The measurement of the pressure in the channel, however, is a rather complicated experimental task due to the presence of high electric voltage in the measurement zone. It is a much simpler process to measure the pressure in the compression wave radiated by the discharge. It is, therefore, this latter quantity that is used in the comparison of theoretical and experimental results.

The measurements of the pressure in the compression pulse are usually done using large-band pressure detectors. There are two types of such detectors: detectors in which the sensitive element is directly exposed to the effect of the pressure being measured, and waveguide type detectors, in which the sensitive element reacts to the deformation wave generated in a long metallic rod that is affected on one its end by the pressure being measured; the lateral surface of the rod is acoustically insulated from the external medium with a metallic tube.

The more convenient sensitive elements are the piezoelectric type, made of piezoceramic, e.g., barium titanate with an admixture of cobalt or piezoceramic ZTS-200. If the pressure on the piezoelement exceeds a few hundred atmospheres, then, in order to prevent nonlinear distortions, it is necessary to adopt a protective reinforcement of the piezoelement. Piezoelements in the shape of cylinders with a diameter and height of $3\,mm$ and a wall thickness of $0.3\,mm$ have a capacitance of about $1000\,pF$ and a lowest natural frequency of about $0.5\,MHertz$. With an input resistance of the oscillograph of a few megaohms, the receiving length allows us to reproduce screen pressure pulses on the oscillograph of duration from 10^{-3} to $10^{5}\,sec$ without any noticeable distortions.

In receivers of the first type (Fig. 6.1), the piezoelement is attached to one end of a coaxial holder using flexible resin. A flexible fixture is needed to prevent the elastic waves, generated in the holder under the effect of a compression wave, to be transmitted to the piezoelement. We must remember the following circumstance. In a compression wave of large amplitude, the displacement speed of the fluid particles is large.

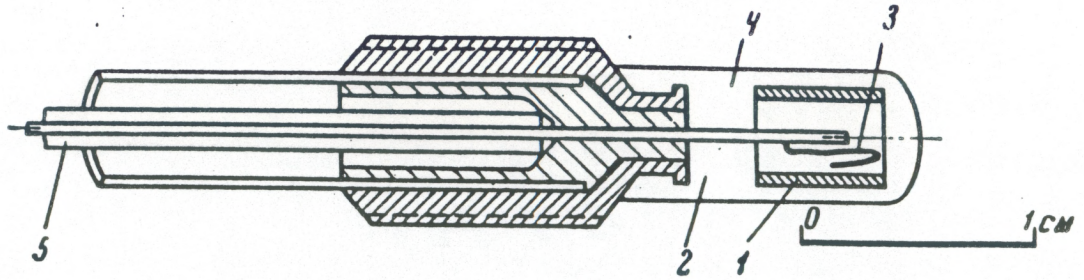

Fig. 6.1. Hydrophone's design: 1. Piezoceramic cylinder. 2. Resin filling. 3, 4. Connectors to the electrodes. 5. Single-wire cable.

Fig. 6.2. Design of a waveguide type hydrophone: 1. Waveguide. 2. Piezoelement. 3. Screening tube. 4. Thread.

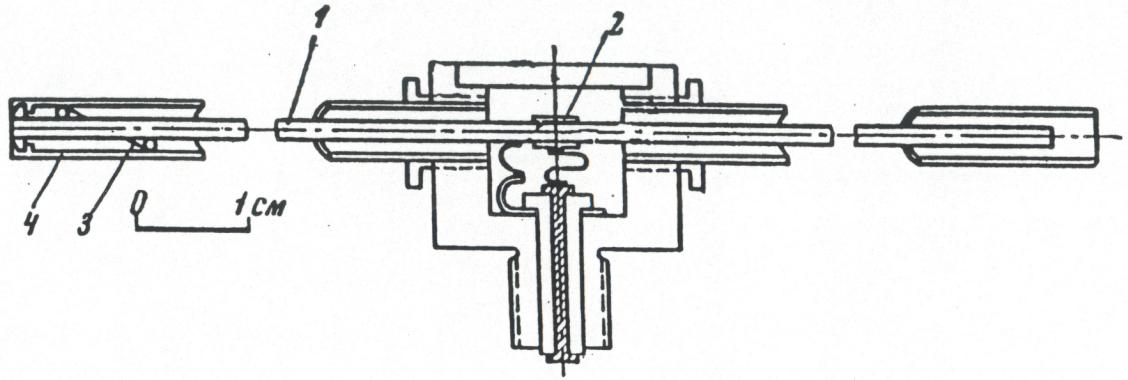

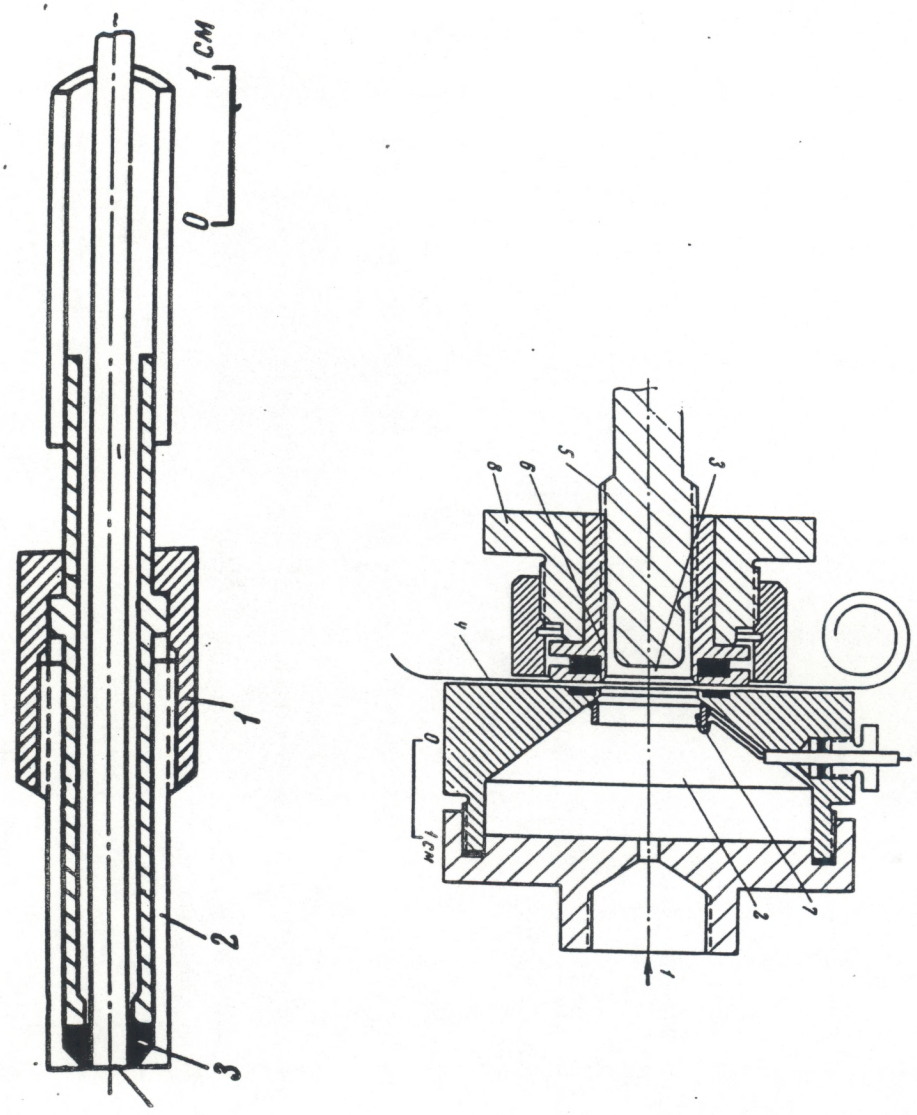

Fig. 6.3. Scketch of a gasket: 1. Sleeve nut. 2. Adjustable sleeve. 3. Resin ring. 4. Waveguide's end.

Fig. 6.4. Sketch of a calibrator: 1. Inlet. 2. Large chamber. 3. Small chamber. 4. Film separating the chambers. 5. Pressure receiver under calibration. 6. Knife cutting the fim at the rotation of the nut 8. 7. Ring-shaped piezoelement to trigger the oscillograph.

The motion of the piezoelement caused by the fluid generates in it mechanical tensions of inertial nature. If the piezoelement has a smaller sensitivity to volume compression than to lateral compression, the results of the pressure measurement are not accurate if the calibration of the piezoelement was done in the absence of lateral compression. A cylindrical piezoelement, due to its axial symmetry, is not sensitive to compression in a direction normal to its axis. Therefore, under the effect of a compression pulse in this direction, such a receiver reacts only to the volume compression. A piezoelement in the shape of a piezoceramic cube or disk may give false readings about the pressure in a compression wave if it has been calibrated under volume compression.

In waveguide type receivers (Fig. 6.2), a cylindrical piezoelement is slipped on a waveguide and firmly fixed to it. The distance between the free end of the waveguide and the piezoelement must be no less than half the pulse length in the material of the waveguide to avoid the superimposition of the reflected with the direct pulses. It is necessary to provide good acoustic insulation between the waveguide and the screening tube. To achieve this it is sufficient, for example, to wind a half-millimeter wool thread around the waveguide with a $1\,cm$ step. An important element is the gasket on the working end of the waveguide, which prevents the water from falling into the screening tube without, at the same time, creating a strong acoustic connection between screening tube and waveguide. A measure of the smallness of such a connection is the absence of transmission of compression pulses to the waveguide when tapping with a metallic object on the screening tube and on the end of the gasket. Fig. 6.3 shows a sketch of a gasket.

The calibration of receivers of the first type can be done in air, for instance, acting on the piezoelement with stepwise pressure pulses of known values. To this end, the piezoelement is put into a small chamber separated by a breakable membrane from a chamber of a larger size, in which there is air at a known pressure. Fig. 6.4 shows a sketch of the setup for the calibration of pressure receivers of the fist type. Fig. 6.5 show a sample of a pressure oscillogram taken during a calibration. In the oscillogram we can see damping oscillations superimposed on the exponential component of the electric voltage. These oscillations are related to the transitory process initiated by the breaking of the membrane. To determine the sensitivity of the receiver, these oscillations must be averaged out. The constant in the exponent is determined by the quantity RC of the receiving length. For a piezoelement with capacitance $1000\,pF$ and the input resistance of an oscillograph IO-4, such a quantity equals $10\ msec.$ For receivers of the first type which have a piezoelement with an epoxide resin protection, a typical value of the sensitivity is about $0.3\,V/atm.$

A convenient method for the calibration of waveguide type receivers is that of "colliding rods ." For the calibration a rod-calibrator is made out of the same material as the waveguide. The ends of the waveguide and the rod are polished so that the limiting pressure can be reached at the instant of the "collision" as quickly as possible.

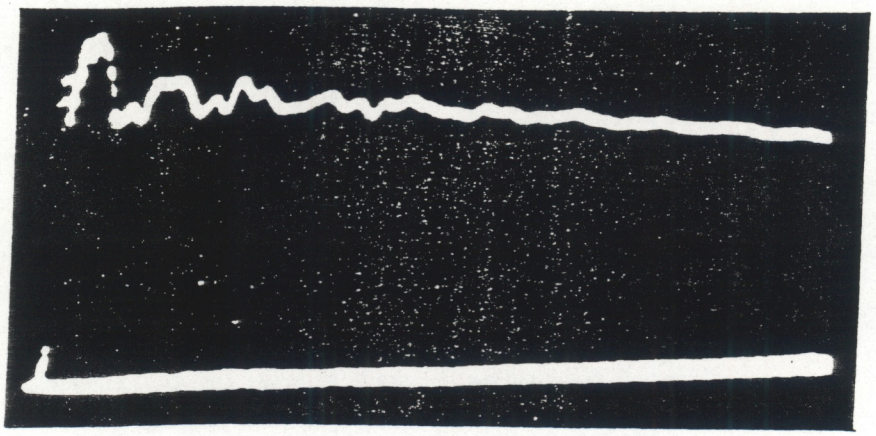

Fig. 6.5. Calibration oscillogram for a hydrophone.

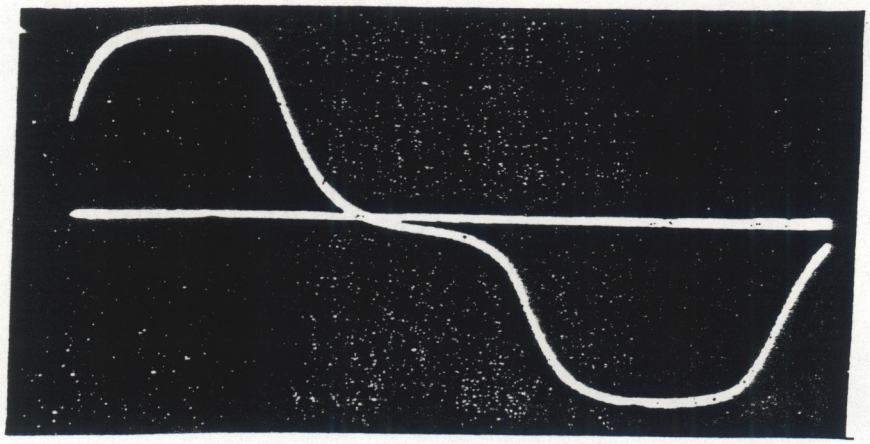

Fig. 6.6. Calibration oscillogram for a waveguide type receiver.

The value of the limiting pressure acting on the ends of the waveguide and the rod is determined by the formula

$$p = \rho c \frac{v}{2} \ , \tag{6.1}$$

where ρc is the wave resistance of the rod and waveguide material, and v is the collision speed given by

$$v = \sqrt{2gh} \ , \tag{6.2}$$

where g is the acceleration due to gravity and h is the free- fall height of the rod.

The rod length is chosen such that during the time of the collision the limiting pressure is established at the point of contact between the waveguide and the rod. For a typical value of the sensitivity rods of $2mm$ diameter , such time is usually about $10^{-5} sec.$ Fig. 6.6 shows a sample of a calibration oscillogram for a waveguide type receiver. There we can see the first compression pulse generated at the collision of the rods, and the subsequent rarefaction pulse, reflected from the free end of the waveguide. In order to separate these pulses it is necessary to put the piezoelement at a distance from the free end of the waveguide which is larger than the length of the rod. In the oscillograms we can sometimes notice small perturbations caused by the reflection of the pulses traveling in the waveguide from the non-uniformity of the waveguide crosssection due to the piezoelement. The sensitivity of waveguide type receivers is a few hundredths of Volts per atmosphere.

The accuracy of pressure measurements carried out with the receivers described above is 10%.

6.2. Spherical Discharges

In the integration of the system of equations (5.14) describing the channel expansion in the spherical model, we used the function $f(x)$ (line 1, Fig. 3.12) corresponding to the approximation of the power by an isosceles triangle. The initial conditions were chosen from the following considerations. The photograms of the channel expansion show that the initial values of the channel radius and the expansion rate are at least one order of magnitude less than their characteristic values during the discharge. Therefore, the numerical integration of the system (5.14) was performed taking various small initial values y_0, z_0 small compared with unity. It proved that the choice of the initial values of these parameters did not have any important effect on the results of the integration provided that $y_0 \ll 1$ and $z_0 \ll 1$. Physically, this may be explained by the fact that the channel expansion law is mainly determined by the law of energy release in the channel, and not by the initial conditions. Below we give the results of the calculation with $y_0 = 0.03$ and $z_0 = 0.00001$.

In Table 6.1 we give the values of the functions needed for the calculation of the hydrodynamic characteristics using Eqs. (5.16)–(5.22). Let us remind the reader that

$y(x)$, $g = f(x)/y^2$ and $\zeta = (f(x)/y^3) - z^2/2y^4$ represent, in a dimensionless form, the time dependence of the channel radius, pressure in the compression pulse and pressure in the channel, respectively.

Table 6.1

x	$f(x)$	z	y	g	ζ
0.0	0.00	0.000	0.000	0.000	0.00
0.1	0.02	0.045	0.178	0.632	2.52
0.2	0.08	0.119	0.310	0.831	1.91
0.3	0.18	0.210	0.428	0.978	1.63
0.4	0.32	0.314	0.540	1.090	1.45
0.5	0.50	0.429	0.645	1.200	1.33
0.6	0.68	0.551	0.746	1.220	1.15
0.7	0.82	0.671	0.843	1.150	0.92
0.8	0.92	0.781	0.935	1.050	0.73
0.9	0.98	0.881	1.020	0.939	0.56
1.0	1.00	0.968	1.100	0.821	0.43

The results of the calculations are given in Table 6.1 and are also plotted in Figs. 6.7, 6.8 and 6.9 (line 1). As we mentioned in Section 3.2, the normalized functions $f(x)$ describing the energy release law differ somewhat from each other. The difference between them is approximately the same as the difference between the lines obtained by integrating over time the power functions approximated by an isosceles triangle and by a triangle in which the perpendicular drawn from the vertex is shifted from the origin of the x axis by $1/3$ of the base length.

In order to clarify the degree of applicability of the adopted approximation for the function $f(x)$, in Figs. 6.7, 6.8 and 6.9 are plotted the functions $y(x)$, $g = f(x)/y^2$ and $\zeta = (f(x)/y^3) - z^2/2y^4$ (line 2), calculated using the approximation of the scalene triangle for the power .

In Fig. 6.7 we see that the value of $y(x)$ at $x = 1$ (i.e., $t = \tau$), is close to 1.1 for any of the approximations adopted for $f(x)$. Therefore, with accuracy up to this coefficient, the channel radius at the end of the discharge, is, according to Eqs. (5.16), equal to R_0.

The function $f(x)/y^2$also not too sensitive to the choice of the approximation . The maximum value of this function equals 1.2–1.3. Thus, from Eq. (5.12), we find that the maximum pressure in a compression pulse is equal to the product of this coefficient times the quantity $\rho_0 R_0^3/\tau^2 r$, which is determined by the square of the average rate of channel expansion with a correction for spherical divergence.

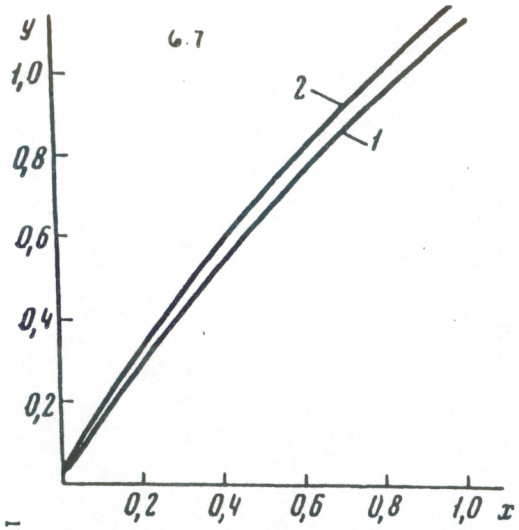

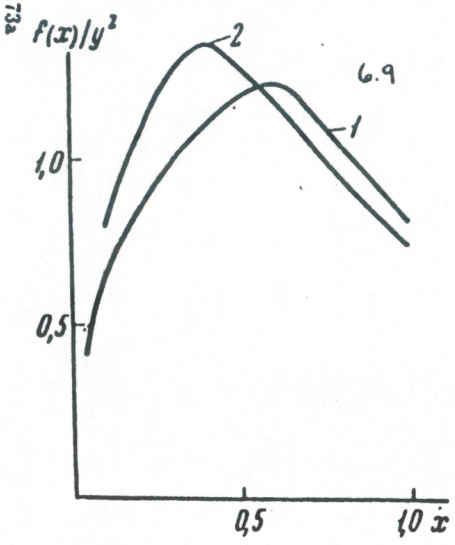

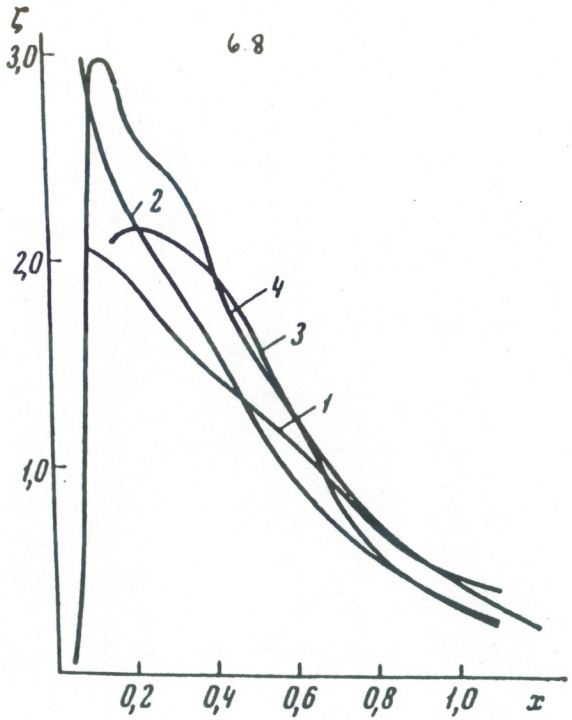

Fig. 6.7. Dimensionless channel radius as function of time. Line 1: case of energy release function approximated by $f(x)$ (Eq. (3.1)). Line 2: case of energy release function approximated by $f_1(x)$ (Eq. (3.2)).

Fig. 6.8. Dimensionless pressure in the channel as function of time. Lines 1 and 2: cases of energy release function approximated by $f(x)$ and $f_1(x)$. Lines 3 and 4: experimental data.

Fig. 6.9. Dimensionless profile of pressure in the compression wave radiated by the channel. Lines 1 and 2: cases of energy release function approximated by $f(x)$ and $f_1(x)$, respectively.

Unlike the dimensionless radius and the pressure in the compression pulse, the pressure in the channel depends strongly on the choice of the approximation for $f(x)$ for small x ($x < 0.2$) due to the presence of the term $f(x)/y^2$ in the expression of the pressure in the channel. This circumstance makes the calculation of the pressure in the channel at the beginning of the discharge unreliable, and, in particular, it does not allow one to determine the value of the maximum pressure in the channel. For this reason, for the spherical model the calculation of the pressure was carried out using other, more accurate approximations of $f(x)$. The first of them was an approximation of the experimental time dependence of the energy by a polynomial of degree 10. Results are shown in Fig. 6.8, line 3. There, line 4 corresponds to the pressure in the channel calculated using a $f(x)$ obtained by approximating the power function with a composite curve: a parabola up to $x = 0.3$ and an isosceles triangle from $x = 0.3$ to $x = 1$. On the basis of the obtained results, we may conclude that the maximum value of the dimensionless function that determines the pressure in the channel is close to 2.

For determination of the efficiency it is necessary to know the value of the integral in Eq. (5.23). Calculations show that this integral is practically equal to unity for any of the approximations adopted for $f(x)$.

Let us now give a few examples of calculations of hydrodynamic characteristics of discharges whose parameters are reported in Table 3.5. As we see, the condition fo applicability of the spherical model of discharge ($l \ll R_0 \ll \lambda$) is satisfied by discharges $Nos.$ 1, 2, and 3; discharge $No.$ 4 lies on the boundary of the applicability region of this model.

Discharges $Nos.$ 1, 2, and 3 were produced near the surface of a solid plate with electrodes machined so tthat they were flush with the surface of the plate. The shape of the channel in such a discharge is close to hemispherical, a fact thatmust be taken into account in the calculations (see remarks at the end of Section 5.2). Discharge $No.$ 1 was ignited with a corona discharge in the interelectrode gap generated by an auxiliary electrode. The gap was $l = 0.3\,cm$ and in $50 \cdot 10^{-6} sec$ an energy released of $E = 510\,J$ occurred . Using formulas (5.16)– (5.22) and values in Table 6.1, we determine that the channel radius at the end of the discharge was $R \approx 1.2\,cm$. This means that the mean expansion rate was $U \approx 2.4 \cdot 10^4\,cm/sec$. The pressure P in the discharge channel reached $\approx 1000\,atm$, the maximum pressure in the compression wave at a distance of $50\,cm$ from the discharge was $13\,atm$; the theoretical profile of the compression wave is shown in Fig. 6.10, line 1. Line 2 in the same figure represents the experimental form of the signal. The jagged behavior of this line is evidently due to the excitation of vibrations of the reflecting plate and pressure receiver under the effect of the compression pulse. From formula (5.28), the energy of the compression wave is about 12% of the energy release in the channel.

Fig. 6.11 shows the distribution of the hydrodynamic speed v in the compression wave calculated with Eq. (5.21). Lines 1 and 2 of the plot correspond to the first and second terms of this formula.

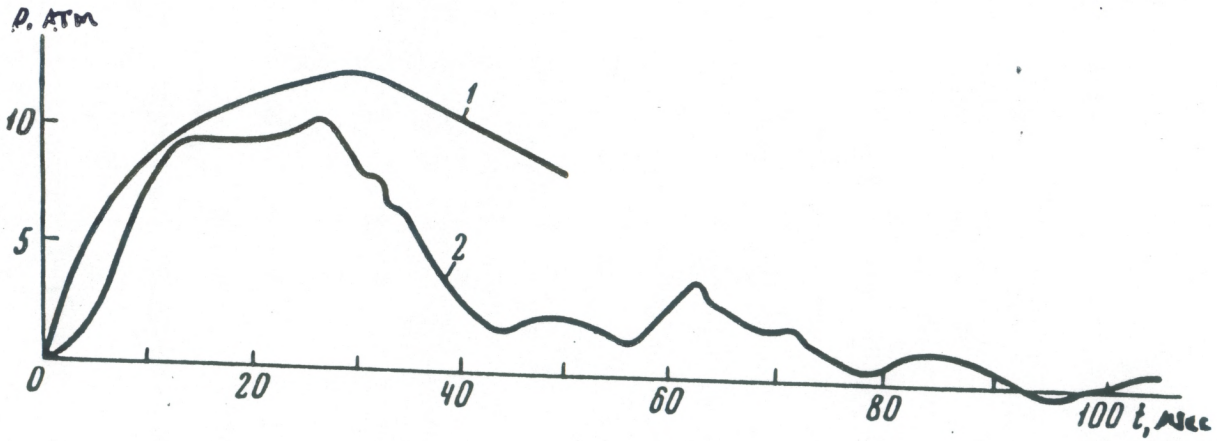

Fig. 6.10. Pressure in the the compression pulse as function of time for discharges *No. 1* of Table 3.5.

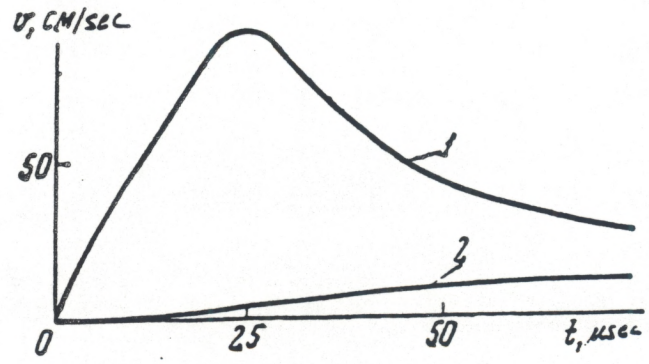

6.11

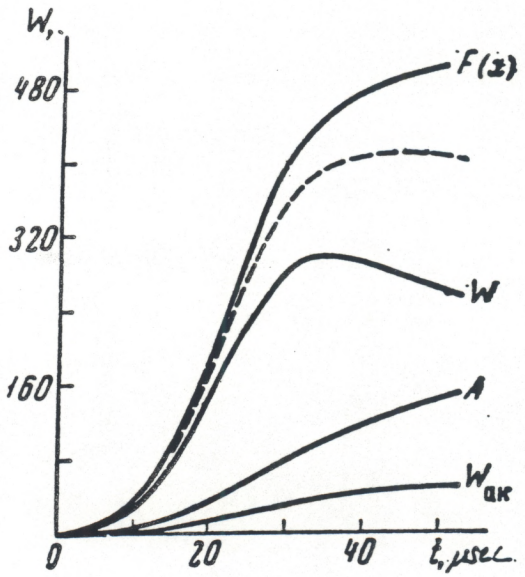

6.12

Fig. 6.11. Hydrodynamic speed distribution in a compression pulse, whose pressure profile is shown in Fig. 6.10.

Fig. 6.12. Energy balance for discharge: *No. 1.* W_{ac} is the radiated acoustic energy; A is the work of the channel expansion; W is the channel internal energy; $F(x)$ is the total energy released in the channel. The broken line indicates the sum of A and W.

Fig. 6.12 shows the time dependence of the energy of the channel plasma, of the expansion work A, and of the acoustic energy W_{ac} transported by the compression wave. These lines were calculated using Eqs. (5.18), (5.19) and (5.22), respectively. In the same figure the time dependence of the energy released in the channel is also plotted : $E(x) = f(x)E$.

The broken line represents the sum $W + A$; the difference between this sum and $E(x)$ characterizes the calculation error due to the approximate nature of the solution of the original equation of energy balance. As we can see, the error does not exceed 20%.

Discharges $Nos.\,2$ and 3 differ from discharge $No.\,1$ because of a narrower discharge gap broken down directly by the working voltage. As we see from Table 3.5, in the channel of discharge $No.\,2$, in $30 \cdot 10^{-6} sec$ there was a release of $376J$ of energy. The radius of the channel at the end of the discharge was $R \approx 0.9\,cm$, the characteristic rate of channel expansion was $U = 2.8 \cdot 10^4 cm/sec$, and the maximum pressure in the channel was $P \approx 1600\,atm$. The maximum pressure p in the compression wave at a distance of $100\,cm$ from the discharge $\approx 8\,atm$. The profile of the compression wave at the same distance is plotted in Fig. 6.13. Line 1 represents the theory, line 2 the experiment. The energy of the compression wave is about 13% of the energy released in the channel.

The hydrodynamic characteristics of discharge $No.\,3$ are close to those given above for discharge $No.\,2$. The profile of the compression wave at a distance of $100\,cm$ from the discharge is shown in Fig. 6.14. The theoretical electroacoustic efficiency of the discharge is 13%; the corresponding value determined from the shape of the signal recorded experimentally is 10%.

To conclude, let us examine discharge $No.\,4$ (Table 3.5), which is characterized by a large amount of energy stored in the capacitors: $169J$ [1]. The discharge was initiated with a wire $7.5\,mm$ long. The duration of the discharge and the quantity of energy release in the channel are not given in Ref. [1]. Assuming that all the energy of the capacitor battery was released in $400 \cdot 10^{-6} sec$ in agreement with the experimental duration of the compression wave, for discharge $No.\,4$ we obtain: $R \approx 7.5\,cm$, $U \approx 1.7 \cdot 10^4 cm/sec$, $P \approx 500\,atm$, $p \approx 26\,atm$ and $efficiency = 9\%$. The theoretical (line 1) and experimental (line 2) profiles of the compression wave at a distance of $100\,cm$ from the discharge are shown in Fig. 6.15.

For the same discharge we also calculated the maximum pressure in the compression pulse as a function of the initial voltage and of the capacitance of the capacitor battery expressed through the number of capacitors in the battery. In Fig. 6.16, the solid line represents the theoretical dependence of the maximum pressure on the voltage, while the circles denote the experimental results. In Fig. 6.17, the solid line represents the dependence of the maximum pressure in the compression pulse on the number of capacitors in the battery, while crosses and circles denote experimental data.

Let us focus on a feature common to all the cases considered. While the absolute value of the maximum pressure in the compression pulses

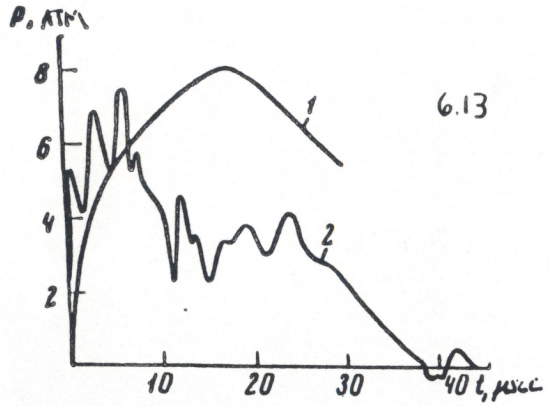

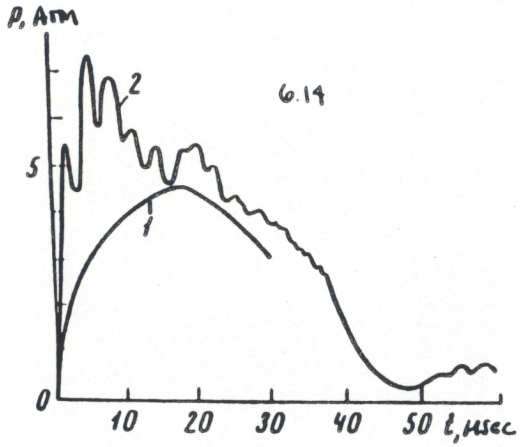

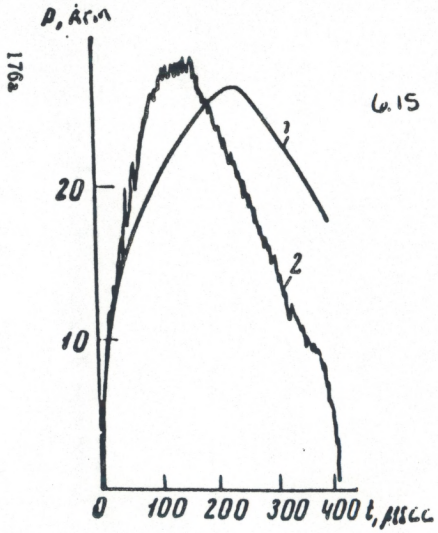

Fig. 6.13. Pressure profile in a compression wave for discharge *No. 3.*

Fig. 5.14. Calculated (1) and experimental (2) pressure profiles in a compression wave for discharge *No. 3.*

Fig. 6.15. Calculated (1) and experimental (2) pressure profiles in a compression wave for discharge *No. 4.*

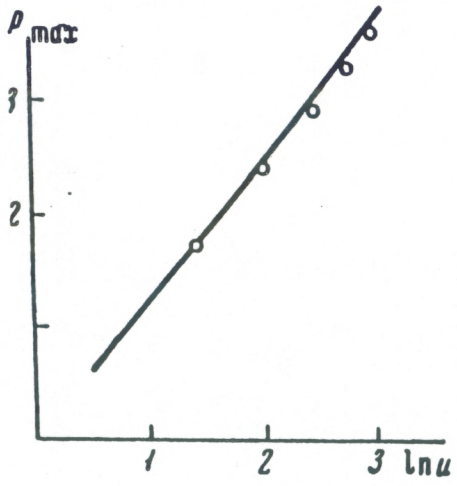

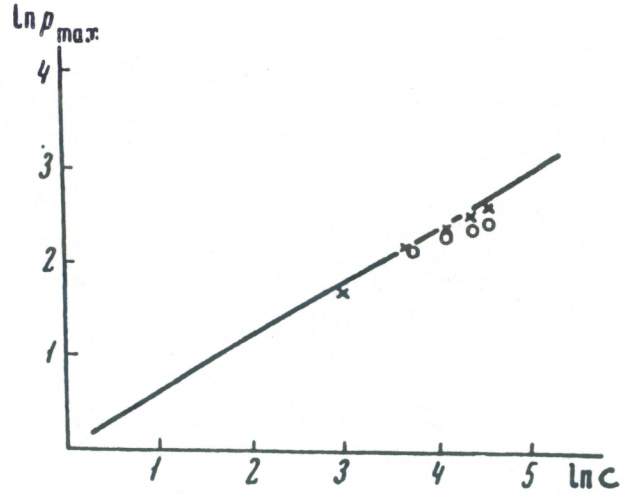

Fig. 6.16. Maximum pressure in a compression pulse as function of the initial voltage. The solid line represents the theory, the circles the experimental data.

Fig. 6.17. Maximum pressure in a compression pulse as function of the capacitance.

is in rather good agreement with the theory, the same is not true for the final stage of the compression pulses. There, the theory always overestimates, approximately by a factorof 2, the experimental values taken at the corresponding times. A possible cause of this effect may be the fast cooling of the plasma in the discharge channel.

6.3. Discharges related to the Model of a Short Cylinder

In order to progress from spherical discharges to discharges that correspond to the model of a short cylinder, it is necessary to increase the length of the channel so that it exceeds the channel radius, while, at the same time, remaining smaller than the length of the compression pulse. These requirements are satisfied by discharges $Nos.$ 5–10 of Table 3.5. The relatively long, but always shorter than the length of the compression pulse, channels in these discharges were obtained by using relatively low-voltage discharges with working voltages of a few kilovolts initiated by thin tungsten wires with a diameter of $0.04\,mm$. All the cited discharges were produced in free space, i.e., far away from the container walls and without using any reflectors. The electrodes had a small diameter compared with the length of the compression pulse, and could not introduce substantial distortions in the acoustic field generated by the discharge.

The acoustic field generated by discharges corresponding to the model of a short cylinder no longer possesses a spherical symmetry : the compression pulse radiated by the channel has a smaller amplitude and a longer duration in a longitudinal direction with respect to the channel axis than it has in the transverse direction; this occurs because the perturbations generated by the different portions of the channel lag behind in the propagation. Therefore, a comparison with the experiment will be done for the transverse direction. The results of the numerical integration of the system Eq.(5.39) do not have the universal character that they had for the case of the spherical discharges. The universal character is lost because of the presence in the first equation of the system Eq.(5.39) of the ratio l/R_0, appearing under the logarithm sign. However, since the solution of the system Eq. (5.39) depends weakly on the ratio l/R_0, we may also apply, without introducing any substantial errors, the results of the integration obtained for a certain value of this ratio to the discharges having a different l/R_0. In Table 6.2 are given the results of the integration of the system Eq.(5.39) for $l/R_0 = 6$, $y_0 = 0.1$ and $z_0 = 0$. The cylindrical discharges investigated experimentally had for l/R_0 a value close to the one given above for l/R_0. As in the case of spherical discharges, the choice of the initial condition y_0 does not affect the results of the calculation much, provided that $y_0 \ll 1$.

Table 6.2

x	$f(x)$	z	y	g_1	ζ
0.0	0.00	0.000	0.000	0.000	0.00
0.1	0.02	0.016	0.104	0.500	1.84
0.2	0.08	0.095	0.145	1.020	3.60
0.3	0.18	0.202	0.225	1.080	3.15
0.4	0.32	0.319	0.319	1.070	2.67
0.5	0.50	0.417	0.418	1.070	2.36
0.6	0.68	0.523	0.518	1.030	2.02
0.7	0.82	0.622	0.619	0.942	1.63
0.8	0.92	0.711	0.719	0.839	1.29
0.9	0.98	0.790	0.817	0.737	1.00
1.0	1.00	0.858	0.912	0.638	0.76

In Fig. 6.18 the solid line gives the plot of the function $y(x)$, and the various symbols denote the experimental values (in dimensionless units) of the radius of the channel as a function of time, taken with the high-speed photographic camera SFR-1.

Figs. 6.19 and 6.20 show the plots of the functions $[f(x)/y^2 - z^2/2y^2]$ and $f(x)/y^2 \ln(l/R_0 y)$, which characterize the form of the radiated compression pulse in a direction tranverse with respect to the channel axis and the pressure in the channel as a function of time. In order to obtain the absolute values of the hydrodynamic quantities, these functions are to be multiplied by the corresponding dimensional coefficients as in Eqs. (5.42) and (6.45).

Let us note that the dimensionless functions plotted in Figs. 6.18, 6.19 and 6.20 are not that sensitive to the choice of the approximation used for $f(x)$ both in the model of a short cylinder and in the model of a long cylinder, which we will consider in the next section.

Let us give examples of the calculated hydrodynamic characteristics for discharges that correspond to the model of a short cylinder. For discharge $No.\,7$ (Table 3.5) we have: discharge gap $l = 6\,cm$, discharge duration $\tau = 53 \cdot 10^{-6} sec$, energy released $E = 2260 J$. Using the formulas of Section 5.3 and the values of Table 6.2, we obtain that the radius of the channel at the end of the discharge is $R \approx 0.9\,cm$, the characteristic expansion rate $U \approx 1.8 \cdot 10^4 cm/sec$, and the pressure in the channel reaches the value $P \approx 1200\,atm$. The maximum pressure in the compression wave in the normal direction and at a distance of $100\,cm$ from the channel is $p \approx 12\,atm$. The profile of the compression wave at the same point in space is shown in Fig. 6.2.

The electroacoustic efficiency of the discharge can be calculated using formulas (5.46) and (5.47) where the integrals, calculated on the basis of the data in Table 6.2, equal $J_1 = 0.83$ and $J_2 = 6.6$ respectively.

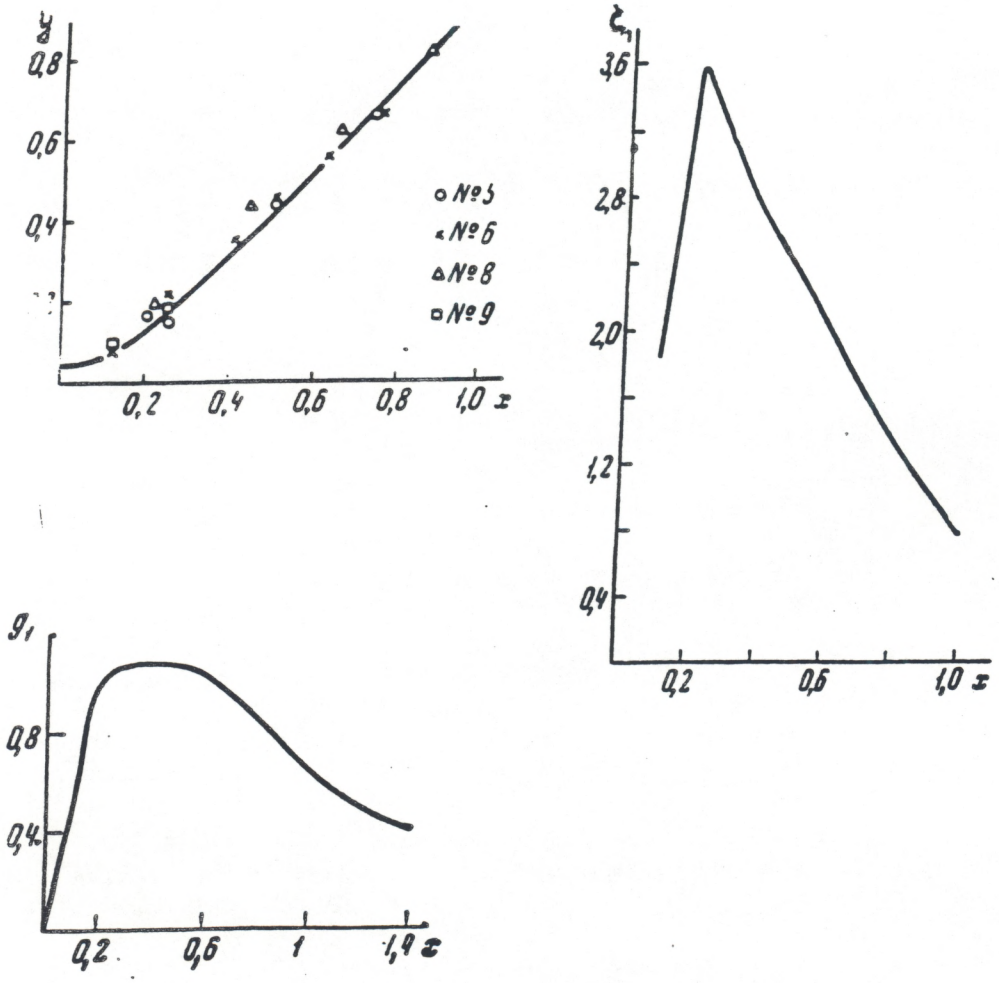

Fig. 6.18. Dimensionless channel radius as function of time. The solid line represents the theory, the circles the experimental data relative to the discharges №. 5. 6. 8 and 9 of Table 3.5.

Fig. 6.19. Dimensionless pressure in the channel as function of time.

Fig. 6.20. Dimensionless pressure in a compression wave.

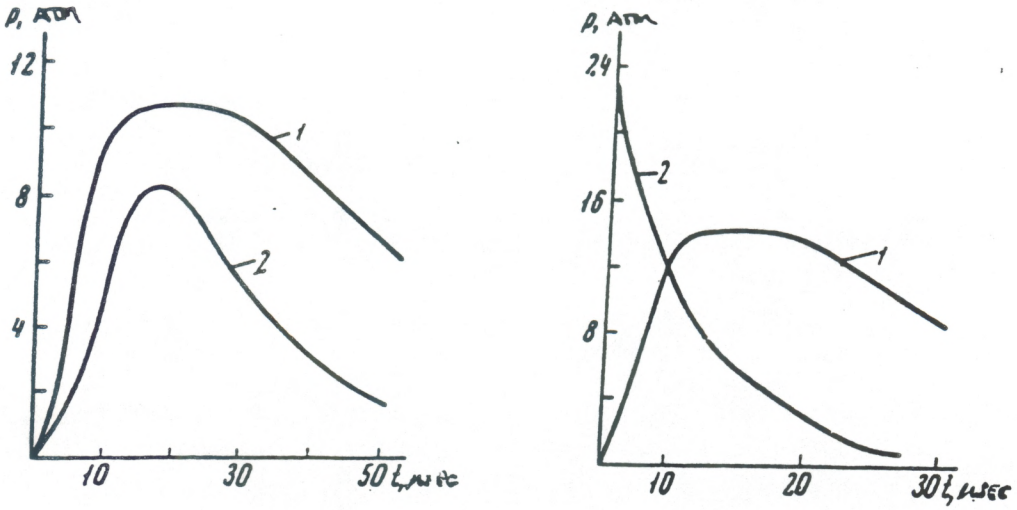

Fig. 6.21. Theoretical (1) and experimental (2) profiles of the compression wave pressure for discharge *No. 7* of Table 3.5 in a direction normal to the channel axis.

Fig. 6.22. Theoretical (1) and experimental (2) profiles of the compression wave pressure for discharge *No. 10* of Table 3.5 in a direction normal to the channel axis.

For the discharge $No.7$ we obtain: $\eta_{theory} = 14\%$, $\eta_{exp} = 12\%$. As a second example, let us consider the discharge $No.10$. The larger power of discharge $No.10$ compared with discharge $No.7$ was achieved by using a low inductance discharge loop (capacitor IMM-5-150 and feeding circuit of seven parallel PK-6 cables $120\,cm$ long) and by decreasing the length of the channel to $3\,cm$. The latter factor was responsible for cutting the discharge duration down to $3 \cdot 10^{-6} sec$ while keeping the amount of energy released in the channel almost the same as for discharge $No.7$: $E \approx 2500j$. The channel radius at the end of the discharge is $R_0.8\,cm$, the characteristic expansion rate $U = 2.9 \cdot 10^4 cm/sec$, and the maximum pressure in the channel $P = 3000\,atm$.

The peak pressure in the compression wave at a distance of $100\,cm$ from the discharge in a direction normal to the channel axis is $p \approx 14\,atm$. The profile of the compression wave at the same point in space is shown in Fig. 6.22.

We can see there that the experimental profile has, unlike the theoretical one, a shock front and a higher peak pressure. We may point to several possible reasons for this discrepancy.

Firstly, the ratio l/R for discharge $No.10$ is about twice as small as the value taken for this parameters in calculating the values reported in Table 6.2, which were used for the theoretical calculation. This circumstance led to a decrease of the calculated pressure in the compression wave by about factor 1.2. Secondly, the form of the function $f(x)$ taken for the calculation is only an approximation of the actual energy release law.

Furthermore, to the relatively high pressure and temperature in the channel for the discharge $No.10$ correspond also a higher value of the effective adiabatic index compared with the mean value used in the calculation $\gamma = 1.6$. From the formula for the pressure in the compression pulse it follows that to higher values of γ correspond higher pressures. This is also one reason for which the calculated compression pulse turns out to be less than the experimental value.

The hydrodynamic characteristics of discharge $No.10$ were calculated, as all the previous ones, under the assumption that the expansion rate is small compared with the speed of sound. An estimate of the expansion speed expressed as R_0/τ gives for the discharge $No.10$ the value $0.2c_0$, where c_0 is the speed of sound. Judging from the experimental results, at such expansion speeds it is already necessary to take into account the compressibility of the fluid and the nonlinear effects in the description of the propagation of compression pulses. In Section 6.5 we shall compare the results of the calculations performed including the nonlinear effect with the experimental data obtained for discharge $No.10$.

Discharge $No.10$ has another peculiarity. As the photograms show, the expansion speed of the near-electrode portions of the channel is higher than for the middle part. The film taken with SFP-1 shows that the form of the channel for discharges with short channels reminds one of a dumbbell formed by joining the spherical near-electrode section. Fig. 3.15 shows one photogram of this kind of channel in the final stage of the discharge.

6.4. Discharges related to the Model of a Long Cylinder

To the model of a long cylinder correspond usually high-voltage discharges generated using accumulators of relatively low capacitance. The working voltage is no less than tens of kV, the capacitance of the order of a few μF, the interlectrode gap no less that several cm, the inductance a few μH.

With these parameters for the discharge loop, experiment shows that the discharge occurs in a near-critical regime. The length of the compression pulse radiated perpendicularly to the channel axis does not exceeds the length of the channel, and the channel radius at the end of the discharge is less than the length of the compression pulse. In other words, the condition $R < \lambda < l$, characteristic of the model of a long cylinder, is fulfilled.

Discharges of this type in low-conductivity water are initiated through a high-voltage breakdown of the interelectrode gap, while in high-conductivity water wire bridges are adopted.

The discharge associated with the model of a long cylinder create highly spatially nonhomogeneous acoustic field: the shape of the radiated compression pulse, its duration and amplitude depend strongly on the angle between the channel axis and the direction to the point of observation.

Let us now turn to the results of the numerical integration of the system (5.52). As in the case of the model of a short cylinder, the solution of this system of equations depends on the parameter that characterizes the geometry of the model, in the present case the quantity $c\tau/R_0 = a$. However, such dependence is not a strong one, because this parameter appears also in the argument of the logarithm. A twofold variation of this parameter does not change, in practice, the solution of system (5.52). The integration of (5.52) was performed with the initial values $y_0 = 0.03$ and $z_0 = 0.01$. The quantity $2c\tau/R_0$ was set equal to 10, which is in agreement with typical experimental data.

Table 6.3

x	$f(x)$	z	y	g_2	ζ
0.0	0.00	0.01	0.03	0.00	0.00
0.1	0.02	0.08	0.09	1.02	2.06
0.2	0.08	0.18	0.18	0.98	1.85
0.3	0.18	0.28	0.28	0.95	1.77
0.4	0.32	0.37	0.38	0.94	1.73
0.5	0.50	0.46	0.48	0.93	1.71
0.6	0.68	0.56	0.58	0.88	1.59
0.7	0.82	0.64	0.67	0.78	1.37
0.8	0.92	0.71	0.77	0.67	1.14
0.9	0.98	0.77	0.87	0.57	0.93
1.0	1.00	0.82	0.95	0.47	0.74

In Table 6.3 we give the values of the dimensionless functions

$$y(x)\,, \quad f(x)/y^2 \ln(2c\tau x/R_0 y)\,, \quad \text{and} \quad f(x)/y^2 - z^2/2y^2\,,$$

which characterize the time dependence of the channel radius, the pressure in the compression pulse radiated by the channel perpendicularly to the channel axis and the pressure in the channel. Figs. 6.23, 6.24 and 6.25 show the plots of these functions.

To the type of discharges of the model of a long cylinder belongs the discharge $No.\,16$ (Table 3.5). In this case, in the discharge channel $l = 4.5$ long $E = 160J$ of energy was released in $5 \cdot 10^{-6} sec$. The channel radius at the end of the discharge was $R \simeq 0.16\,cm$, the expansion rate $U = 3.3 \cdot 10^4 cm/sec$, and the maximum pressure in the channel $P \approx 2300\,atm$.

Figs. 6.26 show the calculated (1) and experimental (2) forms of the compression wave radiated perpendicularly to the channel axis and at a distance of $100\,cm$ from the channel. There are also plotted the theoretical (3) and experimental (4) forms of the wave in the longitudinal direction. As expected, the greater disagreement exists between theory and experiment for the pulse in the direction transverse with respect to the channel axis (24.5 and $8.1\,atm$, respectively), while the pulse in the longitudinal direction differ much less drastically (3.4 and $2.5\,atm$). As we have already indicated, the reason for the large discrepancy between theory and experiment for the pulse in the transverse direction is the *tortuous* pattern of the channel, and, possibly, the higher absorption due to a rather large pulse amplitude.

Let us calculate the electro-acoustic efficiency for the discharge $No.\,16$ using Eq. (5.65). Approximating the transverse pulse with a Gaussian curve with width equal to 0.7τ, where τ is the discharge duration, we obtain $\eta \approx 29\%$.

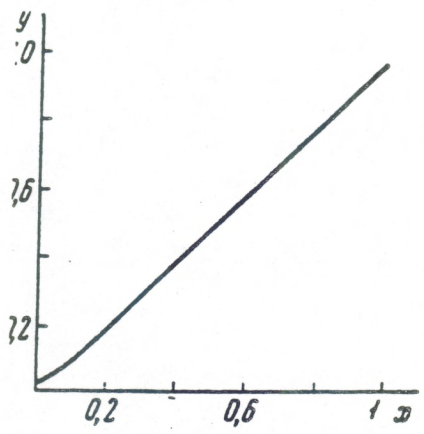

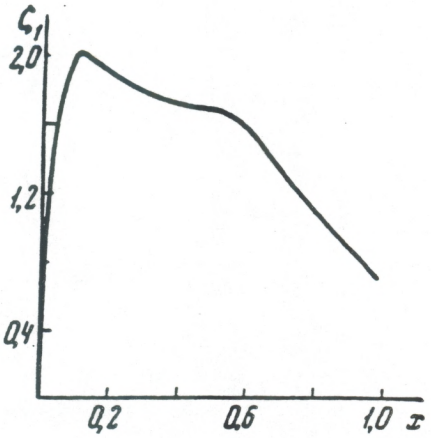

Fig. 6.23. Dimensionless channel radius as function of time.

Fig. 6.24. Dimensionless pressure in the channel as function of time.

Fig. 6.25. Dimensionless pressure profile in a direction perpendicula to the channel axis.

Fig. 6.26. Theoretical (1,3) and experimental (2,4) profiles of the compression wave pressure for discharge *No. 16* in a direction transversal (1, 2) and longitudinal (3, 4) with respect to the channel axis.

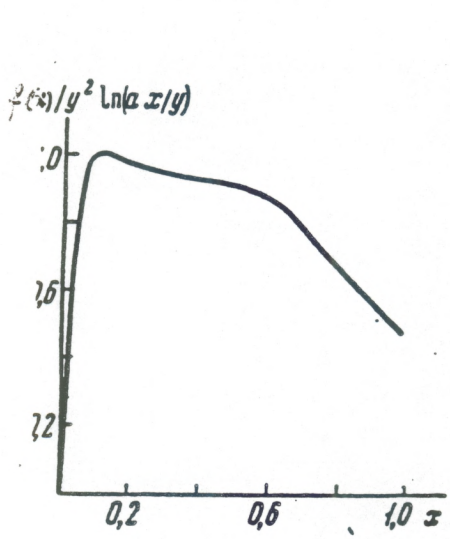

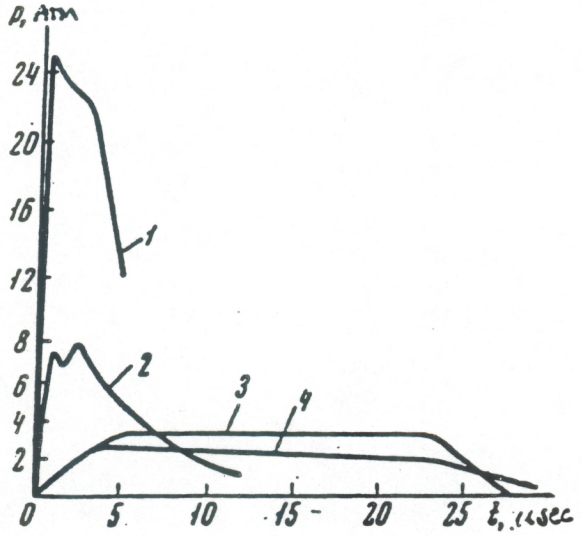

The experimental value of the electro-acoustic efficiency is determined as follows. Oscillograms of the compression pulses are taken at different observation angles with respect to the channel axis, and the pulse energy per unit area is determined for each direction. Then, taking into account the axial symmetry of the compression pulse, the energy through the spherical zone containing the given angles is calculated. The ratio of the sum of these energies to the the energy release in the channel gives the experimental electro-acoustic efficiency. Usually, the experimental value for the electro-acoustic efficiency is 15–20%. As we saw in the case of the spherical model and the model of a short cylinder, the experimental values of the electro-acoustic efficiency are always smaller than the theoretical ones. In the model of a long cylinder this difference is even more noticeable. In this case, to the inaccuracy of the calculations, we must add the effect of the *tortuous* behavior of the channel. The *dephasing* of the elementary compression pulses decreases the amplitude of the compression pulses. At the same time, the area of the total pulses is unchanged, but their energy substantially decreases due to the its quadratic dependence on the pressure. The decrease in the work done by the channel to generate the acoustic field is accompanied by an increase of the kinetic energy of the divergent fluid flux.

6.5. Spherical Model with High Channel Expansion Rates

The basic equations of the spherical model of a discharge at high channel expansion rates, with inclusion of the effect of the fluid compressibility, were given in Section 5.5 (Eqs. (5.68)–(5.74).

In the present section we shall examine the results of the numerical integration of these equations. In performing the integration it was assumed, as in previous cases, that the energy release is described by the function (3.1), which gives the *triangle* approximation of the dimensionless power function $f(x)$ appearing in the rhs of Eq. (5.68),

$$f(x) = \begin{cases} 4x, & 0 \leq x \leq \frac{1}{2}; \\ 4(1-x), & 1_{\frac{1}{2} \leq x \leq 1}; \\ 1, & 1 \leq x. \end{cases} \tag{6.3}$$

First of all, let us note that the system of equations (5.68)–(5.71), which describes the expansion process of the channel, contains one dimensionless parameter, the number M. Furthermore, Eqs. (5.72)–(5.74), which describe the compression waves, contain one additional parameter, namely the reduced distance to the point of the observer: R_0/r. These two parameters may be regarded as similarity criteria in the sense that all the discharges that belong to a spherical model (in which the fluid compressibility effect is included) and are characterized by the same values of the above two parameters, are described by the same equations. This feature gives a certain universality to the calculation.

The results of the calculations for three values of M with $R_0/r = 10^{-2}$, are given in Table 6.4 and in Fig. 6.27-6.29.

Fig. 6.27 shows the dependence of the dimensionless radius $y = R/R_0$ on the dimensionless time $x = t/\tau$ for $M = 0.12$ (line 1) and $M = 2$ (line 2). We see that the result of the calculation does not vary much with the value of M, which indicates that the effect of the fluid compressibility is small. This feature shows up also in the calculation of the pressure in the discharge channel; the plot in dimensionless units of this quantity as a function of the dimensionless time is shown in Fig. 5.28 for $M = 0.12$ (1) , $M = 1$ (2) and $M = 2$ (3).

Fig. 6.29 shows the results of the calculation of the function $g(x)$, which plays an important role in the calculation of the compression waves radiated by the discharge. In fact, the pressure in the compression wave is described by formula (5.78):

$$p = \rho_0 \frac{R_0^3}{\tau^2 r} g(\bar{x}) ,$$

whence we see that function $g(\bar{x})$ characterizes the profile of the wave radiated by the discharge.

It is important to emphasize that, although the form of $g(x)$ varies relatively little as M increases (see Fig. 6.29), which points to a weak effect of the water compressibility on the channel expansion even at supersonic expansion

Table 6.4

M=0,12

x	y	γ	ξ	t	g
0,10	0,186	1,50	2,49	12,7	1,665
0,20	0,324	1,29	1,89	12,8	0,876
0,30	0,448	1,19	1,61	12,9	1,03
0,40	0,564	1,12	1,45	13,	1,16
0,50	0,673	1,07	1,32	13,1	1,27
0,60	0,778	1,02	1,15	13,2	1,30
0,70	0,877	0,962	0,947	13,3	1,23
0,80	0,971	0,903	0,764	13,4	1,13
0,90	1,06	0,845	0,609	13,5	1,02
0,00	1,14	0,792	0,479	13,6	0,899
1,1	1,22	0,743	0,382	13,7	0,796
1,2	1,29	0,701	0,313	13,8	0,715
1,3	1,36	0,664	0,262	13,9	0,622
1,4	1,42	0,632	0,223	14,0	0,596
1,5	1,48	0,603	0,193	14,1	0,551

M=1,0

0,1	0,183	1,48	2,62	117	0,557
0,2	0,321	1,30	1,95	115	0,750
0,3	0,445	1,20	1,64	114	0,892
0,4	0,562	1,13	1,45	113	1,01
0,5	0,673	1,09	1,32	112	1,11
0,6	0,779	1,03	1,15	112	1,14
0,7	0,877	0,951	0,945	112	1,08
0,8	0,969	0,877	0,768	113	1,00
0,9	1,05	0,806	0,619	114	0,904
1,0	1,13	0,739	0,494	115	0,799
1,1	1,20	0,683	0,402	116	0,711
1,2	1,27	0,636	0,337	117	0,642
1,3	1,33	0,598	0,288	117	0,586
1,4	1,39	0,565	0,251	118	0,541
1,5	1,44	0,536	0,221	118	0,503
1,6	1,49	0,5	0,198	119	0,471
1,7	1,54	0,490	0,178	119	0,443
1,8	1,59	0,471	0,162	119	0,419
1,9	1,64	0,454	0,148	120	0,398
2,0	1,68	0,438	0,137	120	0,380

M=2,0

x	y	y	ζ	t	g
0,1	0,177	1,43	2,91	210	0,497
0,2	0,310	1,26	2,16	201	0,673
0,3	0,431	1,16	1,81	196	0,802
0,4	0,544	1,10	1,60	192	0,909
0,5	0,651	1,06	1,45	189	1,00
0,6	0,754	0,977	1,26	188	1,03
0,7	0,851	0,926	1,04	190	0,984
0,8	0,939	0,854	0,842	192	0,912
0,9	1,02	0,756	0,678	195	0,827
1,0	1,1	0,720	0,540	199	0,734
1,1	1,17	0,665	0,439	203	0,656
1,2	1,23	0,620	0,378	206	0,594
1,3	1,29	0,582	0,314	208	0,545
1,4	1,35	0,550	0,273	210	0,504
1,5	1,40	0,522	0,241	212	0,470
1,6	1,45	0,498	0,215	214	0,441
1,7	1,50	0,476	0,194	215	0,416
1,8	1,55	0,458	0,177	216	0,394
1,9	1,59	0,441	0,162	218	0,375
2,0	1,64	0,425	0,149	219	0,358

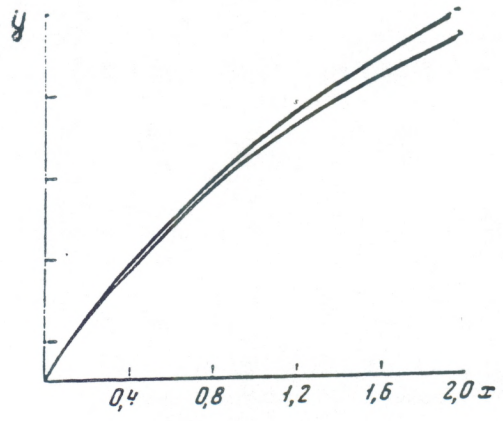

6.27

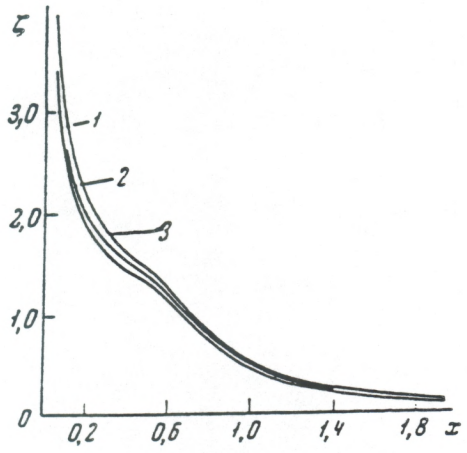

6.28

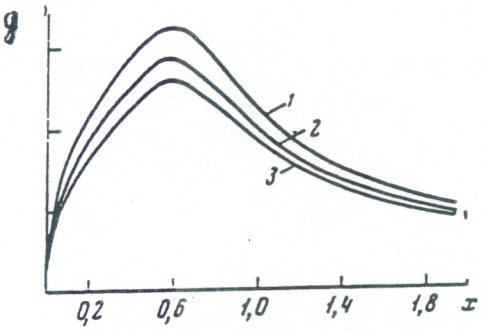

6.29

Fig. 6.27. Dimensionless channel radius as function of time.

Fig. 6.28. Dimensionless pressure in the discharge channel as funtion of time.

Fig. 6.29. Dimensionless kinetic entalpy on the surface of an expanding sphere as function of time for M = 0.12(1), M = 1 (2) and M = 2 (3).

rates, the profile of the compression wave at a fixed distance from the discharge changes dramatically as the rate of the channel expansion increases. This is related to the difference in the process of propagation of small amplitude waves, radiated by discharges of small intensity, and waves of finite amplitude, radiated at near- or supersonic channel expansion rates.

Formally, this difference comes about because for small M the time t at the point of the observer differs, according to Eq. (5.75), from x only by the constant $\frac{r-R}{c_0}$, which is the same at all the points in the profile and takes into account the wave travelling time. In this case, the wave is propagated without changes in the profile. Fig. 6.30 shows the plot of the function $g(t)$ for $M = 0.12$ and $r/R_0 = 10^2$.

As M increases, the relation between t and x changes (see Eqs. (5.72) and (5.76)). For different values of g, the propagation time is different, and, as we can see from Eq. (5.86), to larger g correspond smaller propagation times. As a result, the wave profile is strongly distorted. This is illustrated in Fig. 6.31, which shows the plot of the function for $M = 0.4$ and $r/R_0 = 10^2$.

As we already noted, the "overshoot" of the profile indicates the formation of a shock front, whose position can be approximately determined using the *equal area* rule (see Fig. 6.31).

Let us now utilize the theoretical notions presented above to describe various experimental results. Let us consider the propagation of a compression wave radiated by discharge $No.$ 10 (Table 3.5).

The hydrophone recording of the signal from such discharge in a direction perpendicular to the channel axis is shown in Fig. 6.32 (line 1), which clearly indicates that at the front of the signal there is a shock wave. The characteristic channel radius of discharge $No.$ 10 is $R_0 = 0.887$, which is a small value compared with the channel length. Consequently, it is difficult to apply the spherical model presented in this section for the calculation of the radiation of the compression pulse. It is, however, possible to consider a discharge, equivalent to discharge $No.$ 10 in the sense that such discharge, being spherically symmetric, radiates in all the directions a compression wave of amplitude and duration equal to the amplitude and duration of the pulse radiated by discharge $N_o 10$ in the direction perpendicular to the channel axis. It is possible, in other words, to determine the characteristic radius $\overline{R_o}$ of the spherical discharge from the condition

$$\rho\frac{\bar{R}_0^3}{\tau^2} = \rho\frac{R_0^2 l}{2\tau^2}$$

whence $\bar{R}_0 = 1.18\,cm$. Taking from Table 3.5 $\tau = 30\cdot 10^{-6} sec$, we obtain $M = \frac{\bar{R}_0}{c\tau} = 0.26$.

The result of the integration of Eqs. (5.68)–(5.74) for $M = 0.26$ and $r/R_0 = 10^2$ are plotted in Fig. 6.32 (line 2).

As we can see, the theoretical profile of the compression wave also shows a trend towards an increased steepness of the wave front. In conclusion, we will note that the experimental investigations of electric discharges in fluids

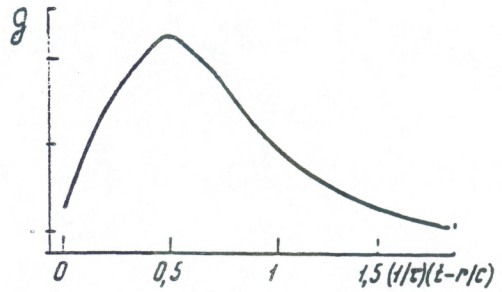

6.30

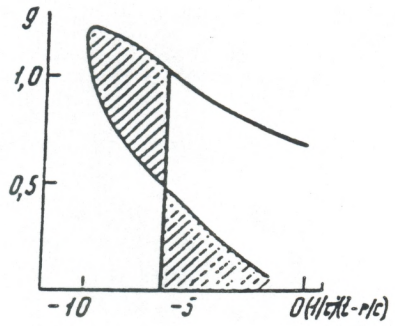

6.31

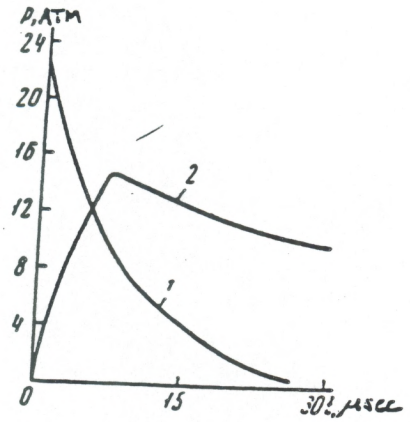

6.32

Fig. 6.30. Dimensionless kinetic entalpy at the point of observation as function of time for $M \approx 0.12$.

Fig. 6.31. Dimensionless kinetic entalpy at the point of observation as function of time for $M \approx 0.4$.

Fig. 6.32. Theoretical (2) and experimental (1) pressure profiles in a compression wave for discharge *No. 10* of Table 3.5.

have been conducted during the last years by several researches (see, e.g., [5–7]). The data obtained in this work agree with the results of the calculations performed using the approximated theory presented above.

6.6. Comparison of Electric Discharges in Water with underwater Explosions

The results reported above show that the hydrodynamic phenomena that accompany electric discharges are, to a large extent, similar to the corresponding phenomena taking place during the explosion of solid explosive charges in liquids. It is interesting to carry out a qualitative comparison between these two processes.

Let us begin with the quantities involving energy. The explosive used is usually trinitrotoluene (TNT) with energetic capacity of about 4200 J/g. Since this energy/weight relation is a constant, we may characterize the energy of the TNT in units of weight. The weight range of the charges used in practice is rather wide. The charges used, for instance, in ocean researches and for industrial technological purposes vary in weight from tens of grams to tens of kilograms. In energy units, this translates into a range from few tens of kJ to several tens of MJ. Because the energy capacity of a condensor is small, being only about $0.1\, J/cm^3$, it is difficult to generate high-energy spark discharges. According to the data in the literature, the maximum energy for electric discharges in a fluid does not exceed a few hundred kilojoules, and the accumulator volume requires to store such energy is no smaller than several cubic meters.

Let us compare now an electric discharge with a TNT explosion of equal energy. The energy release rate in a TNT explosion depends on the rate of detonation which is about $7 \cdot 10^5\, cm/sec$. Taking into account that the TNT density is about $1.5\, g/cm^3$, it is easy to find that the typical linear dimensions of the charges fall in a range from a few cm to several tens of cm. Correspondingly, the energy release time lies between a few μsec and several tens of μsec. The electric discharges in water take typically from tens to hundreds μsec. Therefore, the electric discharges are characterized by a much smaller energy release rate than TNT explosions. This does not mean, of course, that with electric discharges it is not possible, in principle, to obtain a high release rate for the major portion of the energy available. However, the problem of reaching energy release rates comparable with those of TNT explosions entails great technical difficulties.

Due to the high energy release rate during a TNT explosion, the compression pulse possesses an energy that may reach 60% of the energy of the charge. The pressure in the pulse amounts to several tens of thousands of atm, and therefore the pulse has a shock front. The strong energy dissipation leads to a fast drop of the pressure in the compression pulse. Furthermore, because of the high propagation speed of the shock wave, the duration of the compression pulse increases. At reduced (units of length over units of mass) distances on the order of $100\, cm/g$ the compression pulse generated by the explosion is described by the expression [1] (using Coles's data]

$$
\begin{aligned}
p &= p_m \exp(-t/\theta), \\
p_m &= 7200(W^{1/3}/r)^{1.13} \text{ [atm]}, \ \theta = 5.58 \cdot 10^{-6} W^{1/3} (r/W^{1/3})^{0.22} \text{ [sec]}.
\end{aligned}
$$

where W is the charge weight (in g) and r is the distance (in cm).

From these data we can easily find that the ratio of the energy in the compression pulse to the energy of the charge at reduced distances of the order $100\,g/cm$ equals 20%, which is close to the value of the electro-acoustic efficiency of electric discharges in water.

The pulsation energy of a gas bubble formed in a TNT explosion is approximately equal to 40% of the charge energy, while in an electric discharge such energy amounts to 25–30% of the discharge energy. The difference can be explained by the fact that the discharges are accompanied by rather large energy losses, due to high temperatures (on the order of several tens of thousands of degrees) of the matter in the discharge channel, while in explosions the temperature is only about a few thousand degrees.

REFERENCES to Chapter VI

[1] Cole R., *Underwater explosion*, (Princeton UP, Princeton,1948).

[2] Flinn H. G., *Physics of acoustic cavitation in fluids*, in:Physical Acoustics, ed. by W. P. Mason, (Academic Press, NY, 1964), Vol. 1B.

[3] Kersavog G., in *Electric explosion of conductors*, (Moscow, Nauka, 1965).

[4] Landau L. D., Lifshitz E. M., *Fluid Mechanics*, Pergamon Press, N.Y. (1975).

[5] Arsen'ev D. V., *On the theory of high-power electric discharges in liquids* (Dissertation), Rostov-on-the-Don University, (1966).

[6] Filippov I., Zhurin V., Suljaev V., Ing.Fiz. Zh, **2** (4), 341 (1962).

[7] Okun' I. Z., "The application of dimensional and similaeity methods to the investigation of pulsed discharges in water," Zh.Tekh. Fiz., **37** (9), 1724-1738 (1967).

CONCLUSION

The development of technology presents physics with the problem of investigating processes involving large concentration of energy, high pressure and high temperatures. The impulsive spark discharge in a liquid is one such process. As a result of the fast release of the capacitor energy into the discharge channel high temperatures and pressures are generated,accompanied by the intense sound wave radiation. The theoretical model and the results of experimental investigations of hydrodynamical and thermodinamical phenomena stimulated by the underwater pulse discharge are considered in the present book. A qualitative picture of the phenomena occurring in a spark discharge in water and of the actual sequence in which they take place is given. The methods used in experiment for the initiation of spark discharges in a liquid are described. The processes occurring in the discharge channel and the properties of the matter in it are examined. The experimental information on the electric characteristics of the discharge, the rate of the channel expansion and also estimates of pressure and temperature in the discharge channel is given. The properties of the dense low-temperature plasma generated in the discharge channel are examined and the equation of energy balance is derived. The concrete form of this equation depends on the form of the equation which determines the pressure in the channel as a function of the channel radius and its derivatives. In order to find this dependence for various cases, the hydrodynamic problem of the expansion of a bubble in a liquid is considered. then the theoretical models for the pulse spark discharge in water are developed and the results of theoretical considerations are compared with the experiments. The theory of hydrodynamical effects accompanied by the intense sound wave radiation stimulated by fast energy release in liquid developed in the book is applicable to the description of some other effects such as laser induced optical breakdown of a fluid. When the light from a Q-switched laser is focused into a liquid, an optical breakdown may occur that leads to plasma formation, emission of an acoustic transient, and generation of a cavitation bubble [1-5]. This method can be used to study transient cavitation and sonoluminescence [6-7].

REFERENCES to Conclusion.

1. Askary'an G. A., Prokhorov A. M., Chanturia G. F., and Shipulo G. P., "The effects of a laser beam in a liquid," Sov. Phys. JETP **17**, 1463-1465 (1963).

2 Carome E. F., Moeller C. E., and Clark N. A., "Intense ruby-laser-induced acoustic impulse in liquids," J. Acoust. Soc. Am. **40**, 1462-1466 (1966).

3. .Bell C. E., and Landt J. A., "Laser-induced high-pressure shock waves in water," Appl. Phys. Lett. **10,** 46-48 (1967).

4. Barnes P. A.,and Rieckhoff K. E., "Laser-induced underwater sparks," Appl. Phys. Lett. **13,** 282-284 (1968).

5. Ioffe A. I., Melnikov N. A., Naugolnykh K. A., and Upadyshev V. A., "Shock wave at optical breakdown of a liquid," Zh. Prikl. Math. Tekh. Fiz. **3**,125-127 (1970).

6. Vogel A., and Lauterborn W., "Acoustic transient generation by laser-produced cavitation bubbles near solid boundaries," J. Acoust. Soc. Am. **84**, 719-731 (1988).

7. Gaitan D. F., Crum L. A., Church C. C., and Roy R. A., "Sonoluminescence and bubble dynamics for a single, stable cavitation bubble," J. Acoust. Soc. Am. **91**, 3166-3183 (1992).